Characterization of iron uptake into mitochondria of *Saccharomyces cerevisiae*

by

Jing Wang

A dissertation submitted to the Graduate Faculty of
Auburn University
in partial fulfillment of the
requirements for the Degree of
Doctor of Philosophy

Auburn, Alabama
August 1, 2015

Key words: Iron reductase, Heme, *Saccharomyces cerevisiae*.

Approved by

Paul A. Cobine, Chair, Associate Professor of Biological Sciences
Mark R. Liles, Associate Professor of Biological Sciences
Stuart Price, Associate Professor of Veterinary Medicine
Aaron M. Rashotte, Associate Professor of Biological Sciences

Abstract

Iron is abundant in the environment in the oxidized ferric state. However this form is not bioavailable. Cells require soluble ferrous iron and therefore many reduction strategies have evolved. *FRE5* encodes a putative iron reductase in *Saccharomyces cerevisiae.* The gene product is found in mitochondria where iron is converted into the essential cofactors heme and Fe-S. Overall this dissertation investigates the hypothesis that Fre5 reductase activity is required for optimal Fe utilization. I uncover iron related phenotypes in *S. cerevisiae* that lack the *FRE5* gene (referred to throughout as *FRE5* null or *fre5Δ)* including a heme defect compared with the isogenic wild type. This defect could be reversed by adding supplemental iron to the medium, suggesting Fre5 is involved in iron availability in yeast. In addition I found an H_2O_2 resistance phenotype for *fre5Δ*. I hypothesize that the Fre5 reductase activity creates redox cycling of iron that increases the potential for Fenton chemistry to explain the H_2O_2 resistance of this mutant. These phenotypes in *fre5Δ* are reversed by the introduction of *FRE5* gene on a vector. However the overexpression of *FRE5* in high copy number also resulted in iron related phenotypes. A reduction in total mitochondrial iron was observed in *fre5Δ* compared with wild type. *FRE5* overexpression increased mitochondrial iron reductase activity compared to *fre5*Δ. Based on statistical analysis of metal profiles in WT, *fre5Δ* and *fre5Δ* with *FRE5* overexpression strain, I found that *fre5Δ* has a lower level of mitochondrial iron and magnesium and a higher level of mitochondrial copper and zinc compared to the overexpression strain. Fre reductases are required for both copper and iron transport at the plasma membrane so we compared copper and iron phenotypes in mitochondria.

Ferrous iron is transported into mitochondria by Mrs3. Pic2 is a copper transporter in mitochondria but deletion of both *PIC2* and *MRS3* led to a severe respiratory growth defect independent of iron concentrations therefore we suggest that Mrs3 has a low affinity for copper. To investigate this overlap between copper and iron I studied the affect of copper on heme synthesis and found an overlap that results in a copper-induced heme defect that may be relevant to human health in copper overload disorders.

Acknowledgments

I'd like to thank Dr. Paul A. Cobine for the opportunity to conduct research under his guidance. I really appreciate his constant support and patience during my five year research and dissertation work. I feel very lucky to have him as my advisor, his wisdom and humor always inspires me, and he is a good example not only in academic way but also in life. I also want to thank my advisory committee members, Dr. Mark R. Liles, Dr. Stuart Price and Dr. Aaron M. Rashotte to be always available and willing to provide advice and support whenever requested. I also want to thank Dr. Zhongyang Cheng for serving as University Reader. I would also like to thank my colleagues in Dr. Cobine's lab for their encouragement, help and friendship. I appreciate the support from National Science Foundation grant MCB 1158497 (to P.A.C). Specially, I want to thank my wife Ying Su, without her support I would not finish all this. Finally, I want to express my gratitude to my parents and those who help me out in my difficult times.

Table of Contents

List of Tables

List of Figures

Chapter 1
Literature Review

1.1 The importance of iron

Organisms require iron for a wide array of metabolic functions, such as cellular respiration, DNA synthesis, lipid metabolism and many other biochemical activities [1]. Iron must be maintained at a balanced level as excess reactive iron is toxic and deficient iron level will lead to physiological and developmental disorders. Excessive ferrous iron in the cell will react with hydrogen peroxide and lipid peroxide and generate reactive oxygen species (ROS) by Fenton reaction and lipid radicals. ROS and lipid radicals can damage membrane phospholipids, cause vacuolar fragmentation and generate reactive aldehydes that damage proteins, leading to the accumulation of misfolded protein aggregates [2]. While iron deficiency will cause defects in heme and Fe-S cluster synthesis, severe iron deficiency causes cell death. The requirement for iron is conserved between eukaryotes and prokaryotes. *Borrelia burgdorferi* and Lactobacilli are the only two exceptions known not require iron at all and they both require manganese instead [3, 4].

Iron deficiency is the most common nutritional disorder in the world [5]. Iron is not only important for hemoglobin for oxygen transport in humans but also involved in many other processes that are dependent on heme and Fe-S cluster cofactors. The manifestations of iron deficiency include negative effects on work capacity and endurance, low birth weight, preterm delivery as well as motor and mental development in infants, children and adolescents [6-9]. The cause of iron deficiency are affected by many factors: the stage of life, gender, socioeconomic circumstances, dietary, increased iron loss, decreased absorption of iron and so on. Iron deficiency and iron deficiency anemia are especially prevalent among children and women of childbearing age, where they are associated with perinatal mortality. People in underdeveloped countries are also vulnerable to iron deficiency, even in developed countries, certain subgroups are at risk for iron deficiency due to higher requirement of iron. Iron deficiency also impairs neurological

development and cognitive function in children, and some of these defects appear to be irreversible [10]. Although the pathogenesis of anemia in iron deficiency is well understood, other manifestations of iron deficiency are not understood at the cellular or metabolic level, and not all of the clinical manifestations of iron deficiency can be attributed to a reduction in the oxygen-carrying capacity of the blood.

Iron overload is also a common disorder and can be divided into genetic iron overload and non-genetic iron overload. Iron overload is typically manifest as an accumulation of iron in organs, especially in the liver, heart, and pancreas, leading to organ dysfunction and failure. The mechanisms by which excess iron causes organ failure are unknown. Hereditary hemochromatosis is a major type of genetic iron overload, and the most common one is HFE hemochromatosis [11]. HFE protein is a membrane protein that is a member of the MHC class I family, it functions in the regulation of iron homeostasis. Several autosomal recessive mutation in *HFE* gene causes HFE hemochromatosis [12]. There are other cases of hemochromatosis caused by non-HFE proteins, like TfR2, and they share the same histological presentation of HFE hemochromatosis [13]. Other than hemochromatosis, other genetic iron overload syndromes include ferroportin disease and more rarely aceruloplasminemia or hypoceruloplasminemia [13-15].

Non-genetic iron overload includes excessive iron supply, inflammatory syndromes, chronic liver diseases and blood disorders [16, 17]. Excess iron has several severe outcomes. First, excess iron is toxic because of its capacity to produce free radicals. Second, increased iron status is often associated with poor prognosis in the setting of infection, such as malaria, HIV, tuberculosis and Hepatitis C virus [18-21]. Third, iron overload always leads to subsequent disease, like cirrhosis [22].

Baker's yeast *Saccharomyces cerevisiae* serves as a model eukaryote to study the basic of

cellular processes that are common in all eukaryotic cells, including iron homeostasis, uptake and utilization. Proteins found in higher multicellular eukaryotes usually function similarly to their orthologous proteins in yeast and can be frequently substituted and studied in yeast cells. This functional similarity and the genetic tractability of yeast have allowed researchers studying human proteins of iron metabolism to quickly focus their efforts based on the known functions of the yeast ortholog. The limitation of yeast would be that it is a single cell organism, it is impossible to study cell to cell or tissue problems in yeast.

1.2 Iron uptake and storage

In human cells, the principle source of iron is transferrin bounded ferric iron. Unlike human cells, yeast don't have transferrin [23]. The major iron source for *S. cerevisiae* is absorbed through two major pathways: non-reductive pathway and reductive pathway. In the non-reductive pathway, yeast cells absorb iron from siderophore-iron complex from the environment. Siderophore-iron complex are absorbed by ARN 1-4 family in yeast plasma membrane [24]. Siderophores are molecules synthesized and secreted by many species of bacteria and fungi, and grass plants. There are two major groups of siderophores [24]. Hydroxamate-type siderophores are mainly produced by fungi, such as ferrichromes. Catecholate-type siderophores are generally produced by Gram-negative bacteria, such as enterobactin. After secretion, siderophores can bind and solubilize ferric iron, thereby making it available to cellular uptake systems [25]. *S. cerevisiae* differ from other fungi in that it does not synthesize siderophores itself, but similar to most fungi, it can take up iron bound to a variety of these iron chelates [26]. When intracellular iron depletion occurs, more than half of activated genes are directly or indirectly involved with the siderophore-bound iron uptake [26]. Siderophore-bound iron need to pass through the cell wall first in order to reach the plasma membrane. When cellular iron levels decrease, yeast expresses FIT family Fit1, Fit2, and Fit3.

They are GPI-linked cell wall mannoproteins. Of all the genes expressed during cellular iron depletion, the *fit* genes are the most strongly induced, expression of the FIT proteins enhances the retention of ferrichrome in the cell wall and enhances its uptake at the cell surface [27].

In the reductive system, the ferric substrate is reduced to ferrous form at the cell surface before uptake. This reduction step is carried out by a group of broad-specificity metalloreductases known as the FRE family [28]. Fre1 and Fre2 are responsible for the majority of the cell surface reductase activity and are strongly induced by cellular iron depletion, or copper depletion in the case of Fre1 [29]. The FRE reductases are integral membrane proteins with binding sites for heme, FAD, and NADPH, and Fre1 has been shown to bind heme as a b-type flavocytochrome [30]. Although they were initially characterized as ferric citrate reductases, Fre1 and Fre2 can also reduce the ferric iron in siderophore chelates, such as ferric enterobactin, ferrichrome, and ferrioxamine B [31]. Fre3 and Fre4 are two other paralogs of FRE family, which are also expressed under cellular iron depletion. Fre3 and Fre4 showed the reductase abilities by reducing ferric hydroxamte siderophores [31]. FRE family has sequence conservation with the STEAP family in mammals. Studies showed Steap3 is a ferric reductase required in red blood cells for transferrin dependent iron uptake [32]. Steap2 is another ferric reductase and Steap4 is a cupric reductase, they are predicted to use flavin, heme and NADPH cofactors [33].

Based on the fact siderophores only bind ferric iron with high affinity, reduction by this family of reductases would lead to the dissociation of the ferrous iron from the siderophore, making it available to specific transporters. When intracellular iron is deplete, cells transcriptionally upregulate the high-affinity ferrous iron uptake complex Fet3/Ftr1, and uptake iron primarily through this high-affinity complex. In this high-affinity complex pathway, even though cells require ferrous iron for solubility it must be oxidized prior to uptake. The oxidation is performed

by the multicopper oxidase Fet3. The ferric iron is then delivered to the cytosol by the Ftrl permease [34]. Ferrous iron is the only known substrate for this Fet3/Ftr1 complex. The reason why iron must be oxidized before its uptake is unknown, it might contribute to the uniqueness for ferrous iron uptake. Atx1 and Ccc2 are the two proteins that are involved in copper insertion into Fet3. Atx1 is a cytosolic copper chaperone, it binds cytosolic copper and delivers it to the methionine-rich domain of Ccc2 [35]. Ccc2 is a copper ATPase pumps the copper into the post-Golgi vesicle to synthesize Fet3 [36]. Interestingly, both *ATX1* and *CCC2* are regulated by iron transcriptionally rather than copper, meaning their primary role are in iron homeostasis.

When cells contain adequate iron cells downregulate the high-affinity ferrous iron uptake transporter Fet3/Ftr1 complex transcriptionally [37]. The iron uptake occurs through low-affinity transporters with broader transition metal specificity. Yeast express three members of the Nramp family of divalent metal transporters, called Smf1, Smf2 and Smf3 [38]. Smf1 is primarily a plasma membrane transporter of manganese, but can also transport iron and cobalt, and overexpression of Smf1 accumulates higher levels of intracellular iron [39]. Another low-affinity transporter of broad metal ion specificity is Fet4, which exhibits transport activity for ferrous iron, zinc, copper, and cadmium [40]. Fet4 is strongly induced under low oxygen conditions and may become the major iron transporter during hypoxic or anaerobic growth, when the oxygen-dependent Fet3/Ftrl complex is inactive [41].

Pathogenic yeast strains such as *Candida albicans* can utilize heme as their primary iron source. However, this is not the case for *S. cerevisiae* [42]. A study showed under iron depletion conditions, *S. cerevisiae* does not elevate their heme uptake [43]. However, *S. cerevisiae* does have the ability to take up heme and this can be activated under the condition of heme deficiency [44]. Heme deficiency often occurs under hypoxic growth, because the synthesis of heme is highly

dependent on oxygen concentration. No high-affinity heme transporters have been found in any *Saccharomyces* species. The only heme related transporter discovered in *S. cerevisiae* is Pug1, it has limited capacity of heme efflux and protoporphyrin IX (final tetrapyrrole intermediate which is converted to heme by the addition of Fe) uptake [44].

Ferritin is one of the major eukaryotic proteins involved iron storage and maintaining iron homeostasis. In *S. cerevisiae* there is no ferritin or other proteinaceous means to store excess iron. Initially one potential iron storage protein identified in yeast is the homologue of human frataxin (Yfh1) [45]. However most recent studies suggest that this would be a minor secondary function with its main function being delivery of sulfur in Fe-S cluster assembly [46]. Lysosome is the organelle used for iron storage in human cells. In *S. cerevisiae*, excess iron is stored in the vacuole, however the molecular form of the iron in the vacuole is unknown. When yeasts are grown in media containing high concentrations of iron, vacuoles accumulate iron through Cccl, a transporter specific for iron and manganese located on the vacuolar membrane [47]. Overexpression of *CCC1* in yeast result in accumulation of iron in the vacuole, and conversely, deletion mutants accumulate less iron and are sensitive to elevated levels of iron, indicating that sequestrating iron in the vacuole is important for detoxification. *CCC1* is transcriptionally activated under iron-replete conditions by the transcription factor Yap5 [48]. Yap5 is a member of a family of basic-region leucine zipper transcription factors. Other members of this family respond to oxidative stress and cadmium, while Yap5 appears to be the only family member that responds to excess iron.

Growth in iron-poor medium activates the expression of several genes involved in vacuolar iron mobilization, and these genes essentially duplicate the reductive transport system found on the plasma membrane. The vacuole system is made up of Fre6, Fet5 and Fth1. Fre6, a member of the FRE family of metalloreductases, is activated by Aft1 during iron depletion and is expressed

on the membrane of vacuole [49]. Fre6 activity is required for the reduction of vacuolar iron to increase solubility and allow its export from the organelle to the cytosol. The high-affinity vacuolar iron transport complex Fet5/Fth1 is homologous to the high-affinity plasma membrane transport complex Fet3/Ftr1, and are also expressed as a complex on the vacuolar membrane [50]. Smf3 is a paralog of Smf1 and is also found on the vacuolar membrane [50]. Together, Fet5/Fthl and Smf3 can transport ferrous iron produced by Fre6 from the vacuole to the cytosol.

Yeast cells growing on iron-poor medium induce the expression of Hmxl, which is a putative yeast heme oxygenase, and involved in heme degradation to liberate the iron for other metabolic purposes [51]. Expression of Hmxl during iron deficiency also serves to downregulate the expression of iron-containing proteins.

1.3 Heme and Fe-S biosynthesis in yeast

Heme is synthesized in both mitochondria and cytosol, it is highly conserved in biology [52]. The first step in heme synthesis pathway happens within mitochondrial matrix by synthesis of D-Aminolevulinic acid (ALA) from succinyl-CoA and glycine, which come from the citric acid cycle. The enzyme for this reaction is ALA synthase, which is the rate-limiting enzyme to this process and is negatively regulated by the concentration of heme and glucose [53, 54]. ALA then outflows into the cytosol and porphobilinogen (PBG) is synthesized from combining two ALA, this step is catalyzed by ALA dehydratase. PBG deaminated by PBG deaminase to form hydroxymethylbilane, which then converted to uroporphyrinogen III by losing a H_2O molecule catalyzed by uro'gen III synthase. Uro'gen III decarboxylase catalyze uroporphyrinogen III to form coprophyrinogen III. Then mitochondria absorb coprophyrinogen III back into matrix and oxidized to protoporphtrinogen IX by copro'gen III oxidase. Protoporphtrinogen IX then oxidized by proto'gen IX oxidase to form protoporphyrin IX. In the last step, ferrous iron is inserted into

protoporphyrin IX by ferrochelatase to form heme. The studies showed ferrochelatase is able to mediate insertion of iron or zinc into the protoporphyrin IX. When suffering from iron deficiency, cells made primarily the zinc protoporphyrin product instead [55]. Human ferrochelatase were shown to contain a [2Fe-2S] cluster so its activities were regulated by the concentration of Fe-S clusters in cell [56]. But in *Escherichia coli* or plants ferrochelatase does not possess a [2Fe-2S] cluster [56, 57]. In yeast, it is reported that *Saccharomyces cerevisiae* ferrochelatase does not possess a [2Fe-2S] cluster [58-60], and interestingly in *Schizosaccharomyces pombe* a ferrochelatase [2Fe-2S] cluster has been found [61].

Photosynthesis, nitrogen fixation and respiration all need Fe-S proteins, such as ferredoxin, cytochrome b and electron transport chain complex I, II, III. The Fe-S cluster plays an important role in electron transfer. Fe-S cluster synthesis blockage will directly affect mitochondrial function. In addition to the role of electron transfer, Fe-S proteins also play roles in enzyme catalysis and the regulation of proteins, the most typical example is iron regulatory protein Aft1. By sensing the concentration of Fe-S cluster in mitochondria, Aft1 regulates the expression of iron proteins [62]. In the mitochondrial citric acid cycle, two enzymes require iron-sulfur cluster as a cofactor, they are aconitase and succinate dehydrogenase. Iron-sulfur clusters exist in many forms, but the most common forms are [2Fe-2S] and [4Fe-4S] [63].

The biogenesis of mitochondrial Fe-S proteins is accomplished in three major steps. First, the [2Fe–2S] cluster is synthesized on the scaffold protein Isu1 [64], the cysteine desulfurase complex Nfs1/Isd11 act as a sulfur donor by releasing sulfur from cysteine [65, 66]. This step also requires Yfh1 interact with Isu1 in an iron dependent manner. Yfh1 may act as an iron donor and/or an allosteric regulator of the desulfurase enzyme [67]. An electron transfer chain consisting of NAD(P)H, ferredoxin reductase (Arh1) and ferredoxin (Yah1) is needed for Fe-S cluster assembly

on Isu1 [64]. In the second step, the Isu1-bound Fe-S cluster is released by a dedicated ATP-dependent Hsp70 chaperone system including Ssq1, its co-chaperone Jac1, and the nucleotide exchange factor Mge1 [64, 68]. The monothiol glutaredoxin Grx5 then helps the Fe-S cluster to transfer toward apoproteins [69]. In the third step, specialized ISC targeting components catalyze the generation of [4Fe–4S] clusters by involving Isa1/Isa2/Iba57 proteins, and they assist the insertion of Fe-S clusters into specific apoproteins [70]. The first two steps are essential for both cytosolic and mitochondrial Fe-S protein and for cellular iron regulation.

1.4 Iron regulation in yeast cells

In *S. cerevisiae*, iron homeostasis is primarily controlled by the transcription factor Aft1 [71] and, to a lesser extent, Aft2 [72]. These two transcription factors activate a set of genes that constitute the major response to iron deficiency in yeast [see table 1.1]. Aft1 and Aft2 recognize and bind to consensus sequences present in one or more copies in the upstream region of their target genes. Aft2 has 39% identity to Aft1 and recognizes a partially overlapping set of genes with similar consensus sequences, but the effects of Aft2 are minor unless Aft1 is deleted. An exception to this is the transcriptional activation of Smf3 and Mrs4, which are targets for Aft2, but not Aft1.

Aft1 is constitutively expressed in growing yeast cells no matter the iron level. Under conditions of iron depletion, Aft1 mobilizes into the nucleus and binds DNA to activate the transcription of the set of genes described in Table 1.1 [73]. Under conditions of iron sufficiency, Aft1 is mainly located in the cytosol, and it is inactive. The karyopherin Psel is required for Aft1 import into the nucleus [74] and the nuclear exportin Msn5 for export to the cytosol [75].

Several components of the mitochondrial iron-sulfur cluster assembly system are responsible for Aft1 inactivation in the presence of iron, leading to the hypothesis that Aft1 senses cellular iron levels in the form of a product from the ISC assembly system. Deletion of the monothiol glutaredoxin Grx5; depletion of the yeast frataxin homologue, Yfh1; or depletion of glutathione all lead to loss of both ISC assembly and iron-dependent Aft1 inactivation [62]. Aft1 inactivation also requires Atm1, a mitochondrial inner membrane transporter that is thought to export products of the ISC assembly system. However the components of the cytosolic ISC machinery appear not to be required for the inactivation of Aft1, as their depletion does not result in the constitutive expression of the Aft1 regulated genes [62]. These observations suggest that Aft1 responds to changes in the levels of a product of the mitochondrial ISC assembly machinery and that the levels of this ISC product are proportional to the levels of metabolically available cellular iron.

The inactivation of Aft1 requires several other proteins that interact with Aft1 directly. Grx3 and Grx4 are monothiol glutaredoxins required for the inactivation and accumulation of Aft1 in the cytosol [76, 77]. Both Grx3 and Grx4 can bind to Aft1, and a conserved cysteine residue in the glutaredoxin active site is required for both binding and inactivation. Fra1 and Fra2 are two additional proteins that are individually required for the inactivation of Aft1 [78]. In vitro, Grx3 and Grx4 can form heterodimers with Fra2 that bind a [2Fe- 2S] cluster, and the presence of the ISC may be communicated to Aft1 as it cycles through the cytosol [79].

Functional Category	Systematic Name	Gene Name	Location	Function
Iron Uptake	YDR534C	*FIT1*	Cell Wall	Siderophore Binding/Uptake
	YOR382W	*FIT2*	Cell Wall	Siderophore Binding/Uptake
	YOR383C	*FIT3*	Cell Wall	Siderophore Binding/Uptake
	YLR214W	*FRE1*	Plasma Membrane	Metalloreductase
	YKL220C	*FRE2*	Plasma Membrane	Metalloreductase
	YOR381W	*FRE3*	Plasma Membrane	Siderophore Reductase
	YNR060W	*FRE4*	Unknown	Rhodotorulic acid-iron Reductase
	YOR384W	*FRE5*	Mitochondria	Metalloreductase
	YMR058W	*FET3*	Plasma Membrane	Multicopper Oxidase/Fe(II) Uptake
	YER145C	*FTR1*	Plasma Membrane	Permease/Fe(II) Uptake
	YNL259C	*ATX1*	Cytosol	Copper Chaperone
	YDR270W	*CCC2*	Post-Golgi Vesicle	Copper Transport
	YNL040C	*ARN1*	Plasma Membrane/Endosome	Ferrichrome Transport
	YNL047C	*ARN2*	Unknown	Triacetylfusarinine C Transport
	YEL065W	*ARN3*	Plasma Membrane/Endosome	Hydroxamate Siderophore Transport
	YOL158C	*ARN4*	Plasma Membrane	Enterobactin Transport
Efflux of Iron From Vacuole To Cytosol	YLL051C	*FRE6*	Vacuole	Metalloreductase
	YFL041W	*FET5*	Vacuole	Multicopper Oxidase/Fe(II) Uptake
	YBR207W	*FTH1*	Vacuole	Permease/Fe(II) Uptake
Other Transporter	YGR065C	*VHT1*	Plasma Membrane	Biotin Transporter
	YOR316C	*COT1*	Vacuole	Zic and Cobalt Storage/Detoxification
Low iron adaptation genes	YLR205C	*HMX1*	Endoplasmic Reticulum	Heme Oxygenase
	YLR136C	*CTH2*	Cytosol	mRNA Degradation

Table 1.1 Aftl target genes and their subcellular location and function.

Table information was acquired from Philpott [26].

1.5 Iron trafficking in mitochondria

Mitochondria play a very important role in iron metabolism for their heme synthesis, in the assembly of Fe-S clusters and their participation in cellular iron regulation. Mitochondria assemble not only mitochondrial Fe-S clusters, but are also involved in the biosynthesis of Fe-S proteins in cytosol and in the nucleus. These cytosolic and nuclear Fe-S proteins with essential functions include the Fe-S ABC protein Rli1(ABCE1), which participates in ribosome assembly and ribosome recycling during termination of polypeptide synthesis [80]. ATP dependent DNA helicases Rad3, FancJ, Rtel1 and XPD involved in DNA damage repair and telomere maintenance are other examples [81]. Eukaryotic replicative DNA polymerases which also contain a Fe-S

cluster in their C-terminal domain, Fe-S cofactor appears to be indispensable for efficient interaction with their accessory proteins during DNA replication [82].

Fe-S clusters are essential cofactors required for the electron transport chain and many other biochemical reactions and processes. Critical cofactor assembly systems are required to sequester, chaperone, and regulate metal ions. This assembly system is not for building Fe-S cluster, because the clusters will self-assemble in solution, but is thought to be necessary to circumvent the toxicity and indiscriminant reactivity of free iron and sulfide. Defects in biosynthesis in Fe-S cluster will cause dysfunction in mitochondria, neurodegenerative and cardiovascular disease, genomic instability, and the development of aging and cancer [83].

Iron can enter mitochondria through multiple mechanisms, not all of which have been identified. Mrs3 and Mrs4 encode mitochondrial carrier proteins that can transport iron into the mitochondrial matrix [84]. Mrs4 is transcriptionally activated by iron depletion, suggesting the importance of homeostasis of iron in mitochondria. Once iron is diverted into the mitochondrial matrix, frataxin homolog Yfh1 in mitochondria has been proposed to play some role as a chaperone directing iron to produce heme and Fe-S cluster (ISC) [85]. However, recent experimental evidence suggests that this is not a required function of Yfh1. Yfh1 can be bypassed completely by a mutation in the Fe-S cluster scaffold protein IscU suggesting the primary function is sulfur delivery to form Fe-S clusters [86]. Although mutating Fe-chelating residues of Yfh1 reveals no phenotypes it remains possible that Fe binding plays a supporting role in iron availability. Once Fe reaches the ISS machinery it is synthesized into 2Fe-2S clusters that are then inserted in mitochondrial targets or exported to the cytosol where the CIA machinery matures them to 4Fe-4S clusters and/or inserts them into other targets. Fe not recruited into Fe-S clusters is accessed by ferrochelatase for insertion in to PPIX to form heme.

1.6 Iron and Oxidative Stress

Iron has the catalytic properties to catalyze reactions to produce hydroxyl radical ($OH^{\cdot}$), through this property iron is considered to be toxic to cellular function and viability when excess. The $OH^{\cdot}$ is generated through the Fenton reaction. In this reaction superoxide radical ($O_2^{\cdot -}$) reduces ferric iron to ferrous iron, then ferrous iron reacts with hydrogen peroxide (H_2O_2) and produce $OH^{\cdot}$ [87]. Fenton reaction does not require certain place to occur, as long as iron is present. Due to its high potential toxicity it is under tight regulation in cells. The reactive oxygen species (ROS) $O_2^{\cdot -}$ and H_2O_2 are produced by NADPH oxidase and by the aerobic respiration reactions [88]. Iron is also able to catalyze peroxynitrite ($ONOO^-$) to nitronium anion (NO_2^+). $ONOO^-$ is formed with the presence of $O_2^{\cdot -}$ and $NO^{\cdot}$ produced by nitric oxide synthase [89].

$$Fe^{3+} + O_2^{\cdot -} \longrightarrow Fe^{2+} + O_2$$

$$Fe^{2+} + H_2O_2 \longrightarrow Fe^{3+} + OH^- + OH^{\cdot}$$

$$O_2^{\cdot -} + H_2O_2 \xrightarrow{Fe^{3+}} OH^- + OH^{\cdot} + O_2$$

Figure 1.1 Fenton reaction.

The above two equations represent the chemical process, the bottom equation is the expression of the outcomes.

$OH^{\cdot}$ and NO_2^+ are highly reactive and are responsible for lipid peroxidation as well as DNA and protein damage. Organelles such as mitochondria and peroxisomes produce high level of ROS in normal conditions. To prevent the potential damage of ROS produced by them, cells express enzymes such as catalase, superoxide dismutase (Sod1) and glutathione (GSH) peroxidase to break down ROS [90]. On the other hand, there are many antioxidants providing a passive protection form against ROS. For example, GSH neutralize ROS and free radicals by itself or in combination

with other enzymes like glutathione peroxidase and glutathione reductase [91]. Diallylsulfide inhibits cytochrome P4502E1 which is considered a ROS generator in aerobic respiration reactions, in consequence diallylsufide reduces the availability of $O_2^{\cdot -}$ [92]. When suffering iron overload, such as that seen in the genetic disorder hemochromatosis, cellular iron overwhelms these antioxidants and produce more ROS, then ROS reacts with polyunsaturated phospholipids in organelles and cell membranes. Oxidized amino acids leads to DNA strand breaks, protein adducts formation and protein fragmentation [93].

$OH^{\cdot}$ is also able to catalyze electron transfer from lipids in the cell membrane back to free radical, this is known as lipid peroxidation. Lipid peroxidation affects polyunsaturated fatty acids because they contain methylene groups within their double bonds that possess especially reactive hydrogens which are very susceptible to peroxidation [94]. Intramolecular rearrangement of double bonds in these polyunsaturated fatty acids yields conjugated dienes, in the presence of oxygen, lipid radicals form lipid peroxyl radicals [95]. These lipid peroxyl radicals can keep reacting with more fatty acids and form lipid hydroperoxide, which is susceptible to cleavage by ferrous and ferric iron chelates with decomposition to alkoxyl and peroxyl free radicals, respectively. Lipid hydroperoxides undergo intramolecular cyclization and decomposition to generate thiobarbituric aid (TBA)-reactants and the breakdown by-products malondialdehyde (MDA), 4-hydroxynonenal (4-HNE), ketones, alcohol, ethane and pentane [95, 96]. In turn, MDA and 4-HNE are frequently used as markers of oxidative stress as they are readily localized using antibodies. Lipid peroxidation of membranes throughout the cell results in membrane fragility and can lead to dysfunction of a number of different organelles which compromises cell function. These organelles include mitochondria and endoplasmic reticulum, leading to problems with energy and protein production [97].

In conclusion, iron is an important transition metal, it is essential for organisms to live and reproduce. Iron is a cofactor required in heme and Fe-S cluster biosynthesis. Iron homeostasis is tightly regulated in cells, high iron concentration introduces oxidative stress to cells. Organisms can only utilize the reduced form of iron in cells. To better obtain ferrous iron, many metalloredutases are involved in iron reduction processes, iron reductases have been found in plasma membrane as well as vacuole membrane. Mitochondrion is the place where heme and Fe-S cluster synthesized. In yeast mitochondria, there is a putative iron reductase Fre5 reported [98]. In this study, Fre5 is identified as an iron reductase located in mitochondria, the characteristics of which are presented in chapter 2 and chapter 4.

The correlation of iron and copper has been shown in many cases, like multicopper protein Fet3 and its copper transporter Atx1. No overlap of copper and iron uptake in yeast mitochondria has been reported. In this study, the yeast mitochondrial iron transporter Mrs3 has been shown to have an overlap in copper transport in chapter3.

References

1. Lill, R. and U. Muhlenhoff, *Maturation of iron-sulfur proteins in eukaryotes: mechanisms, connected processes, and diseases.* Annu Rev Biochem, 2008. 77: p. 669-700.
2. Corson, L.B., et al., *Oxidative stress and iron are implicated in fragmenting vacuoles of Saccharomyces cerevisiae lacking Cu,Zn-superoxide dismutase.* J Biol Chem, 1999. 274(39): p. 27590-6.
3. Imbert, M. and R. Blondeau, *On the iron requirement of lactobacilli grown in chemically defined medium.* Curr Microbiol, 1998. 37(1): p. 64-6.
4. Posey, J.E. and F.C. Gherardini, *Lack of a role for iron in the Lyme disease pathogen.* Science, 2000. 288(5471): p. 1651-3.
5. Zimmermann, M.B. and R.F. Hurrell, *Nutritional iron deficiency.* Lancet, 2007. 370(9586): p. 511-20.
6. Haas, J.D. and T.t. Brownlie, *Iron deficiency and reduced work capacity: a critical review of the research to determine a causal relationship.* J Nutr, 2001. 131(2S-2): p. 676S-688S; discussion 688S-690S.
7. Halterman, J.S., et al., *Iron deficiency and cognitive achievement among school-aged children and adolescents in the United States.* Pediatrics, 2001. 107(6): p. 1381-6.
8. Algarin, C., et al., *Iron deficiency anemia in infancy: long-lasting effects on auditory and visual system functioning.* Pediatr Res, 2003. 53(2): p. 217-23.
9. Verdon, F., et al., *Iron supplementation for unexplained fatigue in non-anaemic women: double blind randomised placebo controlled trial.* BMJ, 2003. 326(7399): p. 1124.
10. Beard, J.L., *Why iron deficiency is important in infant development.* J Nutr, 2008. 138(12): p. 2534-6.
11. Feder, J.N., *The hereditary hemochromatosis gene (HFE): a MHC class I-like gene that functions in the regulation of iron homeostasis.* Immunol Res, 1999. 20(2): p. 175-85.
12. Sebastiani, G. and A.P. Walker, *HFE gene in primary and secondary hepatic iron overload.* World J Gastroenterol, 2007. 13(35): p. 4673-89.
13. Pietrangelo, A., *The ferroportin disease.* Blood Cells Mol Dis, 2004. 32(1): p. 131-8.
14. Miyajima, H., Y. Takahashi, and S. Kono, *Aceruloplasminemia, an inherited disorder of iron metabolism.* Biometals, 2003. 16(1): p. 205-13.
15. Kono, S., et al., *Hepatic iron overload associated with a decreased serum ceruloplasmin level in a novel clinical type of aceruloplasminemia.* Gastroenterology, 2006. 131(1): p. 240-5.
16. Deugnier, Y., et al., *Increased body iron stores in elite road cyclists.* Med Sci Sports Exerc, 2002. 34(5): p. 876-80.
17. Bottomley, S.S., *Secondary iron overload disorders.* Semin Hematol, 1998. 35(1): p. 77-86.
18. Prentice, A.M., et al., *Iron metabolism and malaria.* Food Nutr Bull, 2007. 28(4 Suppl): p. S524-39.
19. McDermid, J.M., et al., *Elevated iron status strongly predicts mortality in West African adults with HIV infection.* J Acquir Immune Defic Syndr, 2007. 46(4): p. 498-507.

20. Boelaert, J.R., et al., *The effect of the host's iron status on tuberculosis.* J Infect Dis, 2007. 195(12): p. 1745-53.
21. Isom, H.C., E.I. McDevitt, and M.S. Moon, *Elevated hepatic iron: a confounding factor in chronic hepatitis C.* Biochim Biophys Acta, 2009. 1790(7): p. 650-62.
22. Detivaud, L., et al., *Hepcidin levels in humans are correlated with hepatic iron stores, hemoglobin levels, and hepatic function.* Blood, 2005. 106(2): p. 746-8.
23. Cmejla, R., et al., *Human MRCKalpha is regulated by cellular iron levels and interferes with transferrin iron uptake.* Biochem Biophys Res Commun, 2010. 395(2): p. 163-7.
24. Lesuisse, E., et al., *Siderophore uptake and use by the yeast Saccharomyces cerevisiae.* Microbiology, 2001. 147(Pt 2): p. 289-98.
25. Neilands, J.B., *Siderophores: structure and function of microbial iron transport compounds.* J Biol Chem, 1995. 270(45): p. 26723-6.
26. Philpott, C.C., et al., *The response to iron deprivation in Saccharomyces cerevisiae: expression of siderophore-based systems of iron uptake.* Biochem Soc Trans, 2002. 30(4): p. 698-702.
27. Protchenko, O., et al., *Three cell wall mannoproteins facilitate the uptake of iron in Saccharomyces cerevisiae.* J Biol Chem, 2001. 276(52): p. 49244-50.
28. Dancis, A., et al., *Genetic evidence that ferric reductase is required for iron uptake in Saccharomyces cerevisiae.* Mol Cell Biol, 1990. 10(5): p. 2294-301.
29. Georgatsou, E. and D. Alexandraki, *Regulated expression of the Saccharomyces cerevisiae Fre1p/Fre2p Fe/Cu reductase related genes.* Yeast, 1999. 15(7): p. 573-84.
30. Finegold, A.A., et al., *Intramembrane bis-heme motif for transmembrane electron transport conserved in a yeast iron reductase and the human NADPH oxidase.* J Biol Chem, 1996. 271(49): p. 31021-4.
31. Yun, C.W., et al., *The role of the FRE family of plasma membrane reductases in the uptake of siderophore-iron in Saccharomyces cerevisiae.* J Biol Chem, 2001. 276(13): p. 10218-23.
32. Ohgami, R.S., et al., *Identification of a ferrireductase required for efficient transferrin-dependent iron uptake in erythroid cells.* Nat Genet, 2005. 37(11): p. 1264-9.
33. Ohgami, R.S., et al., *The Steap proteins are metalloreductases.* Blood, 2006. 108(4): p. 1388-94.
34. Stearman, R., et al., *A permease-oxidase complex involved in high-affinity iron uptake in yeast.* Science, 1996. 271(5255): p. 1552-7.
35. Lin, S.J., et al., *A role for the Saccharomyces cerevisiae ATX1 gene in copper trafficking and iron transport.* J Biol Chem, 1997. 272(14): p. 9215-20.
36. Yuan, D.S., et al., *The Menkes/Wilson disease gene homologue in yeast provides copper to a ceruloplasmin-like oxidase required for iron uptake.* Proc Natl Acad Sci U S A, 1995. 92(7): p. 2632-6.
37. Philpott, C.C. and O. Protchenko, *Response to iron deprivation in Saccharomyces cerevisiae.* Eukaryot Cell, 2008. 7(1): p. 20-7.
38. Culotta, V.C., M. Yang, and M.D. Hall, *Manganese transport and trafficking: lessons learned from Saccharomyces cerevisiae.* Eukaryot Cell, 2005. 4(7): p. 1159-65.
39. Cohen, A., H. Nelson, and N. Nelson, *The family of SMF metal ion transporters in yeast cells.* J Biol Chem, 2000. 275(43): p. 33388-94.

40. Hassett, R., et al., *The Fe(II) permease Fet4p functions as a low affinity copper transporter and supports normal copper trafficking in Saccharomyces cerevisiae.* Biochem J, 2000. 351 Pt 2: p. 477-84.
41. Jensen, L.T. and V.C. Culotta, *Regulation of Saccharomyces cerevisiae FET4 by oxygen and iron.* J Mol Biol, 2002. 318(2): p. 251-60.
42. Weissman, Z. and D. Kornitzer, *A family of Candida cell surface haem-binding proteins involved in haemin and haemoglobin-iron utilization.* Mol Microbiol, 2004. 53(4): p. 1209-20.
43. Protchenko, O., et al., *A screen for genes of heme uptake identifies the FLC family required for import of FAD into the endoplasmic reticulum.* J Biol Chem, 2006. 281(30): p. 21445-57.
44. Protchenko, O., et al., *Role of PUG1 in inducible porphyrin and heme transport in Saccharomyces cerevisiae.* Eukaryot Cell, 2008. 7(5): p. 859-71.
45. Babcock, M., et al., *Regulation of mitochondrial iron accumulation by Yfh1p, a putative homolog of frataxin.* Science, 1997. 276(5319): p. 1709-12.
46. Lill, R., et al., *The role of mitochondria in cellular iron-sulfur protein biogenesis and iron metabolism.* Biochim Biophys Acta, 2012. 1823(9): p. 1491-508.
47. Chen, O.S. and J. Kaplan, *CCC1 suppresses mitochondrial damage in the yeast model of Friedreich's ataxia by limiting mitochondrial iron accumulation.* J Biol Chem, 2000. 275(11): p. 7626-32.
48. Li, L., et al., *Yap5 is an iron-responsive transcriptional activator that regulates vacuolar iron storage in yeast.* Mol Cell Biol, 2008. 28(4): p. 1326-37.
49. Singh, A., N. Kaur, and D.J. Kosman, *The metalloreductase Fre6p in Fe-efflux from the yeast vacuole.* J Biol Chem, 2007. 282(39): p. 28619-26.
50. Urbanowski, J.L. and R.C. Piper, *The iron transporter Fth1p forms a complex with the Fet5 iron oxidase and resides on the vacuolar membrane.* J Biol Chem, 1999. 274(53): p. 38061-70.
51. Protchenko, O. and C.C. Philpott, *Regulation of intracellular heme levels by HMX1, a homologue of heme oxygenase, in Saccharomyces cerevisiae.* J Biol Chem, 2003. 278(38): p. 36582-7.
52. Hardison, R.C., *Evolution of hemoglobin and its genes.* Cold Spring Harb Perspect Med, 2012. 2(12): p. a011627.
53. Hoffman, M., M. Gora, and J. Rytka, *Identification of rate-limiting steps in yeast heme biosynthesis.* Biochem Biophys Res Commun, 2003. 310(4): p. 1247-53.
54. Ponka, P., *Tissue-specific regulation of iron metabolism and heme synthesis: distinct control mechanisms in erythroid cells.* Blood, 1997. 89(1): p. 1-25.
55. Camadro, J.M. and P. Labbe, *Kinetic studies of ferrochelatase in yeast. Zinc or iron as competing substrates.* Biochim Biophys Acta, 1982. 707(2): p. 280-8.
56. Dailey, H.A., M.G. Finnegan, and M.K. Johnson, *Human ferrochelatase is an iron-sulfur protein.* Biochemistry, 1994. 33(2): p. 403-7.
57. Dailey, T.A. and H.A. Dailey, *Identification of [2Fe-2S] clusters in microbial ferrochelatases.* J Bacteriol, 2002. 184(9): p. 2460-4.
58. Labbe-Bois, R., *The ferrochelatase from Saccharomyces cerevisiae. Sequence, disruption, and expression of its structural gene HEM15.* J Biol Chem, 1990. 265(13): p. 7278-83.

59. Eldridge, M.G. and H.A. Dailey, *Yeast ferrochelatase: expression in a baculovirus system and purification of the expression protein.* Protein Sci, 1992. 1(2): p. 271-7.
60. Gora, M., et al., *Probing the active-site residues in Saccharomyces cerevisiae ferrochelatase by directed mutagenesis. In vivo and in vitro analyses.* J Biol Chem, 1996. 271(20): p. 11810-6.
61. Medlock, A.E. and H.A. Dailey, *Examination of the activity of carboxyl-terminal chimeric constructs of human and yeast ferrochelatases.* Biochemistry, 2000. 39(25): p. 7461-7.
62. Rutherford, J.C., et al., *Activation of the iron regulon by the yeast Aft1/Aft2 transcription factors depends on mitochondrial but not cytosolic iron-sulfur protein biogenesis.* J Biol Chem, 2005. 280(11): p. 10135-40.
63. Rouault, T.A. and W.H. Tong, *Iron-sulphur cluster biogenesis and mitochondrial iron homeostasis.* Nat Rev Mol Cell Biol, 2005. 6(4): p. 345-51.
64. Muhlenhoff, U., et al., *Components involved in assembly and dislocation of iron-sulfur clusters on the scaffold protein Isu1p.* EMBO J, 2003. 22(18): p. 4815-25.
65. Zheng, L., et al., *Mechanism for the desulfurization of L-cysteine catalyzed by the nifS gene product.* Biochemistry, 1994. 33(15): p. 4714-20.
66. Wiedemann, N., et al., *Essential role of Isd11 in mitochondrial iron-sulfur cluster synthesis on Isu scaffold proteins.* EMBO J, 2006. 25(1): p. 184-95.
67. Muhlenhoff, U., et al., *The yeast frataxin homolog Yfh1p plays a specific role in the maturation of cellular Fe/S proteins.* Hum Mol Genet, 2002. 11(17): p. 2025-36.
68. Dutkiewicz, R., et al., *The Hsp70 chaperone Ssq1p is dispensable for iron-sulfur cluster formation on the scaffold protein Isu1p.* J Biol Chem, 2006. 281(12): p. 7801-8.
69. Kim, K.D., et al., *Monothiol glutaredoxin Grx5 interacts with Fe-S scaffold proteins Isa1 and Isa2 and supports Fe-S assembly and DNA integrity in mitochondria of fission yeast.* Biochem Biophys Res Commun, 2010. 392(3): p. 467-72.
70. Sheftel, A.D., et al., *The human mitochondrial ISCA1, ISCA2, and IBA57 proteins are required for [4Fe-4S] protein maturation.* Mol Biol Cell, 2012. 23(7): p. 1157-66.
71. Yamaguchi-Iwai, Y., A. Dancis, and R.D. Klausner, *AFT1: a mediator of iron regulated transcriptional control in Saccharomyces cerevisiae.* EMBO J, 1995. 14(6): p. 1231-9.
72. Blaiseau, P.L., E. Lesuisse, and J.M. Camadro, *Aft2p, a novel iron-regulated transcription activator that modulates, with Aft1p, intracellular iron use and resistance to oxidative stress in yeast.* J Biol Chem, 2001. 276(36): p. 34221-6.
73. Yamaguchi-Iwai, Y., et al., *Subcellular localization of Aft1 transcription factor responds to iron status in Saccharomyces cerevisiae.* J Biol Chem, 2002. 277(21): p. 18914-8.
74. Ueta, R., A. Fukunaka, and Y. Yamaguchi-Iwai, *Pse1p mediates the nuclear import of the iron-responsive transcription factor Aft1p in Saccharomyces cerevisiae.* J Biol Chem, 2003. 278(50): p. 50120-7.
75. Ueta, R., et al., *Mechanism underlying the iron-dependent nuclear export of the iron-responsive transcription factor Aft1p in Saccharomyces cerevisiae.* Mol Biol Cell, 2007. 18(8): p. 2980-90.
76. Ojeda, L., et al., *Role of glutaredoxin-3 and glutaredoxin-4 in the iron regulation of the Aft1 transcriptional activator in Saccharomyces cerevisiae.* J Biol Chem, 2006. 281(26): p. 17661-9.

77. Pujol-Carrion, N., et al., *Glutaredoxins Grx3 and Grx4 regulate nuclear localisation of Aft1 and the oxidative stress response in Saccharomyces cerevisiae.* J Cell Sci, 2006. 119(Pt 21): p. 4554-64.
78. Kumanovics, A., et al., *Identification of FRA1 and FRA2 as genes involved in regulating the yeast iron regulon in response to decreased mitochondrial iron-sulfur cluster synthesis.* J Biol Chem, 2008. 283(16): p. 10276-86.
79. Li, H., et al., *The yeast iron regulatory proteins Grx3/4 and Fra2 form heterodimeric complexes containing a [2Fe-2S] cluster with cysteinyl and histidyl ligation.* Biochemistry, 2009. 48(40): p. 9569-81.
80. Kispal, G., et al., *Biogenesis of cytosolic ribosomes requires the essential iron-sulphur protein Rli1p and mitochondria.* EMBO J, 2005. 24(3): p. 589-98.
81. Rudolf, J., et al., *The DNA repair helicases XPD and FancJ have essential iron-sulfur domains.* Mol Cell, 2006. 23(6): p. 801-8.
82. Netz, D.J., et al., *Eukaryotic DNA polymerases require an iron-sulfur cluster for the formation of active complexes.* Nat Chem Biol, 2012. 8(1): p. 125-32.
83. Rouault, T.A. and W.H. Tong, *Iron-sulfur cluster biogenesis and human disease.* Trends Genet, 2008. 24(8): p. 398-407.
84. Foury, F. and T. Roganti, *Deletion of the mitochondrial carrier genes MRS3 and MRS4 suppresses mitochondrial iron accumulation in a yeast frataxin-deficient strain.* J Biol Chem, 2002. 277(27): p. 24475-83.
85. Li, H., et al., *Oligomeric yeast frataxin drives assembly of core machinery for mitochondrial iron-sulfur cluster synthesis.* J Biol Chem, 2009. 284(33): p. 21971-80.
86. Yoon, H., et al., *Turning Saccharomyces cerevisiae into a Frataxin-Independent Organism.* PLoS Genet, 2015. 11(5): p. e1005135.
87. Tedesco, A.C., L. Martinez, and S. Gonzalez, *Photochemistry and photobiology of actinic erythema: defensive and reparative cutaneous mechanisms.* Braz J Med Biol Res, 1997. 30(5): p. 561-75.
88. Hampton, M.B., B. Fadeel, and S. Orrenius, *Redox regulation of the caspases during apoptosis.* Ann N Y Acad Sci, 1998. 854: p. 328-35.
89. Videla, L.A., et al., *Oxidative stress-mediated hepatotoxicity of iron and copper: role of Kupffer cells.* Biometals, 2003. 16(1): p. 103-11.
90. Pietrangelo, A., *Iron-induced oxidant stress in alcoholic liver fibrogenesis.* Alcohol, 2003. 30(2): p. 121-9.
91. Wu, G., et al., *Glutathione metabolism and its implications for health.* J Nutr, 2004. 134(3): p. 489-92.
92. Parola, M. and G. Robino, *Oxidative stress-related molecules and liver fibrosis.* J Hepatol, 2001. 35(2): p. 297-306.
93. Sies, H., *Oxidative stress: from basic research to clinical application.* Am J Med, 1991. 91(3C): p. 31S-38S.
94. Yadav, A.S. and D. Bhatnagar, *Inhibition of iron induced lipid peroxidation and antioxidant activity of Indian spices and Acacia in vitro.* Plant Foods Hum Nutr, 2010. 65(1): p. 18-24.
95. Britton, R.S., K.L. Leicester, and B.R. Bacon, *Iron toxicity and chelation therapy.* Int J Hematol, 2002. 76(3): p. 219-28.
96. Bacon, B.R. and R.S. Britton, *The pathology of hepatic iron overload: a free radical--mediated process?* Hepatology, 1990. 11(1): p. 127-37.

97. Ramm, G.A. and R.G. Ruddell, *Hepatotoxicity of iron overload: mechanisms of iron-induced hepatic fibrogenesis.* Semin Liver Dis, 2005. 25(4): p. 433-49.
98. Reinders, J., et al., *Toward the complete yeast mitochondrial proteome: multidimensional separation techniques for mitochondrial proteomics.* J Proteome Res, 2006. **5**(7): p. 1543-54.

Chapter 2
Characterization of Fre5 as an iron reductase

Abstract

Iron is an essential element for eukaryotes. The iron co-factors, heme and iron sulfur clusters are synthesized in mitochondria. Inadequate iron trafficking to mitochondria is lethal due to the requirement for iron sulfur clusters in ribosome assembly. *FRE5* is part of a family of nine homologous genes involved or predicted to be involved in iron uptake. Fre5 is found in mitochondria. Our results show a heme synthesis defect in *FRE5* null cells in both whole cell level and mitochondrial level compared with wild type. This defect could be reversed by adding more iron into media, suggesting Fre5 is involved in iron transport in yeast. We also found iron defect in *FRE5* null cells mitochondrial level compared with *FRE5* overexpression cells. Based on the H_2O_2 resistance phenotype of *fre5* deletion cells, we performed the genetic screen to reverse the phenotype, some candidates were found, which will give us some guidance what genes are involved in the *FRE5* pathway. We propose a hypothesis based on our data that Fre5 is an iron reductase, this reductase activity create redox cycling and therefore increases potential for Fenton chemistry and damage.

Introduction

Yeasts require iron to complete their life cycle. Iron is an essential transition metal for several important cellular processes, such as respiration and ribosome biosynthesis [1, 2]. In mitochondria, Fe is essential for the synthesis of heme and iron sulfur cluster [3, 4]. Iron homeostasis must be tightly regulated, limiting the supply of iron to mitochondria impairs the metabolic and respiratory activities. On the other hand, excess iron is toxic by generating reactive oxygen species. Free iron ions might be particularly harmful to mitochondria, because free reactive oxygen species are generated as a side reaction of electron transport [5]. Even mild iron

insufficiency can lead to heme synthesis defects that can impair metabolic activities. Mrs3 and Mrs4 serve as high affinity transporters of iron but do not constitute the full set of proteins involved [6]. In fact the mechanisms of iron transport to mitochondria are very poorly understood.

Although iron is abundant in the environment, it is not easily available, as it is mainly present as oxidized forms which are poorly soluble. While iron is present as ferric in the environment the majority of intracellular iron is in the reduced state. An intracellular eukaryotic siderophore has been identified, suggesting a portion of the intracellular iron is ferric [7]. The uptake, transport and storage/recycling of iron is extremely important for normal growth of yeasts. Yeasts have developed several iron transporters as well as iron reductases to achieve to goal. Based on amino acid sequence similarity, the *Saccharomyces cerevisiae* genome contains nine open reading frames (ORFs) of iron/copper reductase-related genes, which are YLR214w (*FRE1*), YLK220c (*FRE2*), YOR381w (*FRE3*), YNR060w (*FRE4*), YOR384w (*FRE5*), YLL051c (*FRE6*), YOL152w (*FRE7*), YGL160w (*FRE8*) and YLR047c (*FRE9*). *FRE1* and *FRE2* are the first studied and identified genes in this family [8]. *FRE1* encodes a plasma membrane ferric/cupric reductase and its expression is regulated by iron and copper levels via Aft1 and Mac1, *FRE2* encodes a plasma membrane ferric reductase and its expression is regulated by copper level via Aft1.

Based on bioinformatics studies, these nine ORFs fall into three categories:

1. Mainly *FRE3* and *FRE4*, significantly *FRE5* and *FRE6* exhibit higher similarity to the *FRE2* amino acid sequence;

2. *FRE1* and *FRE7* are similarly distant from all other members;

3. YGL160w and YLR047c are the most distantly related ORFs to all other members but they are more similar to each other.

All these ORFs encode for proteins that should contain transmembrane domains and except *FRE7*, YGL160w and YLR047c, all the other members contain a 17-20 residue N-terminal potentially cleavable signal peptide. A ferric reductase function has been shown for Fre1-Fre4 [1]. All members contain binding sites for the FAD co-factor and NADPH [9]. Fre1 has been shown to be a heme-containing protein, there are four conserved histidine residues responsible for coordinating the two heme groups [10]. These histidines are conserved in all FRE members, however not all contain a heme group, for example, Fre2 [11]. All members contain several (6-11) potential N-glycosylation sites. Finally, a possible vacuolar targeting motif (KLPN) exists in YLR047c sequence. *FRE* family expression in different iron/copper conditions suggests that *FRE2*, *FRE*3, *FRE*4, *FRE*5 and *FRE*6 are iron dependent metalloreductases. These genes are transcriptionally induced by the absence of iron via Aft1. Also, they are weakly induced by the absence of copper if *MAC1* (the copper dependent transcription factor) is deleted. This group can be subdivided into the *FRE2* and *FRE3* gene class, which is highly reducible by iron depletion, and the *FRE4*, *FRE5* and *FRE6* gene class, which is only moderately induced.

FRE1 and *FRE7* are copper-dependent genes. These genes are induced by the absence of copper via Mac1. *FRE1* is also moderately induced by iron depletion via Aft1, whereas *FRE7* is not. YGL160w and YLR047c are not inducible by either iron or copper concentration changes.

In the FRE family, Fre1 and Fre2 are the major cell-surface iron reductases, Fre3, which is a plasma membrane protein, can also reduce iron bound to ferrichrome, triacetylfusarinine C, or rhodotorulic acid, but not enterobactin. Fre1 and Fre2 can reduce enterobactin-iron. Fre4 can reduce rhodotorulic acid-iron at high concentrations [12]. Fre6 is found in the vacuole, and is required for the mobilization of iron in the vacuole [13]. YGL160w is found in the endoplasmic

reticulum, and is a putative NADPH oxidase [14]. The location of Fre5 is not verified, however it has been reported in the mitochondria [15].

This chapter describe the deletion and characterization of the putative mitochondrial iron reductase Fre5 gene in strain BY4741. Our results suggest that *FRE5* null strain generates iron-related phenotypes and that Fre5 exhibits iron reductase activity. *FRE5* null strain also showed oxidative stress resistance phenotype, it might because the reductase activity creates redox cycling and therefore increases the potential for Fenton chemistry and damage.

Material and methods

Mitochondria extraction

Cells were grown in 1 L YPD or synthetic complete glucose media for 2 days to let them reach the optical density (OD) 600 nm to 2, then cells were harvested by centrifugation in a 50 ml VWR centrifuge tube at 4000 rpm for 5 min. Every 1g cells were treated with 4U lyticase in 15 ml 1.2 M sorbitol at 30 degree Celsius for 2 hours, then 35 ml 1.2 M sorbitol were added and centrifuged at 4000 rpm for 10 min to wash off lyticase. Small glass beads and 1.2 M sorbitol were added to a total volume of 15 ml, vortexed each one 30sec for at least 3 times. Kept the 50 ml VWR centrifuge tubes on ice when not use. 35 ml 1.2 M sorbitol added to the tube and centrifuged at 2500X for 10 min, the supernatant were poured to a new 50 ml VWR centrifuge tube. Pellet were repeated the same procedure for another time. Supernatant were centrifuged at 12000X for 20 min, discarded the supernatant, pellets were the cruel mitochondria. Cruel mitos were dissolved in 5 ml 1.2 M sorbitol and 10 ml 22% histodine were added to the bottom of the tube to make it appear two layers. Centrifuged at 12000X for 60 min, the purified mitochondria remained in the

middle layer. Drew out the middle layer with a 1 ml pippet and stored in -80 degree Celsius fridge for future use.

Determination of Iron reductase activity

Mixed 10 μL of PBS washed mitochondria with 90 μL 50 mM sodium citrate pH 6 containing 5% glucose supplemented with 1mM $FeCl_3$ and 1 mM bathophenanthrolinedisulfonate (BPS). Incubated the mixture for 5 min at 30 ℃. The reduction of iron was measured by the formation of the colored Fe (II)-BPS complex and the change in absorbance at 520 nm were monitored [16]. Reductase activity was normalized with protein concentration determined from Bradford optical measurements of culture turbidity [17].

Oxygen consumption assay

Oxygen consumption assay were performed on a YSI 5300A Biological Oxygen Monitor. Cells were grown to mid-exponential phase, washed with PBS 7.0 for three times then diluted ten times in PBS. The rate of oxygen consumption of each strain was calculated based on the linear portion. Each strain was assayed repeatedly three times to get the average rate.

Serial dilution growth test

Cells were grown in 5 ml YPD or synthetic complete glucose media to mid-exponential phase. 200 ul of the culture were transferred into a 96 well plate and dilute in sterilized deionized water as a 1:10 dilution for 5 times, each with a total volume of 200 ul. Then multichannel pippet were used to drop 5 ul of each dilution sample onto YPD or synthetic complete glucose plate media with different conditions to test for growth.

Determination of total iron in whole cell and in mitochondria by inductively-coupled plasma optical emission spectroscopy (ICP-OES)

Cells were grown to exponential phase, spun down the cells and mixed with 150 uL nitric acid, or 100 ug purified mitochondrial lysate were mixed with 150 uL nitric acid, incubated at 90 ℃ for 30 min. Briefly centrifuged, added 450 uL milliQ water. Each sample was repeated with at least with three replicates.

Phenotypes of *fre5* deletion cells compared with WT

Wild type BY4741 and *fre5Δ* cells were grown to exponential phase and diluted ten times and then spotted onto YPD plate, YPLG plate, SCLG plate, SCD containing different concentration of bathophenanthrolinedisulfonate (BPS) from 10 uM to 400 uM, SCD without biotin containing different concentration of BPS from 10 uM to 400 uM, SCD containing different concentration of H_2O_2 from 1 mM to 4 mM, SCD containing different concentration of CCCP from 5 uM to 20 uM, SCD containing different concentration of copper from 1 mM to 3 mM. The phenotype of *fre5*Δ were tested by drop test.

Measurement of heme concentration in the whole cells/mitochondria

5mL cells were grown in YPD (or synthetic complete media) culture overnight to reach an OD of 1-2, cells were collected by centrifugation. Premixed 560uL Acetone and 41uL concentrated HCl were added to pellet then vortexed for 1min. The supernatant were transfer to a new 1.5mL centrifuge tube, added 600uL 50% acetonitrile, 1uL formic acid , and 60-80uL NH_4OH to adjust pH in 3-4. Then loaded liquid sample onto HPLC with a 25 cm x 4.6 mm C18 column. Heme were eluted at a flow rate of 1ml/min using 30% acetonitrile at the beginning 5 min, followed by a 50-

100% linear acetonitrile gradient over the subsequent 25 min. The acetonitrile solutions contained 0.05% trifluoroacetic acid (TFA). The elution of heme compounds was monitored at 400nm for Soret band and the heme peak comes off around 15 min. The heme test procedure for isolated mitochondria by HPLC was the same as whole cells.

Concentration measurement of protoporphyrin IX in the whole cells

Sample preparation method was the same with heme extraction described as above. Scan sample by fluorescence spectrometer from 500 nm to 700 nm, protoporphyrin IX would appear as a peak around 620 nm.

Concentration measurement of ergosterol in the whole cells

Yeast cells were grown in 100 ml YPD medium overnight to reach mid-log phase, centrifuged to collect cells using 50 ml VWR centrifuge tubes, discarded the supernatant. Added 3 ml methanol, 2 ml 0.5% pyrogallol, 2 ml 60% KOH. Vortexed gently to mix. Placed tubes in 90℃ water bath and left for 2h. Samples were removed from water bath and allowed to cool. Sample then extracted with 15 ml heptane, centrifuged at 1000X for 5 min to facilitate phase separation. Scaned the absorbance of extraction samples by spectrometer from 180 nm- 320 nm. The four peak area represented the amount of ergosterol in cells.

Construction of *FRE5* complement cells and reverse phenotypes

Genomic DNA were extracted from WT BY4741, PCR the *FRE5* gene from WT strain BY4741 genomic DNA with 200bp upstream base pair. TA cloned the PCR product of *FRE5* into pGEM-T easy vector and transformed into *E.coli*. Extracted pGEM-T easy plasmid from *E.coli*

and digested with NotI and run agarose gel to separate PCR product from vector, cut the *FRE5* PCR product band from agarose gel and purified with QIAquick Gel Extraction Kit. Digested plasmid pRS423 with NotI and ligated with *FRE5* PCR product. Transformed the ligated plasmid and pRS423 into WT and *fre5*Δ cells by electroporation. Grew the transformation cells on SCD-His plates. Grew the complement cells as well as cells with empty vector with WT and *fre5*Δ cells on different plates that showed phenotypes, complement cells showed reverse the phenotype but not the cells with empty vectors.

β -Galactosidase Assay

Multicopy plasmid contained *fet3::lacZ* fusion was obtained from Dr. Paul Cobine, transformed into WT BY4741 and *fre5*Δ cells by electroporation. Grew cells in YPD, YPD+500 mM $FeSO_4$, YPD+25 uM BPS, YPD+50 uM BPS, YPD+100 uM BPS to mid-log phase. Samples were collected, and β-galactosidase assay was performed using the substrateo-nitrophenyl-β-D-galactose as described [18]. Protein concentration was measured by Bradford method.

Reactive Oxygen Species Measurements of Mitochondrial Fractions

Ninety microliters of the mitochondrial fraction were mixed with 90 μL of a 10 μg/mL dihydroethidium (DHE) solution, 200 μM NADPH in an aluminum foil covered 1.5 mL Eppendorf tube. After a 15 min incubation in the dark at 28 ℃ measureed with an excitation wavelength of 485 nm and an emission wavelength of 595 nm.

Sequence Analysis

DNA and protein sequence information was obtained from the yeast databases: SGD (Saccharomyces Genome Database, http://www.yeastgenome.org). Additional sequence information was obtained from NCBI website (http://www.ncbi.nlm.nih.gov). Sequence analysis was also aligned by clustal omega (http://www.ebi.ac.uk/Tools/msa/clustalo/). A phylogenetic tree was generated from MABL website (http://www.phylogeny.fr). Muscle was used as alignment algorithm, the number of bootstrap was 500.

Genomic library preparation

The genomic library was prepared as described [19]. The plasmid pRS413 was restriction digested with EcoRV and treated with alkaline phosphatase (New England Biolabs). The *S. cerevisiae* BY4743 cell genomic DNA was partially restriction digested with EcoRV to give a maximum number of DNA fragments in the 3-10 kb size range. Then performed electrophoresis with these DNA fragments on an agarose gel, removed the DNA smear range from 3-10kb out of the gel and extracted with a gel extraction kit. The extracted genomic DNA fragments and the treated pRS413 vector were ligated with T4 DNA ligase (New England Biolabs) at 4 degree Celsius overnight. The ligation mixture was used to transform NEB 10-beta Competent Escherichia coli cells (High Efficiency) with electroporation method. The transformants were selected on LB plates with ampicillin. Then the transformants were scraped off with liquid LB medium and used to extract the genomic library plasmid with a Qiaprep Spin Miniprep Kit.

Genomic library Screening

The genome size (g) *of S. cerevisiae* is about 13.5Mb, The average gene size of *S. cerevisiae* is 1.5kb (most genes < 5kb; the longest < 10kb), and the genomic DNA was partially digested to average size of 6kb (3kb-10kb). The insert size (i) $=6X10^3$. Set the probability that any

point in the genome will occur at least once in the library (P) =99%, the number of colonies (N) needs to be screened is:

$$N = \frac{\ln(1-p)}{\ln(1-\frac{i}{g})} = \frac{\ln(1-99\%)}{\ln(1-\frac{6X10^3}{13.5X10^6})} = 10359$$

After extracting the genomic library plasmid, the S. cerevisiae BY4741 *FRE5* null strain was used as a recipient strain in complementation experiments with electroporation method. The transformants were first selected on synthetic complete glucose agar plates minus histidine (SCD-His). In order to have a high confident that our selection includes all genes in the genome, it was necessary to transform and collect enough transformants (10359) on the SCD-His plates according to the formula. Then, transferred the transformants from SCD-His plates to SCD-His+ H_2O_2 by replicating plates. Kept screening the extracted genomic library plasmid until the target genes were identified.

Results

Yeast Genome Codes for a Putative Iron Reductase: *FRE5*.

In a phylogenetic tree of the FRE family, *FRE1-FRE7* cluster together, *FRE8* and *FRE9* (*YNO1*) are distantly related to the other FRE genes (Fig. 2.1A). *FRE5* is very closely related to *FRE6*. Fre1, Fre2 and Fre6 are confirmed as ferric reductases [9, 13]. The common structural features of the FRE family include an N-terminal region made up of six or seven transmembrane helices, two of which contain two strictly conserved histidine residues responsible for coordinating two b-type heme groups [14], which are likely situated one above the other within the membrane and vertical to the plane of the membrane (Figure 2.1C). It is worth noting that the presence of this histidine motif does not necessarily mean the activity requires heme, such as observed in Fre2 [4].

The C-terminal soluble domain contains binding sites for FAD, NADPH and oxidoreductase sequence motifs. Position-specific iterated homology analyses with the sequence of Fre1 and Fre2 against Fre5 showed that all features could be found in Fre5. In Figure 2.1B, four conservative histidine residues could be found between 300 and 400 amino acids. FAD, NADPH and oxidoreductase sequence motifs are highlighted in the boxes. *FRE5* has 25.04% identity compared with *FRE1* and 38.15% identity compared with *FRE2* (Figure 2.1D). Figure 2.1E gives a visualization of a predicted Fre5 structure. The predicted localization of this protein was mitochondria and subsequently Fre5 has been found in the mitochondrial proteome [8].

A

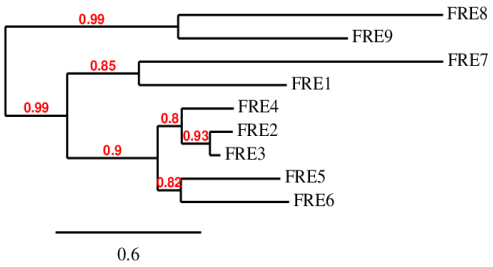

B

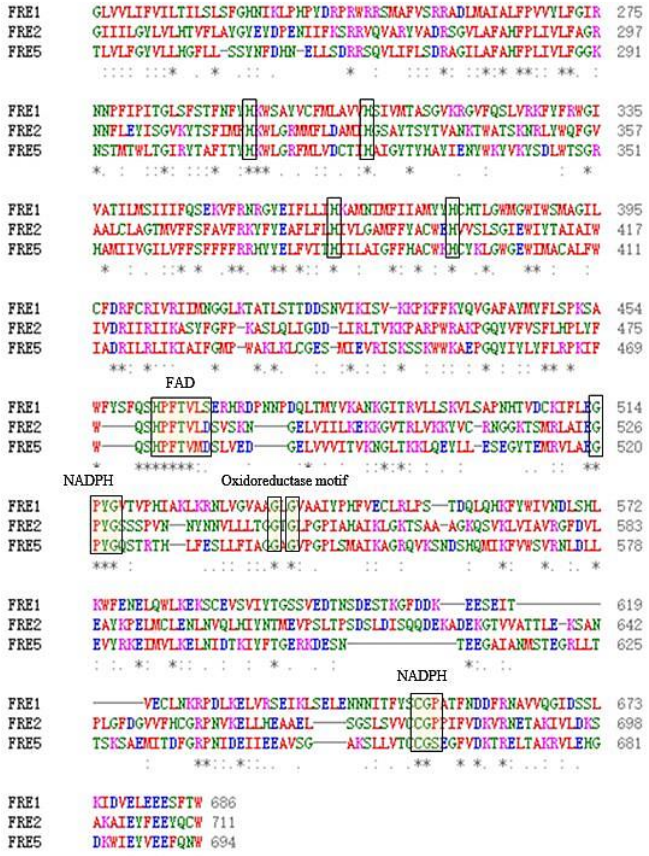

C

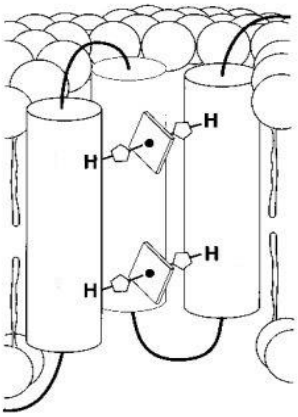

D

Percent Identity Matrix

	FRE1	FRE2	FRE5
1: FRE1	100.00	24.92	25.04
2: FRE2	24.92	100.00	38.15
3: FRE5	25.04	38.15	100.00

E

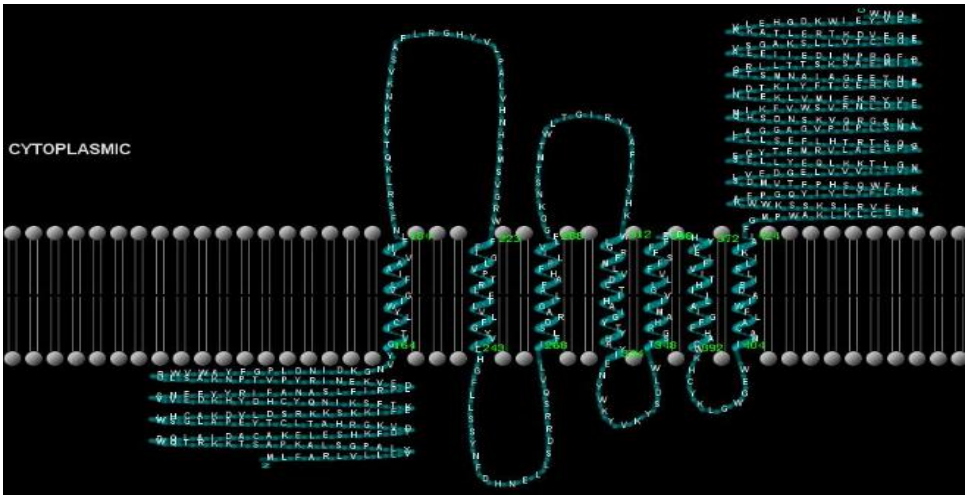

Figure 2.1 Bioinformatic predictions for *FRE5* (YOR384W).

(A) Phylogenetic tree of FRE family. Tree was generated by MABL website (http://www.phylogeny.fr) using the nine homologs within this protein superfamily. *FRE1* and *FRE7* are closely related, whereas *FRE8* and *FRE9* (*YNO1*) clustered together and are distantly related to all other *FRE* proteins. *FRE5* and *FRE6* appear to share a common ancestor. (B) Alignment of Fre1, Fre2 and Fre5. The Fre1, Fre2 and Fre5 amino acid sequences were aligned by using the clustal omega (http://www.ebi.ac.uk/Tools/msa/clustalo/). * indicates conserve amino acids among them. (C) Structural model of stacked intramembranous histidines coordinating two hemes. Membrane is portrayed as two layers of circles with tails to indicate the phospholipid bilayer. Cylinders represent three consecutive transmembrane α helices. Hemes shown as squares contain a hexacoordinate iron (black dots) [10]. (D) Percentage of amino acid residue identity between *FRE1*, *FRE2* and *FRE5*, calculated by clustal omega. (E) Prediction structure for Fre5 obtained from uniport (http://www.uniprot.org/uniprot/Q08908). Seven transmembrane helices are shown. The signal peptides locate in the matrix, and the FAD and NAD(P)H binding regions are in the cytosol.

Fre5 Functions as a Ferric Reductase.

To test if Fre5 exhibits ferric reductase activity, we determined total iron in strains overexpressing *FRE5* and compared the results with controls carrying the empty vector (Figure 2.2). Mitochondria were extracted from mid-exponential grown cells of wild type BY4741 and *FRE5* null strain, then ICP-OES were used to obtain total iron from the sample. The results showed wild type BY4741 and *FRE5* null strain contain similar level of total iron. However, overexpressing of *FRE5* clearly led to a significant accumulation of iron in the mitochondria.

Iron reductase activity were assayed with mitochondria from strain overexpression of *FRE5* and *FRE5* null. The overexpression of *FRE5* was associated with an increase in the mitochondrial capacity to reduce ferric iron (Figure 2.3). To test whether the activity is due to a reductase, several negative controls were used to check the activities. One negative control was pure mitochondria mixed with bathophenanthrolinedisulfonate (BPS) but without addition of $FeCl_3$, the other one was addition of $FeCl_3$ and BPS only without mitochondria. BPS used as a ferrous iron chelator. As shown in the Figure 2.3, all the negative controls confirmed the specificity of the reductase activities.

Taken together, the iron reductase activity measurements, iron uptake data, phylogenetic tree construction, and the transcriptional regulation by Aft1 support a ferric reductase function for Fre5.

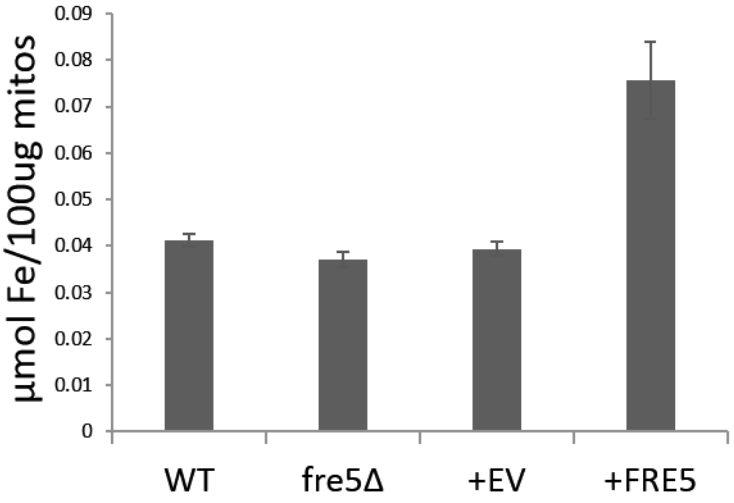

Figure 2.2 Total mitochondrial iron measured by ICP.

Total iron concentrations were significantly increased when the *FRE5* overexpressing strain was compared with the BY4741 WT strain.

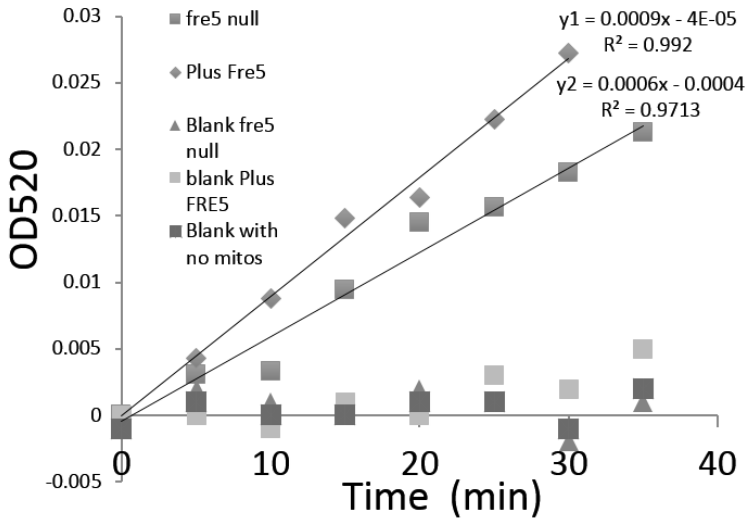

Figure 2.3 Determination of ferric reductase activity in yeast mitochondria.

Ferric reductase activities of mitochondria of strain overexpressing *FRE5* and *FRE5* null were measured. Absorption was normalized by subtraction of blanks. Upper curves were obtained with the overexpression strain (diamond) and the deletion strain (square), respectively, and the overexpression strain is clearly having higher activities. Lower blank curves were obtained by leaving out mitochondria, adding only mitochondria of strain overexpressing *FRE5* or mitochondria being deleted for *FRE5*.

Deletion of *FRE5* causes heme defect.

In mitochondria, iron is required for heme and iron sulfur cluster assembly. Severe defects in iron assimilation would be lethal under aerobic conditions as iron sulfur cluster and heme are required. The *FRE5* null strain grew the same as wild type in aerobic condition by serial dilution growth test (Figure 2.4A). However, the *FRE5* null strain showed a defect in oxygen consumption compared with WT (Figure 2.4B). This phenotype suggested *FRE5* was related with defects in heme and/or iron sulfur cluster assembly, but this defect is not severe enough to be lethal.

Heme concentration was tested in whole cells and in mitochondria (Figure 2.5). After extraction in acid-acetone and reverse phase chromatography an absorbance (at 405 nm to detect the Soret band of heme) peak around 15 min was identified as heme B (as has been seen previously report [20]). A comparison of peak areas in WT sample and *FRE5* null, showed *FRE5* null strain has heme synthesis defect in whole cell as well as mitochondrial by four folds. This heme defect caused by a deletion of *FRE5* could be reversed by overexpression of *FRE5* or by adding ferrous iron into the media (Figure 2.5D), suggesting that the heme synthesis defect was caused by decreased bioavailability of iron in the *FRE5* null strain.

To test if there was also an Fe-S cluster assembly defect we transformed the WT BY4741 and *FRE5* null strains with a vector contains *FET3-LacZ* fusion gene. The expression of *FET3* is tightly regulated by iron global regulator Aft1. Aft1 regulates *FET3* by sensing the concentration of iron sulfur cluster in cell. If the concentration of Fe-S cluster is low, Aft1 upregulates the expression of *FET3*, if the concentration of Fe-S cluster is high Aft1 downregulates the expression of *FET3*. Measuring the expression of FET3 using β-gal assay is an indirect measure of the concentration of Fe-S cluster assembly in mitochondria. We compared the expression level of *FET3* in WT BY4741 and *FRE5* null strain under different iron concentrations by adding exogenous ferrous iron or the iron-chelator bathophenathroline sulfate (BPS) to deplete available iron in the medium. Figure 2.6 showed with different iron concentrations *FRE5* null strain and WT BY4741 have similar *FET3* expression pattern, indicates there is no significant Fe-S cluster assembly defect in *FRE5* null strain.

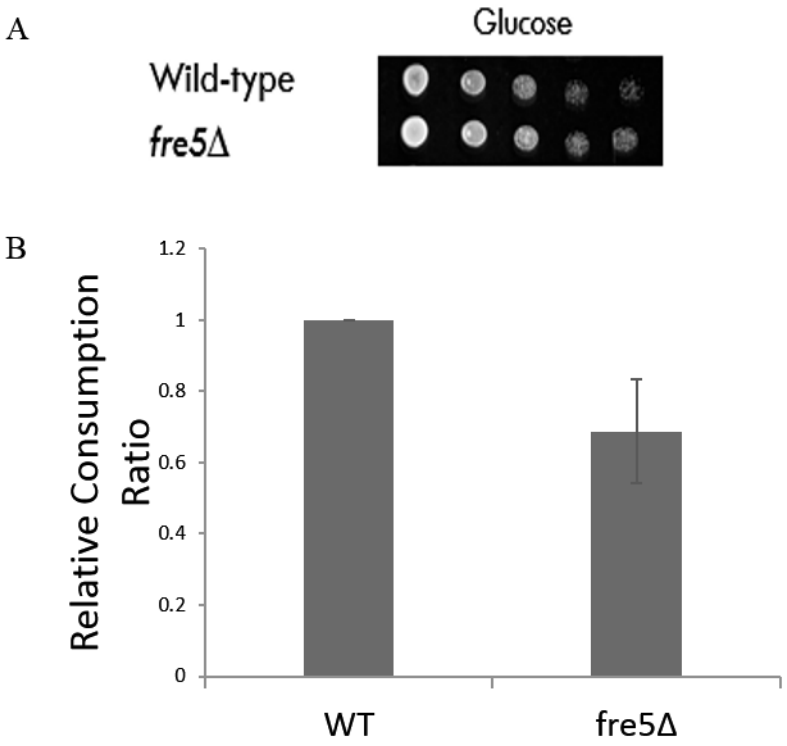

Figure 2.4 Global phenotype of FRE5 null strain.

(A) Serial dilution growth test of WT and *FRE5* null strain on synthetic complete glucose media plate. (B) Oxygen consumption test of WT and *FRE5* null strain. The *FRE5* null strain showed a ¼ defect in oxygen consumption compared with WT.

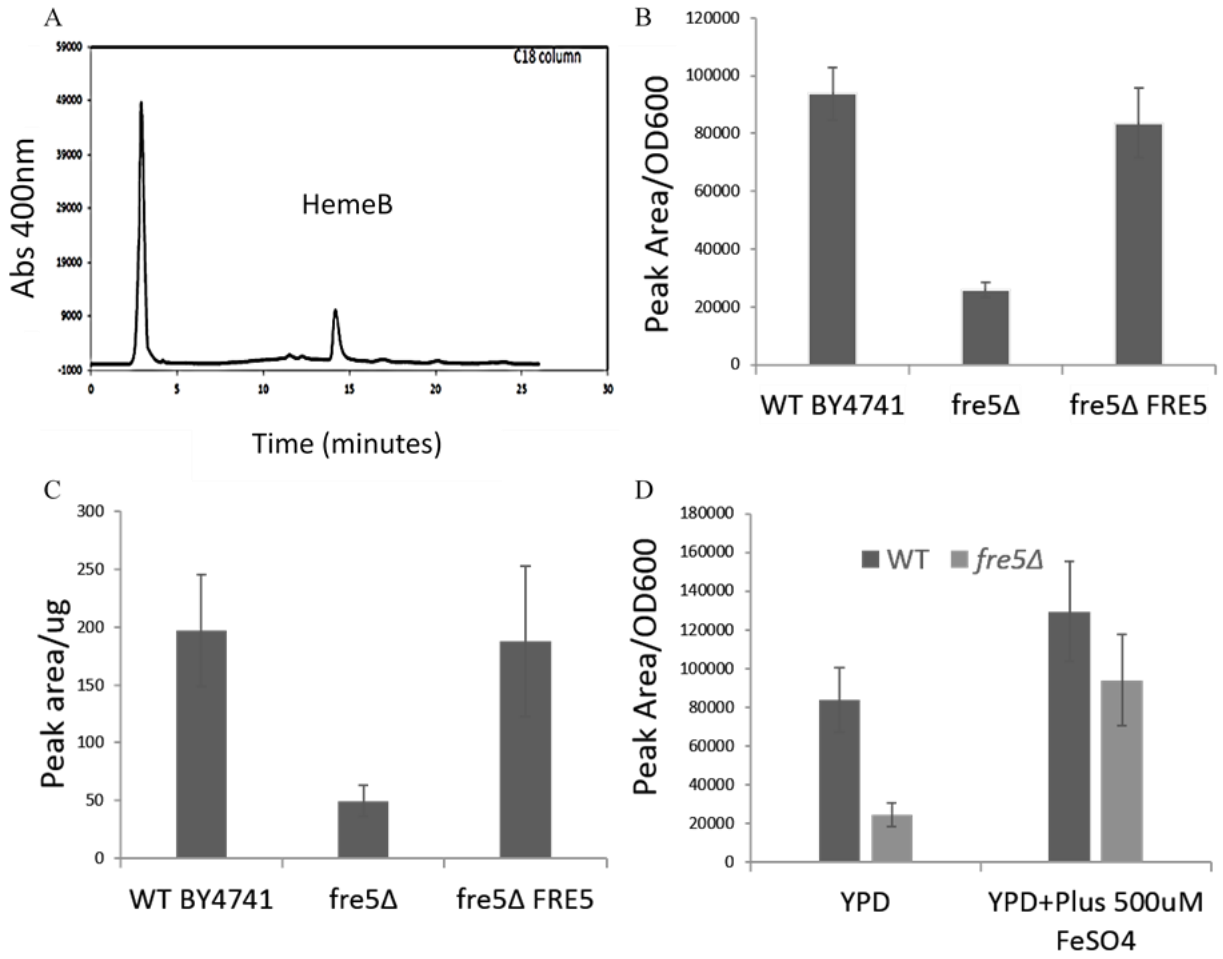

Figure 2.5 Heme defect phenotype of *FRE5* null strain.

(A) Heme profile generated by HPLC. The peak around 15 min indicates the heme level in the sample. (B) Comparison of heme levels in the whole cells of WT BY4741, *FRE5* null and *FRE5* overexpression strains. Heme level was normalized with total cell numbers determined from optical measurements of culture turbidity. (C) Comparison of heme levels in mitochondria of WT BY4741, *FRE5* null and *FRE5* overexpression strains. Heme level was normalized with protein concentration determined from Bradford optical measurements of culture turbidity. (D) Heme level comparison of WT BY4741 and *FRE5* null strain by adding exogenous ferrous iron. Cells were grown in YPD media with and without addition of ferrous iron and then the heme levels in

each were compared. With addition of ferrous iron, *FRE5* null strain had a significant higher level of heme and did not show significant difference compared to WT BY4741 strain.

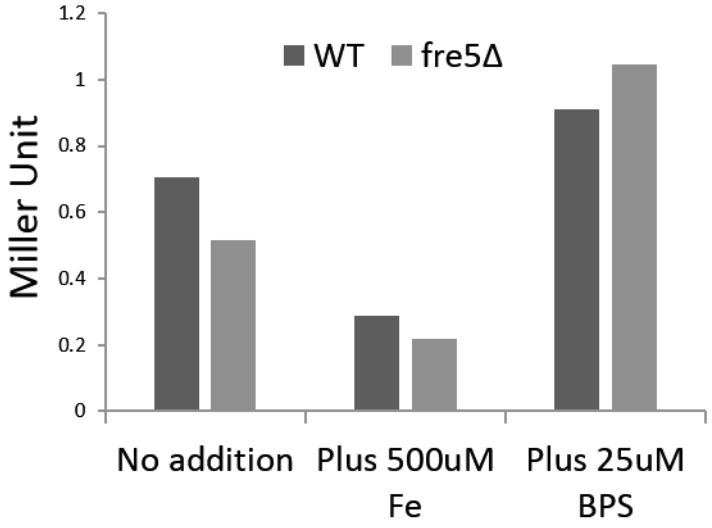

Figure 2.6 Relative Fe-S cluster Concentration test in different iron concentration.

Multicopy plasmid contained *fet3::lacZ* fusion were transformed in WT and fre5 null. Relative Fe-S cluster concentration as tested by the expression of FET3 by β-Galactosidase Assay in the media containing 500 uM FeSO4 or 25 uM BPS.

Other heme related phenotypes.

Mrs3 and Mrs4 are ferrous iron transporters in mitochondrial inner membrane from the mitochondrial carrier family (MCF) [21]. We found that the *MRS3* null strain showed a heme defect similar to the *FRE5* null strain. However, the *MRS4* null strain did not (Figure2.7A). This suggests that Mrs3 and Mrs4 may have separate roles in the iron import pathway in yeast mitochondria in this background.

In order to better understand the cause of the heme defect, several heme related phenotypes were tested. Iron is required to make heme at the final step of heme synthesis pathway. In this step, iron is inserted into protoporphyrin IX by ferrochelatase [3]. We assayed protoporphyrin IX

concentrations in *FRE5* null strain as well as MCF member null strains. Figure 2.7B showed *FRE5* null strain and *MRS3* null strain did not significantly accumulate protoporphyrin IX (PPIX) in their mitochondria compared with WT.

Ergosterol is a sterol found in yeast cell membranes, serving many of the same functions that cholesterol serves in animal cells. Ergosterol bio-synthesis is essential [22], and this biosynthesis pathway is regulated by heme proteins. Many enzymes involved in this pathway contain heme, like Erg1, Erg13, Erg3 [23]. In order to see if this heme defect would affect ergosterol, we examined the ergosterol concentrations in these strains. Figure 2.7C showed ergosterol biosynthesis is slightly perturbed in the *FRE5* null strain compared to WT. Although heme decreased four folds in these strains, it is still enough to maintain sufficient ergosterol biosynthesis.

Heme is also an important component of electron transport chain complexes. We examined the ubiquinol c oxido-reductase (complex III) and cytochrome c oxidase (complex IV) activities. Figure 2.7D showed *FRE5* null strain had a 10-20% defect in complex III activity compared with overexpression of *FRE5* strain. Figure 2.7E indicates *FRE5* null strain did not show any complex IV activity defect compared to WT.

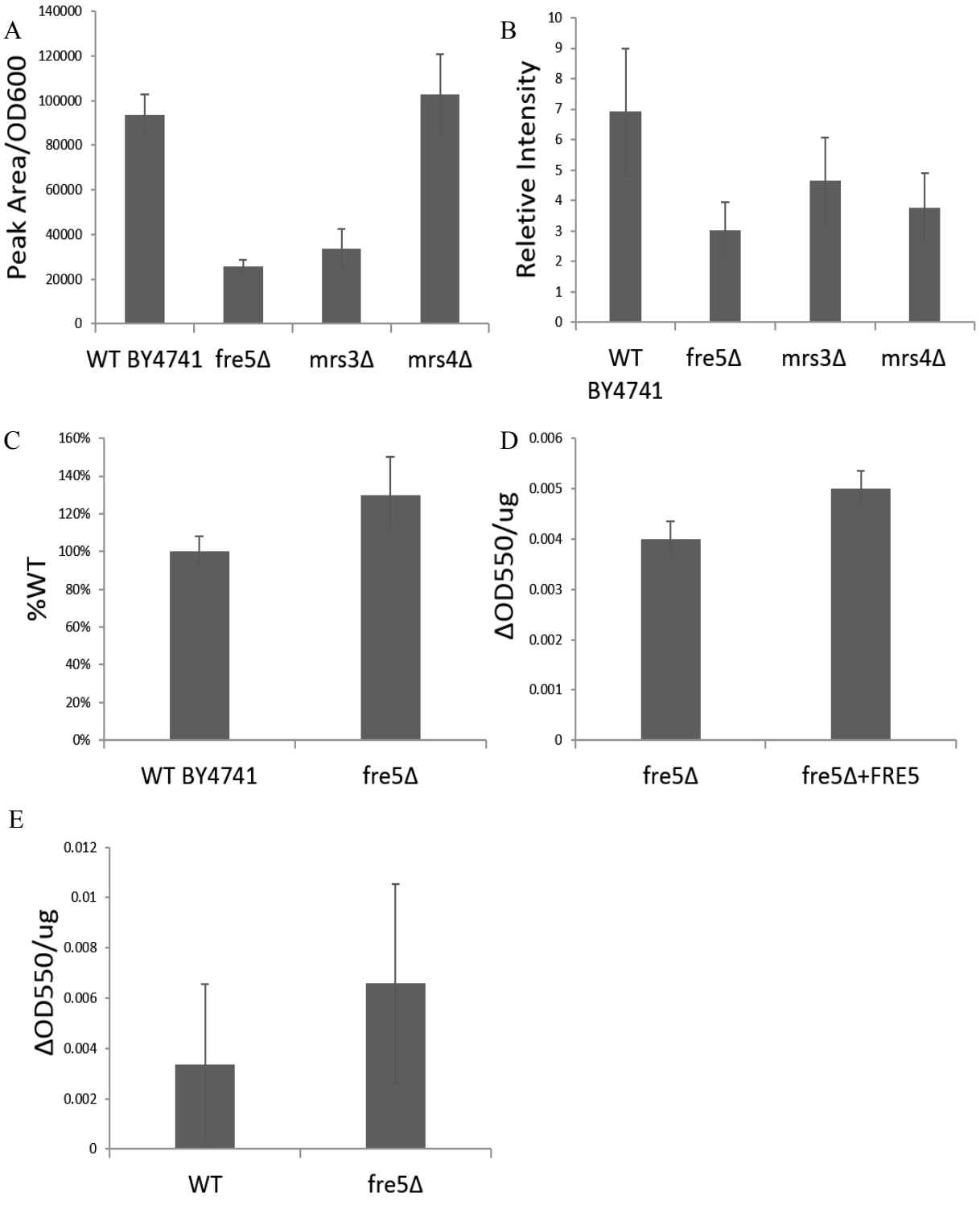
A
Peak Area/OD600
140000
120000
100000
80000
60000
40000
20000
0
WT BY4741
fre5Δ
mrs3Δ
mrs4Δ
B
Reletive Intensity
10
9
8
7
6
5
4
3
2
1
0
WT BY4741
fre5Δ
mrs3Δ
mrs4Δ
C
%WT
160%
140%
120%
100%
80%
60%
40%
20%
0%
WT BY4741
fre5Δ
D
ΔOD550/ug
0.006
0.005
0.004
0.003
0.002
0.001
0
fre5Δ
fre5Δ+FRE5
E
ΔOD550/ug
0.012
0.01
0.008
0.006
0.004
0.002
0
WT
fre5Δ

Figure 2.7 Heme defect related tests.

(A) Heme concentrations in different strains. (B) protoporphyrin IX concentrations in different strains. (C) Total ergosterol concentrations in WT and *FRE5* null strain. (D) Complex III activity assay. (E) Complex IV activity assay.

***FRE5* null strain is resistant to copper.**

Serial dilution growth tests were performed on the synthetic complete glucose plates with the addition of $FeSO_4$, BPS and $CuSO_4$. The *FRE5* null strain did not show a phenotype on either iron deplete or iron rich plates. However, the *FRE5* null strain exhibits a weak resistance to copper compared to WT BY4741 (Figure 2.8).

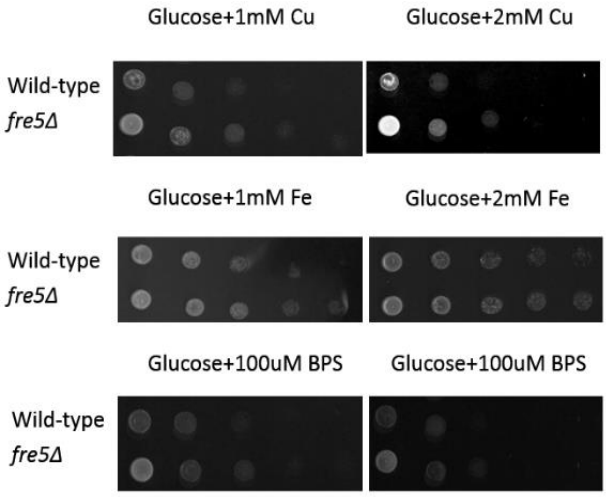

Figure 2.8 Growth test of WT BY4741 and *FRE5* null strain.

BY4741 and *FRE5* null strain were serial diluted and plated onto synthetic complete glucose plates containing different concentration of $FeSO_4$, BPS and $CuSO_4$. On $FeSO_4$ and BPS plates BY4741 and *FRE5* null strain showed same growth pattern. On $CuSO_4$ plates *FRE5* null strain showed resistance to copper compared to WT BY4741.

***FRE5* null strain is resistant to hydrogen peroxide.**

Mitochondria is the major source of superoxide production. To test for the possibility that the ferric reductase activity of Fre5 results in superoxide production, we performed oxidative stress tests.

The *FRE5* null strain was inoculated in YPD liquid media with the addition of different concentration of hydrogen peroxide, *FRE5* null strain showed resistance to H_2O_2 in liquid culture (Figure 2.9A) and on YPD+2.5 mM H_2O_2 plate (Figure 2.9B). To test if this oxidative stress resistance phenotype is specific to H_2O_2 we used the ionophore carbonyl cyanide m-chlorophenylhydrazone (CCCP) which reduces the ability of ATP synthase to function induces stress [24]. Cells grown in synthetic complete glucose media to mid-exponential phase, then transferred onto synthetic complete glucose plates containing different concentration of CCCP, then incubated for two days. Colony forming units were count on each plate. The *FRE5* null strain showed resistance to CCCP (Figure 2.9C) showing this oxidative stress resistance phenotype is not limited to H_2O_2. This oxidative stress resistance phenotype could be reversed by overexpression of *FRE5* in the cell and in fact Figure 2.9D suggests that overexpression of *FRE5* in WT BY4741 increased sensitivity to H_2O_2.

Dihydroethidium (DHE) was used to test for reactive oxygen species (ROS) level in cells. Membrane permeable DHE oxidized 2-electron by superoxide or hydrogen peroxide yields the fluorescent, DNA-binding membrane-impermeable compound ethidium [25, 26]. Figure 2.9E showed overexpression of *FRE5* strain contained higher level of ROS, which explained the oxidative stress resistance phenotype shown in the above experiments.

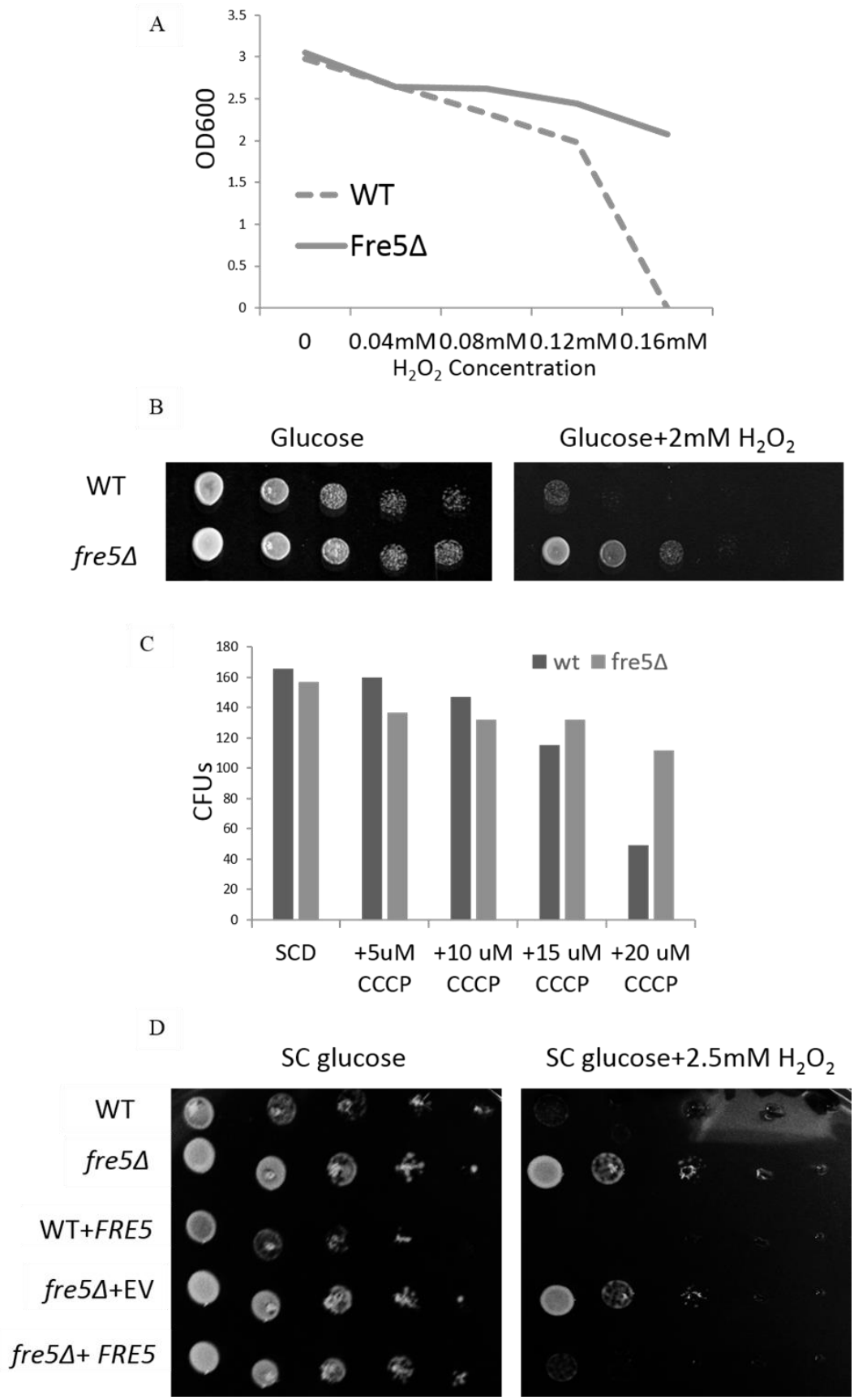
A
OD600
WT
Fre5Δ
0
0.04mM
0.08mM
0.12mM
0.16mM
H_2O_2 Concentration
B
Glucose
Glucose+2mM H_2O_2
WT
fre5Δ
C
wt
fre5Δ
CFUs
SCD
+5uM CCCP
+10 uM CCCP
+15 uM CCCP
+20 uM CCCP
D
SC glucose
SC glucose+2.5mM H_2O_2
WT
fre5Δ
WT+FRE5
fre5Δ+EV
fre5Δ+ FRE5

E

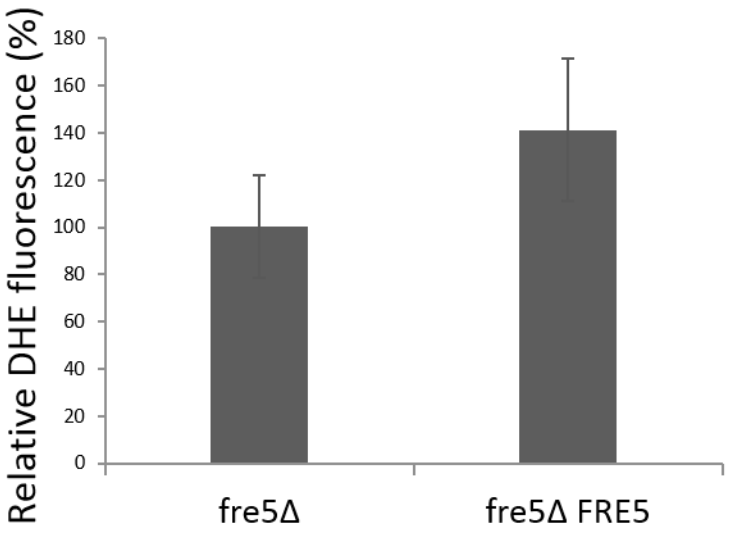

Figure 2.9 Resistance to oxidative stress of *FRE5* null strain.

(A) Growth comparison of WT BY4741 and *FRE5* null strain in different H_2O_2 concentrations. Cells were inoculated in YPD liquid media with addition of different H_2O_2 concentration. The OD at 600 nm were tested by spectrophotometer to obtain total cells in the culture. Black solid line represents the *FRE5* null strain, whereas a grey dash line represents WT. (B) Serial dilution growth test of WT BY4741 and *FRE5* null strain in synthetic complete glucose (SCD) plates with different H_2O_2 concentrations. (C) Colony forming units of WT BY4741 and the *FRE5* null strain in synthetic complete glucose (SCD) plates with different CCCP concentration. (D) Serial dilution growth test of WT BY4741, *FRE5* null strain, WT with overexpression of *FRE5* strain, *FRE5* null strain with empty vector and *FRE5* null strain with overexpression of *FRE5* in synthetic complete glucose (SC glucose) plates with different H_2O_2 concentrations. (E) ROS level in cells tested by DHE assay.

Oxidative stress resistance suppression screen.

The *FRE5* null strain exhibits a hydrogen peroxide resistance phenotype on synthetic complete glucose plate. To discover any other genes involved in the same pathway as *FRE5*, a low copy library was constructed from a BY4743 strain and was screened for candidates that have the ability to reverse the resistance to hydrogen peroxide. Twelve colonies were isolated that reversed the resistance; eight harbored vectors with *FRE5* contained within the insert as assessed by PCR. The other four vectors were sequenced; one was an empty vector (Can7), suggesting that the reversal of the phenotype was mediated by a spontaneous mutant. The other three were *TEX1* (Can4), *CAT8* (Can11) and *YHM2* (Can12). The candidates were retested on hydrogen peroxide plates in comparison to WT and *FRE5* null strain. The growth test suggests that *TEX1*, *CAT8* and *YHM2* can reverse the resistance phenotype of *FRE5* null strain.

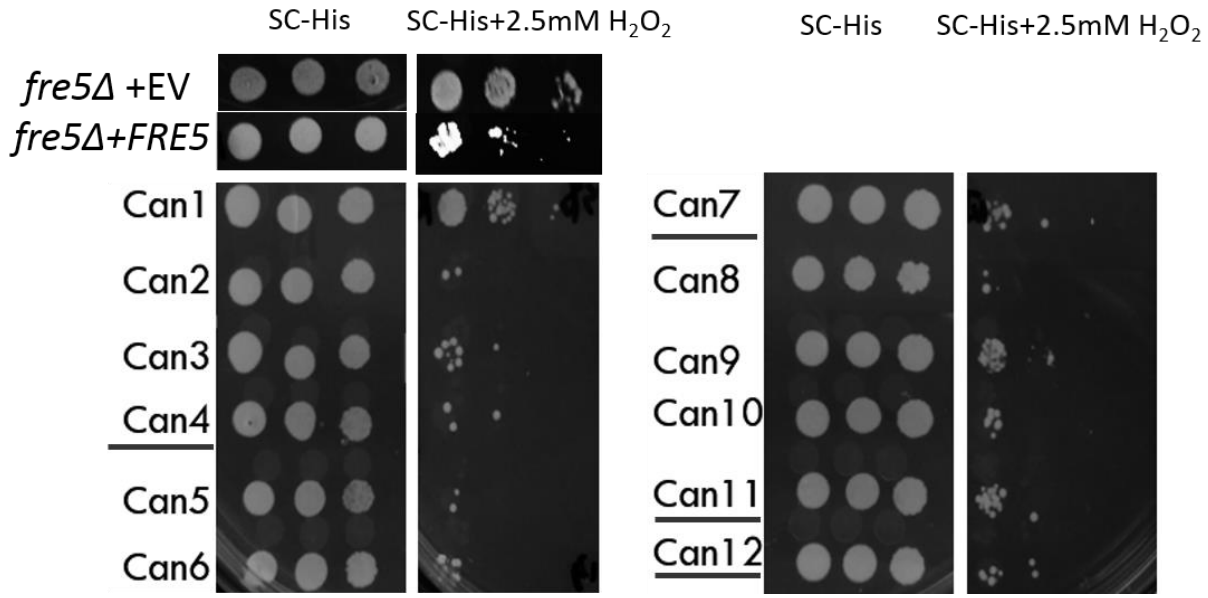

Figure 2.10 Serial dilution growth test of library screened candidates.

Can1-Can12 are twelve candidates selected from genomic library screening that could reverse the oxidative stress resistance phenotype of the *FRE5* null strain. Eight of them were verified as *FRE5*

by PCR, they are those not labelled with underlines. The other four were sequenced, Can7 was an empty vector mutant, Can4 turned out to be *TEX1*, Can11 was *CAT8* and Can12 was *YHM2*.

Deletion mutants array for oxidative stress resistance selection.

We screened the commercial yeast deletion collection to identify single mutants that exhibit the same oxidative stress resistance phenotype as *FRE5* null strain. We found nine candidates that showed increased hydrogen peroxide resistance compared to other single mutants (Table 2.1, Figure 2.11A). To winnow these candidates we tested for heme concentrations in each strain. *PTC6* null strain was found to have very low heme concentration (Figure 2.11B).

Candidate	Systematic Name	Standard Name
1	YNL273W	TOF1
2	YPR017C	DSS4
3	YNR015W	SMM1
4	YNR018W	RCF2
5	YBR025C	OLA1
6	YIL153W	YIL153W
7	YCR079W	PTC6
8	YBR106W	PHO88
9	YIR013C	GAT4

Table 2.1 Single deletion candidates of oxidative stress resistance.

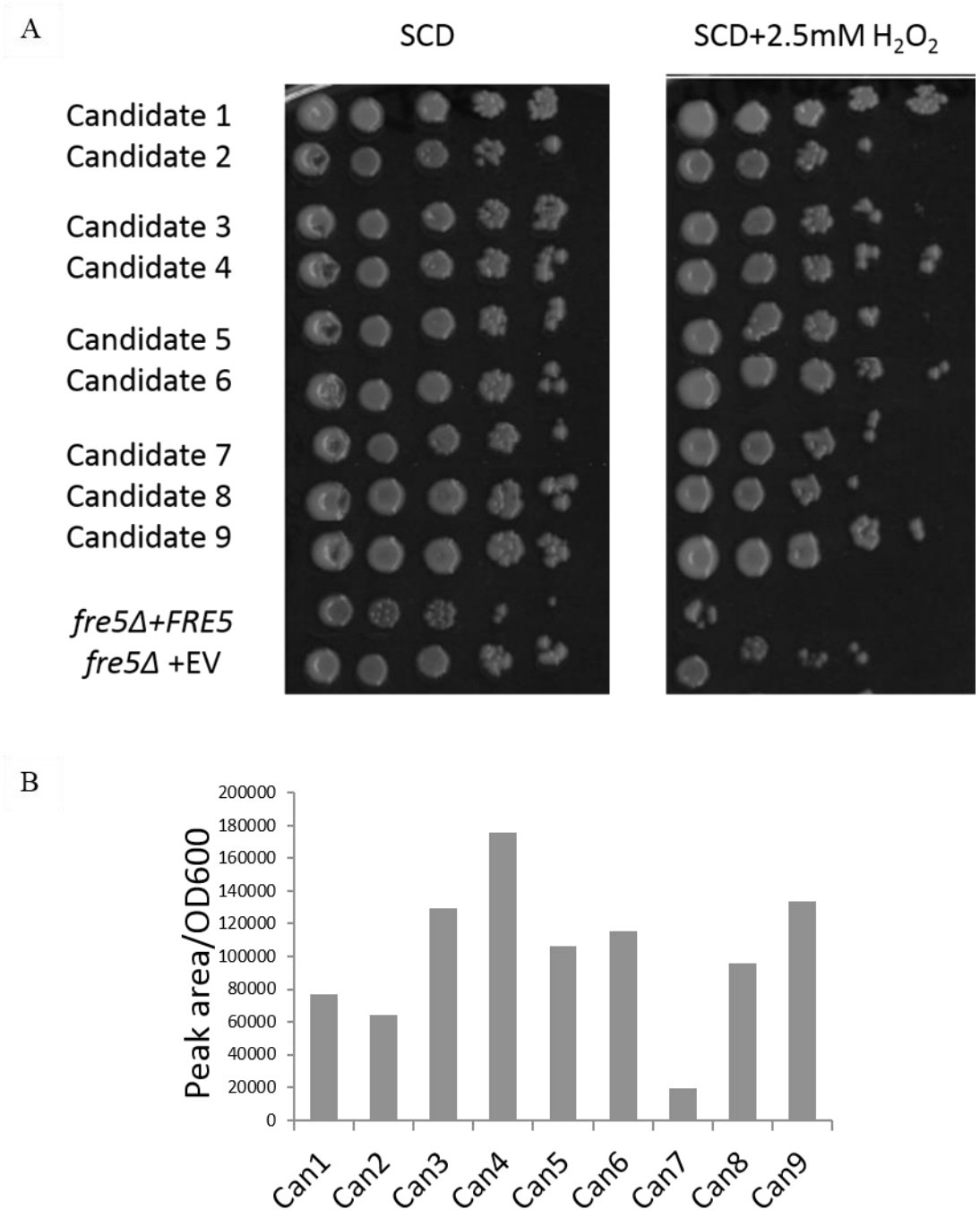

Figure 2.11 Single mutation candidates selected from H_2O_2 plate screen.

(A) Serial dilution growth test of candidates. *FRE5* null strain is a positive control and *FRE5* null with *FRE5* overexpression strain is a negative control. (B) Heme concentration test for Single deletion candidates. Can1-Can9 stand for candidate 1 through candidate 9.

Discussion

Fre5 is a putative iron reductase in the mitochondria. It is one of the nine FRE family proteins found in *Saccharomyces cerevisiae*. This is the first time Fre5 function has been investigated. From the bioinformatics research and previous transcriptional regulation data of Aft1 we found the expression of *FRE5* is regulated by Aft1, which is a global iron protein regulator. The structure of Fre5 shows same conservative motifs as other verified iron reductase, like Fre1 and Fre2. The direct measurement of iron reductase activity in mitochondria suggest expression of Fre5 mitochondria increases activity. However deletion does not completely eliminate reductase activity suggesting that alternative methods exist. The deletion mutant does have decreased iron availability as assayed by a heme defect and overexpression of *FRE5* increases the iron concentration in mitochondria. *FRE5* null has mild oxygen consumption defect related to decreases of 10-20% of complex III activity but not complex IV activity. In addition a small increase in ergosterol intermediates suggest a mild defect in the biosynthesis of ergosterol. Therefore this decreased heme concentration suggests a model where the minimum heme concentration for cell normal activities is much lower than normal concentration accumulated under conditions (Figure 2.12). Although the heme defect is obvious, it seems the iron homeostasis was not significantly affected, as the *FET3* expression was not altered. We could not generate iron defect phenotype in *FRE5* null strain by serial dilution growth tests. However we found a weak copper resistant phenotype in *FRE5* null strain. Free copper could generate ROS [27], since *FRE5* null strain exhibits oxidative stress resistance phenotype, it could show resistance to higher copper concentration for its ROS resistance capability. Free iron also generates ROS, but *FRE5* null strain failed to show more resistance to higher iron concentration. We did not observe iron sulfur cluster synthesis defect either, suggesting iron sulfur cluster biosynthesis is maintained in the *FRE5* null

strain, presumably due to the essential nature of Fe-S clusters for example in ribosome biosynthesis and DNA replication[2].

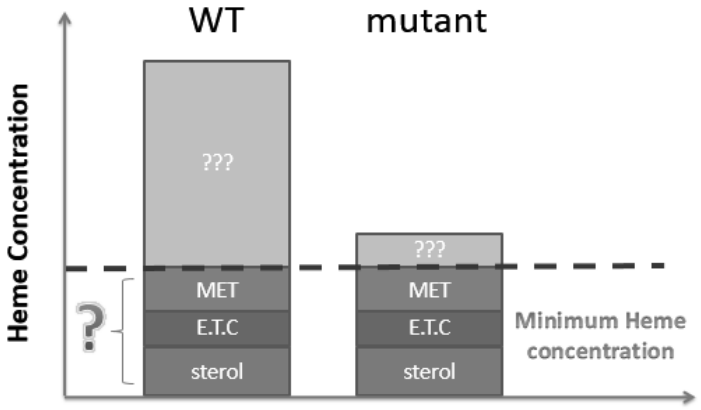

Figure 2.12 Heme model in yeast cells.

Heme distribution in yeast cell. The minimum requirement of heme in yeast cell includes the production of ergosterol, electron transport chain complex and metalloproteins. This minimum requirement is much lower than normal heme concentrations found in yeast cells. The specific level of this minimum requirement is unknown.

Yeast cells need heme for sterol synthesis, electron transport chain complexes synthesis and metalloprotein synthesis. Because yeast cells make many redundant heme, at a relative low heme concentration, cells still have enough heme to produce those components, there might be a minimum heme concentration for yeast cells to maintain regular bioactivities.

Mitochondria is a major source of superoxide production. Complexes I and III of the mitochondrial electron transport chain produce superoxide anions during normal respiration as a by-product. Superoxide is specifically produced in large part by complex III of the mitochondrial ETC [28]. The iron reductase and NADPH oxidase share similar conservative domains. They both contain six to seven transmembrane helices and require three different redox cofactors, namely

two tightly bound b-type hemes, FADH and NADPH [29]. Recently, YGL160w in FRE family was found as a putative NADPH oxidase [14]. The immediate product of NADPH oxidase enzymes is the superoxide radical anion, which then metabolized to other ROS molecules (peroxynitrite, H_2O_2, and hydroxyl radical) relevant for defense in the case of Nox2 [30]. Since they share the same conserved domains, it expected that they may act similar in some ways. Actually, Fre1 the plasma membrane ferric reductase has been shown to be capable of inefficient oxygen reduction [11].Study also showed the *FRE5* null strain overproduce glutathione, this might lead to oxidative stress resistance phenotype [31]. *FRE5* overexpression strain did show higher iron level in mitochondria, suggesting iron involved Fenton reaction might be the reason of decreased ROS level in *FRE5* null strain. Heme is also another cause of oxidative stress. When heme concentration is high, cell tends to produce more complex III, which produces ROS as a by-product. In other hand, heme itself acts as a prooxidant: it converts less reactive oxidants to highly reactive free radicals. Free heme has high affinity for different cell structures (membranes and DNA), triggering site-directed oxidative damage. When under higher ROS environment, higher heme may trigger more damage to cells [32].

By two different types of screening experiments, we found some candidates that could potentially be involved in the same pathway as Fre5. Tex1 is known as a protein involved in mRNA export, it is a component of the transcription export (TREX) complex [33]. Cat8 is a zinc cluster transcriptional activator [34], it is necessary for derepression of a variety of genes under non-fermentative growth conditions, like NADP-dependent cytosolic isocitrate dehydrogenase and lactate permease [35]. Yhm2 is a putative mitochondrial transport protein, known as exporting citrate from and importing oxoglutarate into mitochondria, causing net export of NADPH reducing equivalents [36]. None of the candidates were reported involving in redox pathways, however

Yhm2 showed transporter activities in mitochondria. Ptc6 is a mitochondrial type 2C protein phosphatase. This gene is involved in mitophagy and the null mutant is sensitive to rapamycin. Deletion of *PTC6* results in pyruvate dehydrogenase, phosphorylation of pyruvate dehydrogenase normally inactivates the enzyme [37]. The actual reason for them related in reversing *FRE5* null strain phenotype need further investigation.

Reference

1. Burger, G., et al., *Studies on the mechanism of electron transport in the bc1-segment of the respiratory chain in yeast. II. The binding of antimycin to mitochondrial particles and the function of two different binding sites.* Biochim Biophys Acta, 1975. 396(2): p. 187-201.
2. Kispal, G., et al., *Biogenesis of cytosolic ribosomes requires the essential iron-sulphur protein Rli1p and mitochondria.* EMBO J, 2005. 24(3): p. 589-98.
3. Krawiec, Z., A. Swiecilo, and T. Bilinski, *Heme synthesis in yeast does not require oxygen as an obligatory electron acceptor.* Acta Biochim Pol, 2000. 47(4): p. 1027-35.
4. Duby, G., et al., *A non-essential function for yeast frataxin in iron-sulfur cluster assembly.* Hum Mol Genet, 2002. 11(21): p. 2635-43.
5. Pan, Y., *Mitochondria, reactive oxygen species, and chronological aging: a message from yeast.* Exp Gerontol, 2011. 46(11): p. 847-52.
6. Zhang, Y., et al., *Mrs3p, Mrs4p, and frataxin provide iron for Fe-S cluster synthesis in mitochondria.* J Biol Chem, 2006. 281(32): p. 22493-502.
7. Haas, H., *Molecular genetics of fungal siderophore biosynthesis and uptake: the role of siderophores in iron uptake and storage.* Appl Microbiol Biotechnol, 2003. 62(4): p. 316-30.
8. Georgatsou, E. and D. Alexandraki, *Two distinctly regulated genes are required for ferric reduction, the first step of iron uptake in Saccharomyces cerevisiae.* Mol Cell Biol, 1994. 14(5): p. 3065-73.
9. Georgatsou, E. and D. Alexandraki, *Regulated expression of the Saccharomyces cerevisiae Fre1p/Fre2p Fe/Cu reductase related genes.* Yeast, 1999. 15(7): p. 573-84.
10. Finegold, A.A., et al., *Intramembrane bis-heme motif for transmembrane electron transport conserved in a yeast iron reductase and the human NADPH oxidase.* J Biol Chem, 1996. 271(49): p. 31021-4.
11. Lesuisse, E., M. Casteras-Simon, and P. Labbe, *Evidence for the Saccharomyces cerevisiae ferrireductase system being a multicomponent electron transport chain.* J Biol Chem, 1996. 271(23): p. 13578-83.
12. Yun, C.W., et al., *The role of the FRE family of plasma membrane reductases in the uptake of siderophore-iron in Saccharomyces cerevisiae.* J Biol Chem, 2001. 276(13): p. 10218-23.

13. Singh, A., N. Kaur, and D.J. Kosman, *The metalloreductase Fre6p in Fe-efflux from the yeast vacuole.* J Biol Chem, 2007. 282(39): p. 28619-26.
14. Rinnerthaler, M., et al., *Yno1p/Aim14p, a NADPH-oxidase ortholog, controls extramitochondrial reactive oxygen species generation, apoptosis, and actin cable formation in yeast.* Proc Natl Acad Sci U S A, 2012. 109(22): p. 8658-63.
15. Sickmann, A., et al., *The proteome of Saccharomyces cerevisiae mitochondria.* Proc Natl Acad Sci U S A, 2003. 100(23): p. 13207-12.
16. Wyman, S., et al., *Dcytb (Cybrd1) functions as both a ferric and a cupric reductase in vitro.* FEBS Lett, 2008. 582(13): p. 1901-6.
17. Bradford, M.M., *A rapid and sensitive method for the quantitation of microgram quantities of protein utilizing the principle of protein-dye binding.* Anal Biochem, 1976. 72: p. 248-54.
18. Rose, M. and D. Botstein, *Construction and use of gene fusions to lacZ (beta-galactosidase) that are expressed in yeast.* Methods Enzymol, 1983. 101: p. 167-80.
19. Rodrigues, F., et al., *Construction of a genomic library of the food spoilage yeast Zygosaccharomyces bailii and isolation of the beta-isopropylmalate dehydrogenase gene (ZbLEU2).* FEMS Yeast Res, 2001. 1(1): p. 67-71.
20. Pierrel, F., et al., *Coa1 links the Mss51 post-translational function to Cox1 cofactor insertion in cytochrome c oxidase assembly.* EMBO J, 2007. 26(20): p. 4335-46.
21. Foury, F. and T. Roganti, *Deletion of the mitochondrial carrier genes MRS3 and MRS4 suppresses mitochondrial iron accumulation in a yeast frataxin-deficient strain.* J Biol Chem, 2002. 277(27): p. 24475-83.
22. Weete, J.D., M. Abril, and M. Blackwell, *Phylogenetic distribution of fungal sterols.* PLoS One, 2010. 5(5): p. e10899.
23. Craven, R.J., J.C. Mallory, and R.A. Hand, *Regulation of iron homeostasis mediated by the heme-binding protein Dap1 (damage resistance protein 1) via the P450 protein Erg11/Cyp51*. J Biol Chem, 2007. 282(50): p. 36543-51.
24. Zhang, C.C., et al., *High level expression of full-length estrogen receptor in Escherichia coli is facilitated by the uncoupler of oxidative phosphorylation, CCCP*. J Steroid Biochem Mol Biol, 2000. 74(4): p. 169-78.
25. Benov, L., L. Sztejnberg, and I. Fridovich, *Critical evaluation of the use of hydroethidine as a measure of superoxide anion radical.* Free Radic Biol Med, 1998. 25(7): p. 826-31.
26. Papapostolou, I., N. Patsoukis, and C.D. Georgiou, *The fluorescence detection of superoxide radical using hydroethidine could be complicated by the presence of heme proteins.* Anal Biochem, 2004. 332(2): p. 290-8.
27. Brewer, G.J., *Copper toxicity in the general population.* Clin Neurophysiol, 2010. 121(4): p. 459-60.
28. Turrens, J.F., *Mitochondrial formation of reactive oxygen species.* J Physiol, 2003. 552(Pt 2): p. 335-44.
29. Nauseef, W.M., *Biological roles for the NOX family NADPH oxidases.* J Biol Chem, 2008. 283(25): p. 16961-5.
30. Valko, M., et al., *Free radicals and antioxidants in normal physiological functions and human disease.* Int J Biochem Cell Biol, 2007. 39(1): p. 44-84.
31. Perrone, G.G., C.M. Grant, and I.W. Dawes, *Genetic and environmental factors influencing glutathione homeostasis in Saccharomyces cerevisiae.* Mol Biol Cell, 2005. 16(1): p. 218-30.

32. Atamna, H., *Heme, iron, and the mitochondrial decay of ageing.* Ageing Res Rev, 2004. 3(3): p. 303-18.
33. Strasser, K., et al., *TREX is a conserved complex coupling transcription with messenger RNA export.* Nature, 2002. 417(6886): p. 304-8.
34. Hedges, D., M. Proft, and K.D. Entian, *CAT8, a new zinc cluster-encoding gene necessary for derepression of gluconeogenic enzymes in the yeast Saccharomyces cerevisiae.* Mol Cell Biol, 1995. 15(4): p. 1915-22.
35. Bojunga, N. and K.D. Entian, *Cat8p, the activator of gluconeogenic genes in Saccharomyces cerevisiae, regulates carbon source-dependent expression of NADP-dependent cytosolic isocitrate dehydrogenase (Idp2p) and lactate permease (Jen1p).* Mol Gen Genet, 1999. 262(4-5): p. 869-75.
36. Castegna, A., et al., *Identification and functional characterization of a novel mitochondrial carrier for citrate and oxoglutarate in Saccharomyces cerevisiae.* J Biol Chem, 2010. 285(23): p. 17359-70.
37. Ruan, H., et al., *The YCR079w gene confers a rapamycin-resistant function and encodes the sixth type 2C protein phosphatase in Saccharomyces cerevisiae.* FEMS Yeast Res, 2007. 7(2): p. 209-15.

Chapter 3
Overlap of Copper and Iron Uptake Systems in Mitochondria in *Saccharomyces cerevisiae**

*Modified version from paper: "Overlap of Copper and Iron Uptake Systems *Saccharomyces cerevisiae*" submitted to JBC.

Abstract

In *Saccharomyces cerevisiae*, the mitochondrial carrier family protein Pic2 imports copper into the matrix. Deletion of *PIC2* causes copper-dependent growth phenotypes due to defects in mitochondrial copper uptake that result in decreased activity of cytochrome c oxidase. However, copper import is not completely eliminated in this mutant, so alternative transport systems must 1exist. Deletion of the *MRS3*, a component of the iron import machinery, also causes a copper-dependent growth defect on non-fermentable carbon. Deletion of both *PIC2* and *MRS3* led to a more severe respiratory growth defect than both individual mutant and a double mutant prevented activation of a heterologously expressed copper-requiring enzyme in mitochondrial intermembrane space. When expressed in *Lactococcus lactis*, Pic2 mediates copper and silver import, and purified Pic2 showed an interaction with the copper-ligand complex found in the mitochondrial matrix. In contrast, Mrs3 failed to mediate copper or silver import when expressed in *L. lactis* and showed a decreased interaction with the copper-ligand complex when compared to Pic2 purified from *E. coli*. suggesting Mrs3 has only a low affinity for copper. The low affinity copper transport by Mrs3 was substantiated by a copper induced defect in heme synthesis that was dependent on presence of *MRS3*. Therefore, we conclude that the iron transporter *MRS3* can be used in vivo for maintaining mitochondrial matrix copper and this overlap can lead to a copper induced heme deficiency.

Introduction

Copper is an essential trace element used in various pathways including iron acquisition, respiration, and detoxification of reactive oxygen species. Because of its potential toxicity, the import, localization, and storage of copper is tightly controlled. Cells use a combination of low-affinity and high-affinity transport systems to bring copper into the cytoplasm [1, 2]. Inside the cell, protein and small molecule chaperones sequester copper and deliver it to target enzymes. The chaperone Atx1 carries copper to the P-type ATPase Ccc2 in the trans-Golgi network for incorporation into the multicopper oxidase Fet3, which is required for high affinity iron uptake [3]. Copper is delivered to the Cu, Zn superoxide dismutase (Sod1) by its chaperone Ccs1 in the cytosol and in the mitochondrial inter-membrane space (IMS) [4, 5]. Mitochondrial matrix copper is bound to a small molecule chelate known as the copper ligand (CuL), which is likely involved in recruitment of copper to this compartment [6].

In mitochondria, in addition to Sod1, copper is used by cytochrome *c* oxidase (CcO), the final enzyme complex in the electron transport chain [7]. The CcO complex localizes to the inner membrane (IM) and cofactor insertion must be tightly coordinated with its assembly; a series of chaperone proteins add copper into the forming enzyme complex as the individual subunits are translated and inserted [8]. The soluble IMS protein Cox17 delivers Cu to the IM proteins Sco1 and Cox11, which assemble the Cu_B site in the Cox1 subunit and the Cu_A site in the Cox2 subunit, respectively [9-11]. In addition to these assembly roles Sco1 is required for regulating cellular copper concentration with mutations causing defects in both import and export of copper [12]. While CcO is the major mitochondrial copper enzyme, the bulk of mitochondrial copper exist within the matrix, bound by the CuL [13]. The CuL is transported into the mitochondrial matrix

by the mitochondrial carrier family (MCF) protein Pic2 [14]. It must then be redistributed to the IMS for assembly into CcO and mitochondrial Sod1 [15].

The mitochondrial carrier family proteins (MCF) are exclusive to eukaryotes and are involved in translocation of various TCA intermediates, nucleoside di- and triphosphates, and other substrates across the mitochondrial IM [16]. Multiple MCF proteins are known to play a role in mitochondrial metal homeostasis. Mrs3, Mrs4, and their metazoan homologs are responsible for high-affinity iron transport across the IM [17]. Deletion of both *MRS3* and *MRS4* causes a severe growth defect in yeast grown under iron-depleted conditions while mutation of metazoan mitoferrin was embryonic lethal due to severe anemia [18, 19]. In addition to Mrs3 and Mrs4 in yeast, Rim2 was shown to mediate transport of nucleotide-bound iron across the inner membrane [20].

Other MCF proteins have indirect effects on mitochondrial metal homeostasis. Deletion of *MTM1* was originally shown to affect activity of Mn dependent Sod2, presumably by mismetallation of Sod2 with iron [21]. It was later shown that iron accumulates as Fe (III) in *mtm1*Δ yeast, suggesting that Mtm1 contributes to Sod2 activity by some other mechanism [22]. Ggc1, a GTP/GDP exchanger also is required for correct iron handling [23]. Deletion of Ggc1 caused a defect in Fe-S and heme that was reversed by expression of a nucleoside diphosphate kinase to normalize GTP levels in the mitochondrial matrix [24]. These examples reveal that MCFs can indirectly modify metal-related phenotypes in yeast, highlighting the need for both phenotypic characterization and biochemical assessment.

Pic2 cannot be the only protein involved in mitochondrial copper import. Deletion of the *PIC2* gene causes a growth defect only under copper-limiting conditions [14]. Mitochondria from *pic2*Δ still have 40%-70% of wild-type copper levels and can still import copper, though to a lower

capacity than those from wild-type cells [14]. Therefore, other transporters must exist. We have used complimentary phenotypic and biochemical assays to show that Mrs3, a known component of the mitochondrial iron import machinery, is involved in the mitochondrial copper import pathway.

Material and methods

Yeast strains, culture conditions, and standard methods

Yeast strains used were BY4741 (*MATa, leu2*Δ*, met15*Δ*, ura3*Δ*, his3*Δ) and isogenic kanMX4 mutant from Open Biosystems (Huntsville, AL). Double mutants were constructed by homologous recombination of the *URA3MX* cassette at the *MRS3* locus. The Y8205 (*MATα, can1*Δ*::STE2pr-Sp_his5 lyp1*Δ*::STE3pr-LEU2 his3*Δ *leu2*Δ *ura3*Δ*)* strain was a kind gift from Scot Leary (University of Saskatchewan). Cultures were grown in 1% yeast extract, 2% peptone (YP) medium or in synthetic defined media with selective amino acids excluded using the appropriate carbon source. Bio101 yeast nitrogen base plus 0.1 mM ferrous sulfate was used to give copper deficient conditions. If required, extracellular copper was depleted with bathocuproine sulfonate (BCS) or silver was added as a mitochondrial copper competitor. Exogenous copper was provided by adding $CuSO_4$. Growth tests were performed at 30 ℃ with 1 in 10 serial dilutions of overnight pre-cultures grown in YP plus 1% glucose.

Vector constructs

IM-hSOD1 was constructed by inserting the hSod1 open reading frame in-frame with the sequence encoding the N-terminal 104 residues of Sco2 (YBR024W) that encode a mitochondrial

targeting sequence and a transmembrane domain described previously [15]. Constructs were verified by dideoxynucleotide sequencing prior to use.

Fractionation of mitochondrial Cu pool

Preparation and fractionation of mitochondria was performed as previously described [13]. To extract the matrix Cu pool, cells were extracted in 100% methanol. Resulting extracts were dried and resuspended in water. CuL was prepared using Whatman DE52 anion exchange resin, which was washed in 10 mM ammonium acetate (pH 8.0). Ligand fractions were eluted using two bed volumes of 1 M ammonium acetate, pH 8.0. These were dried and washed in water before being loaded onto a Sonoma C18 column and separated by a 0-100% methanol gradient for 30 minutes on a Shimadzu UFLC. Fractions were collected and analyzed for fluorescence using an excitation maximum of 220 nm and emission maximum of 360 nm or an excitation maximum of 320 nm with an emission maximum of 400 nm (PerkinElmer Life Sciences LS55 spectrofluorimeter) and for copper by ICP-OES (PerkinElmer Life Sciences 9300-DV).

Expression of Mrs3 in *Lactococcus lactis*

L. lactis cells transformed with vector (pNZ8148) alone or pNZ8148 (MoBiTec) carrying the *PIC2* or *MRS3* gene were grown overnight at 30˚C in M17 medium with 0.5% glucose and 10 μg/mL chloramphenicol. Cells were diluted into fresh medium at an OD_{600} of 0.1, grown to an OD_{600} of 0.4, and induced using 1 ng/mL nisin for five hours. For determining silver toxicity in *L. lactis* we inoculated strains expressing vec, *PIC2* or *MRS3* in a 96-well plate in M17 plus 1 ng/mL nisin and increasing concentration of silver (0-250 μM final concentration). Controls of

M17 without nisin or M17 plus silver without nisin were included. Optical density at 600 nm was used to assess growth after 18 hours at 30^{o}C.

Copper uptake assay

Isolated mitochondria suspended in 0.6 M sorbitol were incubated with CuL for 30 second intervals and removed from solution by centrifugation. Uptake was measured by ICP-OES as an increase in copper in mitochondrial pellets over time. Copper uptake was assayed in *L. lactis* using a modified method where whole cells were resuspended in purified CuL or copper or iron salts in water. Cells were incubated for different time points at room temperature, removed by centrifugation, washed in water, and total metals were measured by ICP-OES. Uptake was reported as the increase in copper or iron over time.

Expression of recombinant proteins

The *PIC2, MRS3,* and *MIR1* ORFs were cloned into pHis parallel 1. The fidelity of each construct was verified by dideoxynucleotide sequencing prior to use. BL21 (DE3) cells were transformed with appropriate vectors and protein expression was induced for 3 hours. Inclusion bodies were isolated in a manner similar to that described by Palmieri [16]. Briefly, cells were resuspended in 1X potassium phosphate buffer (140 mM NaCl, 2.7 mM KCl, 8.3 mM K_2HPO_4, 1.8 mM KH_2PO_4), pH 7.5 and disrupted by sonication. Insoluble material was collected by centrifugation at 18,500 *g*. Insoluble material was resuspended in 1X potassium phosphate buffer, pH 7.5, and loaded onto a stepwise 40%, 53%, 70% sucrose gradient. Samples were centrifuged at 18,500 *g* for one hour and inclusion bodies were isolated as a gray colored band at the interface between the 53% and 70% layers. Presence of the protein of interest was confirmed by

immunoblot. To load protein into liposomes, inclusion bodies were solubilized in 6 M urea before overnight dialysis in egg yolk phospholipids dispersed in 1X potassium phosphate buffer. The dialyzed mixture was sonicated to generate the final proteoliposomes and protein concentration was determined by Bradford assay.

Fluorescence anisotropy

CuL was diluted to give a fluorescence intensity of ~30 using an excitation at 320 nm and emissions at 400 nm (slit widths were set to 5 nm). Inclusion bodies and MCF protein incorporated into liposomes were added in 1-5 μL increments. Anisotropy was measured using a PerkinElmer Life Sciences LS55 spectrofluorimeter.

Miscellaneous methods

The monoclonal mouse anti-human SOD1 was purchased from Santa Cruz Biosciences. Secondary antibodies used were Cy3-linked goat anti mouse from GeneScript. Superoxide dismutase (SOD1) activity was measured using a xanthine oxidase linked assay kit (Sigma Life Science) and absorbance was measured on a BioTek 96-well plate reader.

Results

Simultaneous deletion of *PIC2* and *MRS3* results in copper-dependent growth defects

Pic2 was identified using a screen of single MCF gene deletions grown on rich medium with a non-fermentable carbon source in the presence of the cell-impermeable copper chelator BCS and silver as a mitochondrial copper competitor [14]. Under these conditions, the *mrs3Δ* mutants had a growth defect, though it was milder than *pic2*Δ mutants (Figure 3.1A). This defect

was reversed when silver concentrations were decreased, and no defect was observed on glucose at the same concentration of silver (not shown). To test for synergistic phenotypes, we created a *pic2*Δ*mrs3*Δ double mutant. Simultaneous deletion of *PIC2* and *MRS3* resulted in poor growth on copper-depleted rich medium with a non-fermentable carbon source (Figure 3.1B). Deletion of the related gene *MRS4*, which encodes another component of the high affinity iron import machinery, in the *pic2*Δ background did not cause an additional defect when compared to *pic2*Δ alone under any conditions tested (Figure 1B). We also compared the growth of double mutants that lack *PIC2* and *ODC1*, *ODC2* or *MIR1*. No combination showed phenotypes as severe as *pic2*Δ*mrs3*Δ although a silver dependent phenotype was observed in *pic2*Δ*odc2*Δ. When grown on synthetic medium with a non-fermentable carbon source, the *pic2*Δ*mrs3*Δ had a growth defect in the absence of chelators (Figure 3.1C). Even though the deletion are additive, overexpression of *MRS3* from a multi-copy vector could not suppress the silver induced defect in a *pic2*Δ mutant (Figure 3.1D). These results suggest that deletion of both *PIC2* and *MRS3* negatively affects copper delivery to CcO.

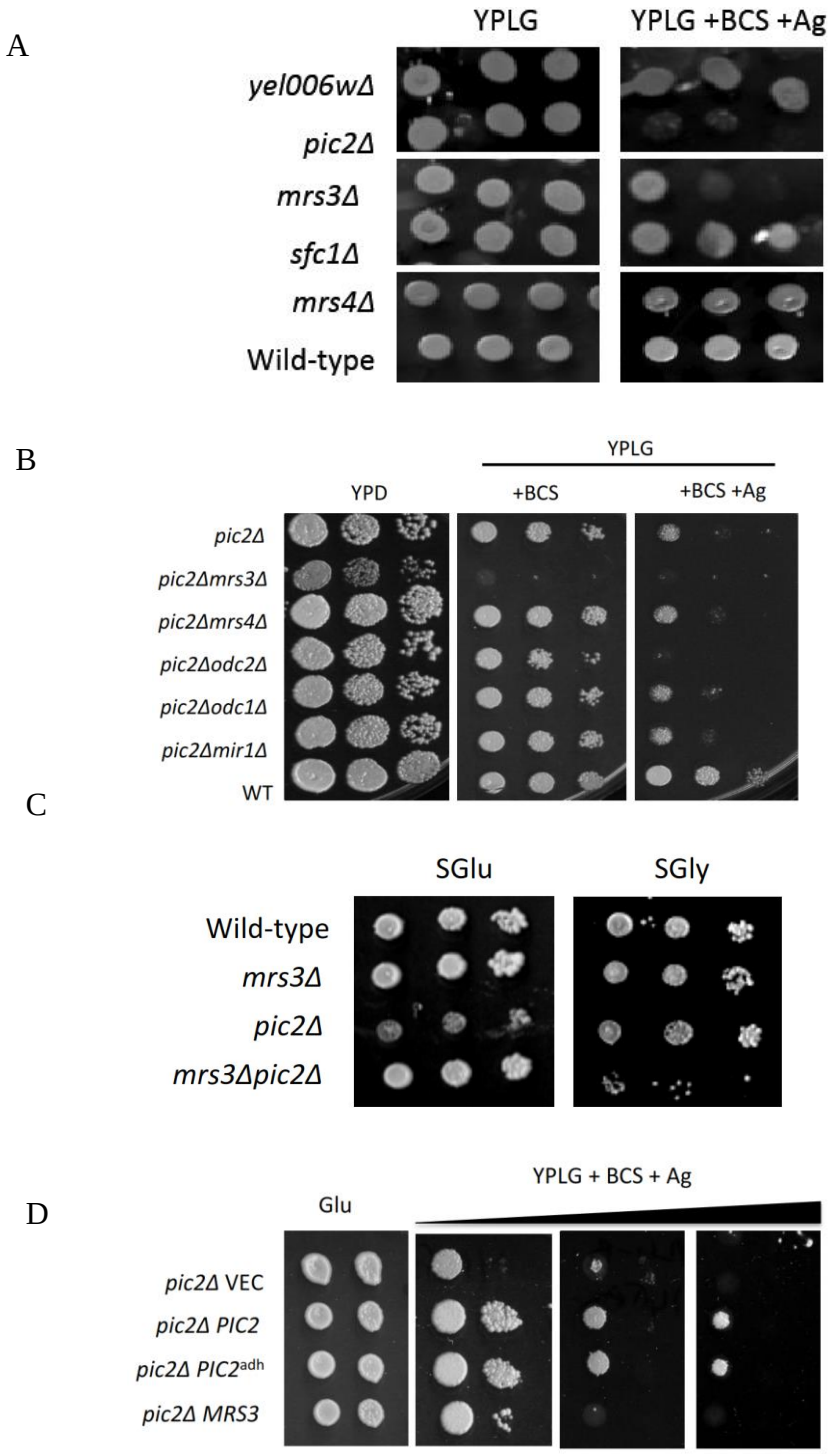

Figure 3.1 Copper related phenotypes in PIC2 and MRS3 null mutants.

(A) Serial dilution drop test of single MCF null mutants on non-fermentable carbon source (glycerol) plates. When adding BCS and silver in the glycerol plates, *pic2*Δ showed severe growth

defect, and *mrs3*Δ showed a mild growth defect. Other single MCF null mutant did not show any growth defect. YEL006W is a putative mitochondrial NAD+ transporter [25]. *SFC1* is a mitochondrial succinate-fumarate transporter gene [26]. (B) Serial dilution drop test of *pic2*Δ, *mrs3*Δ and *pic2*Δ*mrs3*Δ double mutant on fermentable and non-fermentable plates. *pic2*Δ*mrs3*Δ showed growth defect on non-fermentable plate.(C) Serial dilution drop test of different double mutant on fermentable and non-fermentable plates. Only *pic2*Δ*mrs3*Δ showed severe growth defect on non-fermentable plate by just adding BCS. Comparing to *pic2*Δ, *pic2*Δ*odc2*Δ also showed growth defect on non-fermentable plate with addition of BCS and silver. *ODC1* and *ODC2* are paralogs, coding for 2-oxodicarboxylate transporter, which involves in lysine and glutamate biosynthesis [27]. *MIR1* is a mitochondrial phosphate carrier gene [28]. (D) Serial dilution drop test of overexpression of *PIC2* and *MRS3* in *pic2*Δ strains. Only *PIC2* could reverse the growth defect phenotype but not *MRS3*.

Deletion of *PIC2* and *MRS3* results in mitochondrial copper deficiency

Deletion of the gene encoding the copper chaperone for Sod1 (*CCS1*) results in a lysine auxotrophy [29, 30]. The lysine auxotrophy of *ccs1*Δ can be reversed by an IM-tethered human Sod1 (IM-hSod1) (See Figures in [40]). Activity of IM-hSod1 is dependent on available copper within the IMS and this enzyme may be used as a copper sensor that is unaffected by yeast regulatory pathways [15]. Copper used by IMS cuproenzymes originates from the matrix pool so the *ccs1*Δ*::IM-hSod1* background can be used to probe availability of both matrix and IMS copper. Deletion of *PIC2* in this background caused a 40-50% decrease IM-hSod1 activity when these cells were grown in silver, but did not cause a lysine auxotrophy [14]. The *ccs1*Δ*::IM-hSod1* copper-sensing strain was crossed with the *mrs3*Δ single mutant to generate the *mrs3*Δ*ccs1*Δ*::IM-*

hSod1 and the *pic2*Δ*mrs3*Δ double mutant to generate a *pic2*Δ*mrs3*Δ*ccs1*Δ*::IM-hSod1* triple mutant. While the *mrs3*Δ*ccs1*Δ*::IM-hSod1* strain did not have any growth defects, *pic2*Δ*mrs3*Δ*ccs1*Δ*::IM-hSod1* mutant failed to grow on medium lacking lysine (See Figures in [40]). As expected, the triple mutant completely lacked Sod1 activity, indicating a deficiency of available mitochondrial copper, while the *mrs3*Δ*ccs1*Δ*::IM-hSod1* double mutant had a mild deficiency of hSod1 activity. The triple mutant strain was able to grow weakly on glycerol containing media when compared to *pic2*Δ*ccs1*Δ*::IM-hSod1*. These results suggest that both *PIC2* and *MRS3* affect availability of copper in mitochondria.

Mitochondria from *pic2Δ, mrs3*Δ, and *mrs4*Δ isolated from cells grown in rich medium with supplemental iron were analyzed for total metals by ICP-OES and showed decreased copper levels to 30%, 60%, 70% of wild-type respectively (Figure 3.2A). Mitochondria isolated from *pic2Δ*, *mrs3*Δ, and *pic2*Δ*mrs3*Δ cells grown in rich medium or synthetic medium with glucose as a carbon source were analyzed for total metals by ICP-OES showed only a mild decrease in copper relative to mitochondria from wild-type cells (not shown). To exaggerate a difference in mitochondrial copper, wild type, *pic2*Δ, and *mrs3*Δ, and *pic2*Δ*mrs3*Δ cells were grown in synthetic medium supplemented with 0.5 mM $CuSO_4$. *pic2*Δ and *mrs3* Δ mitochondria accumulated copper to 45% and 80% of wild type mitochondria, respectively (Figure 3.2B). The *mrs3*Δ mitochondria showed a defect in total iron under these conditions (Figure 3.2B) while *pic2*Δ mitochondria had copper-specific defect. The *pic2*Δ*mrs3*Δ double mutant accumulated only about 30% of wild-type copper while other metals remained at or greater than wild-type levels, except for manganese (Figure 3.2B). It should be noted that, as previously observed [14], all mutants expanded the mitochondrial copper pool when grown in exogenous copper, but expansion was attenuated relative to wild-type cells.

We compared the accumulation of the CuL complex in *pic2Δ*, *mrs3*Δ, and *mrs4*Δ cells grown in rich medium with supplemental iron. The CuL complex was extracted in organic solvents then isolated by anion exchange and analyzed by reverse phase chromatography. Based on previous studies the levels of anionic complex are reflective of the mitochondrial copper levels. This indirect measure of mitochondrial copper reflected the same level of defect observed in total copper (Figure 3.2C).

A

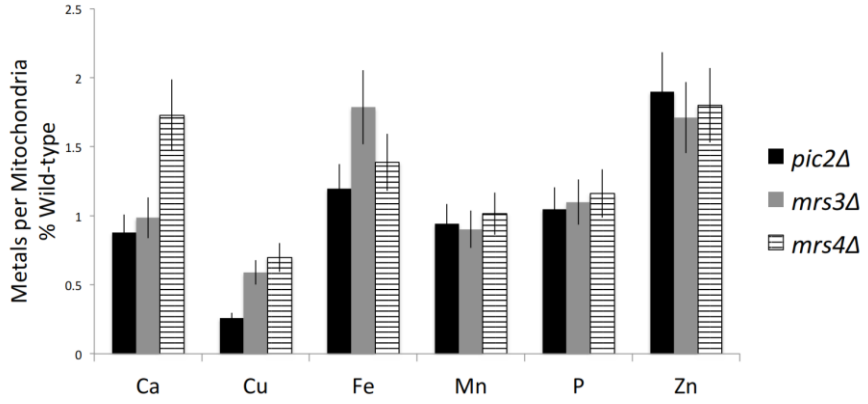

B

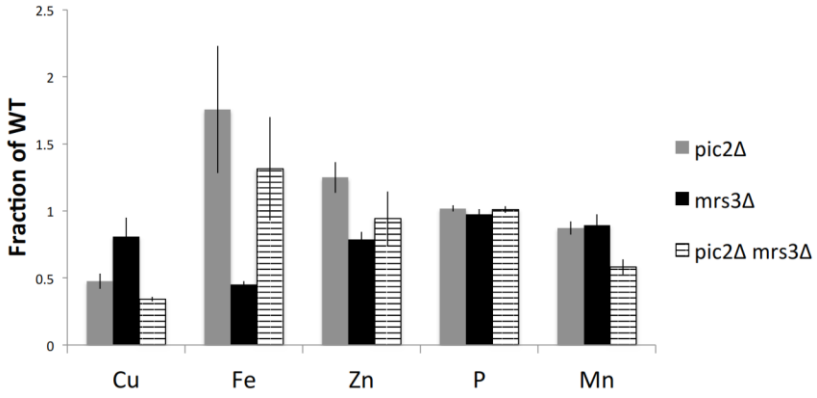

C

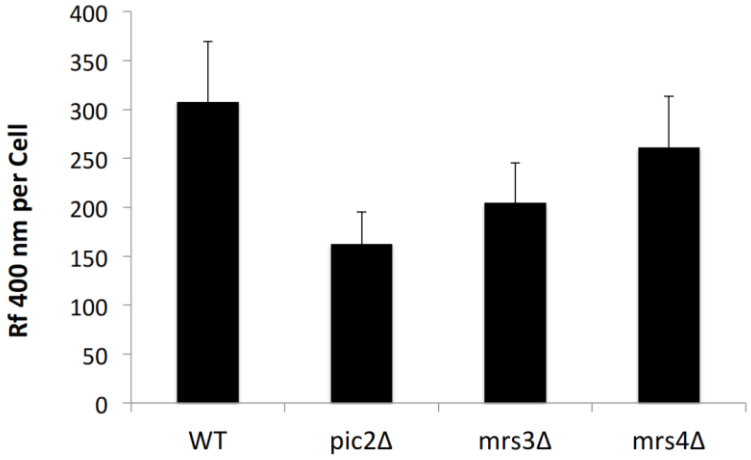

Figure 3.2 Metal concentrations in mutants by ICP-OES.

(A) Relative metal concentrations in mitochondria of *pic2*Δ*, mrs3*Δ and *mrs4*Δ compared with WT. Cells were grown in rich media with supplemental iron, after extraction of mitochondria, metal concentrations were analyzed by running through ICP-OES. Final metal concentrations in the

mutants were calculated by the percentage of that metal in the WT strain. Only copper concentration showed defect in mutants. *pic2*Δ showed 30% copper concentration of wild type mitochondria, *mrs3*Δ showed 60% and *mrs4*Δ showed 70%. (B) Relative mitochondrial metal concentrations of *pic2*Δ, *mrs3*Δ and *pic2*Δ*mrs3*Δ in rich media with supplemental copper. Comparing to WT, *pic2*Δ, *mrs3*Δ and *pic2*Δ*mrs3*Δ *all* showed copper defect when growing with copper supplement. In which *pic2*Δ*mrs3*Δ has the most severe mitochondrial copper defect, then *pic2*Δ. *mrs3*Δ also showed mitochondrial iron defect growing with copper supplement but not *pic2*Δ*mrs3*Δ. (C) CuL concentrations in *pic2*Δ, *mrs3*Δ and *mrs4*Δ cells. CuL concentrations were measured by reverse phase chromatography. The CuL concentrations indirectly reflect the mitochondrial copper level in cells.

MRS3 does not mediate high affinity copper uptake

Intact mitochondria from *pic2*Δ, *mrs3*Δ and wild-type cells were assayed for uptake of copper in the form of purified CuL. Copper was taken into *pic2*Δ mitochondria at a decreased initial rate while uptake into *mrs3*Δ mitochondria resembled wild-type mitochondria. These data indicate that deletion of *MRS3* does not cause a detectable defect in mitochondrial copper import. However the simultaneous deletion of both *PIC2* and *MRS3* does result in a further decrease in initial rates of copper uptake (Figure 3.3).

MRS3 was heterologously expressed in the Gram-positive bacterium *Lactococcus lactis* used previously to demonstrate function of mitochondrial carrier family proteins including copper uptake by Pic2 [14, 31]. Uptake of CuL and $CuSO_4$ was assayed in whole cells containing *MRS3* or the empty vector. *L. lactis* cells expressing Mrs3 failed to increase total copper, provided as purified CuL or as $CuSO_4$ (Figure 3.4A, B). However, these cells expressing Mrs3 were capable

of importing more $FeSO_4$, which is consistent with the role of Mrs3 in the mitochondrial high affinity iron import pathway (Figure 3.4C). The ability of Mrs3 to mediate iron import suggests that the lack of copper import is not due to general defects in the Mrs3 protein.

Because silver acts as a toxic copper mimetic, we designed a silver toxicity assay in *L. lactis* that was dependent on the expression of a functional expression of a Cu importer. We observed dose dependent Ag toxicity in *L. lactis* when Pic2 expression was induced with nisin (Figure 3.4D). Using this assay, we found that expression of Mrs3 did not induce Ag toxicity, indicating the lack of silver import (Figure 3.4D). No toxicity was observed in 119 μM silver in the absence of the inducer nisin (Figure 3.4E).

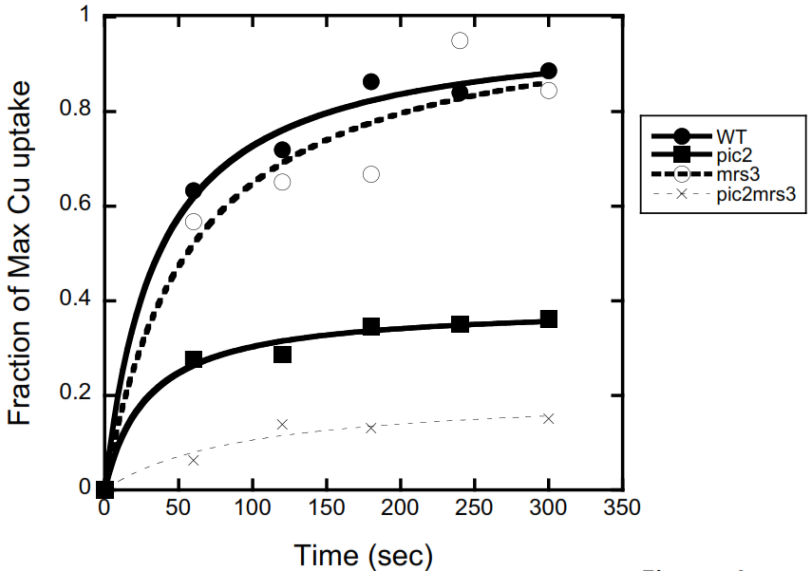

Figure 3.3 Copper uptake assay in mitochondria.

Copper uptake was measured in WT, *pic2*Δ, *mrs3*Δ and *pic2*Δ*mrs3*Δ mitochondria. *mrs3*Δ mitochondria showed similar copper uptake compared to WT, *pic2*Δ showed a copper uptake defect by more than 50%, *pic2*Δ*mrs3*Δ showed most severe copper uptake defect.

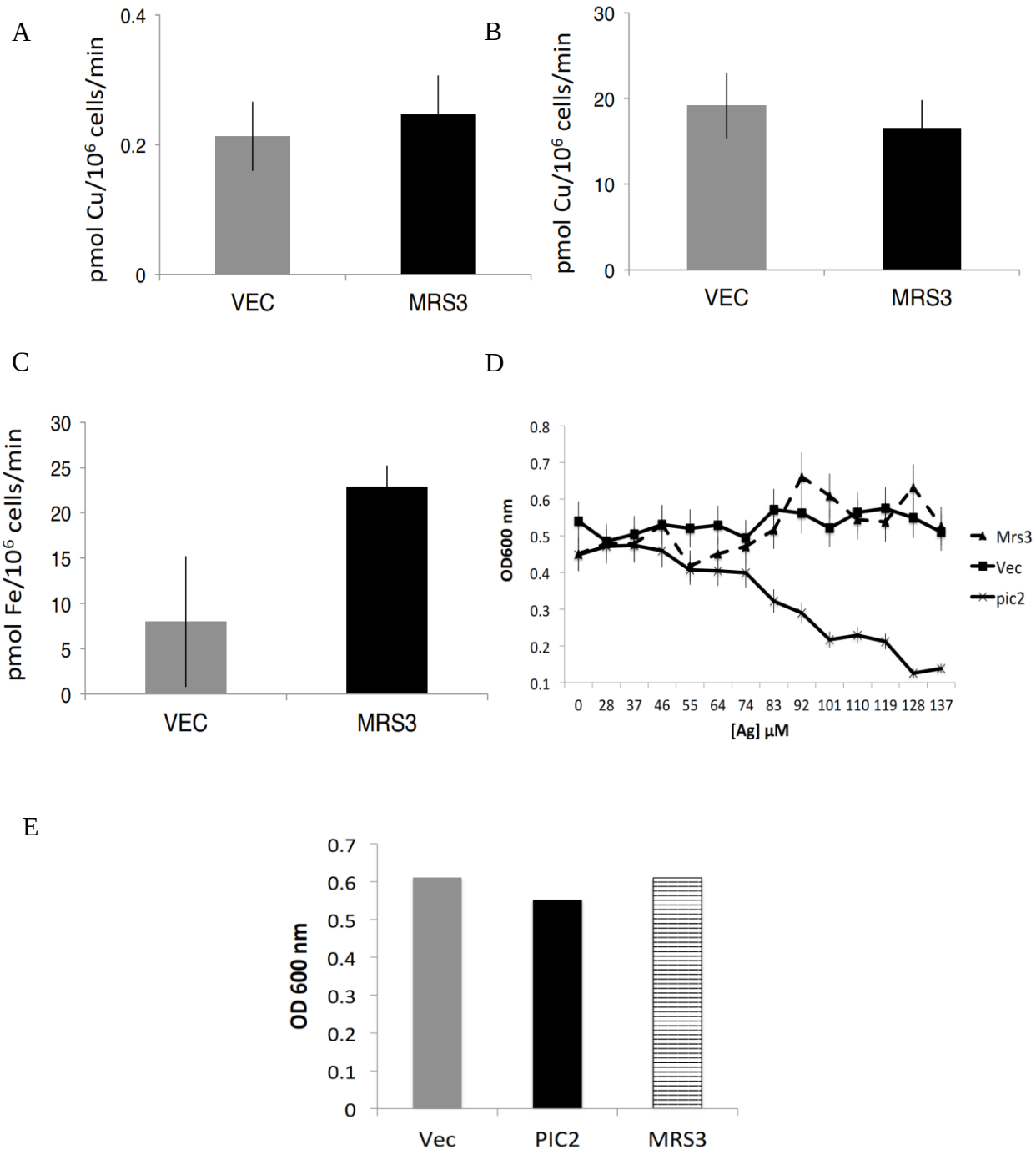

Figure 3.4 Copper uptake assay of Pic2 and Mrs3 in *L. lactis*.

(A) Uptake assay of CuL in *L. lactis* with empty vector or expressing Mrs3. (B) Uptake assay of $CuSO_4$ in *L. lactis* with empty vector or expressing Mrs3. (C) Uptake assay of $FeSO_4$ in *L. lactis* with empty vector or expressing Mrs3. (D) Silver toxicity assay in *L. lactis* with empty vector,

expressing Mrs3 or expressing Pic2. The expression of Pic2 was induced with nisin. Only with the expression of Pic2 cells showed growth defect under higher silver concentrations. (E) OD 600nm test of cells without nisin under 119 μM silver. Without the addition of nisin, cells contain *PIC2* vector did not show growth defect under 119 μM silver, meaning the growth defect under high silver concentration was indeed caused by the expression of Pic2.

Mrs3 has weak interaction with the CuL complex relative to Pic2

The CuL complex has a fluorescent emission at 360 nm when excited at 220 nm that is responsive to the addition or removal of copper [15]. We scanned the excitation and emission profiles to find a unique emission that could be excited without interference from the proteoliposomes to analyze potential CuL-protein interactions by fluorescence anisotropy (FA). Purified CuL had a fluorescent emission at 400 nm upon excitation at 320 nm that could be detected as a single peak on by reverse phase chromatography (Figure 3.5A). This peak and total mitochondrial copper increases with copper supplementation to the media (Figure 3.5B). As previously reported, the fluorescence of the purified molecule was quenched in a concentration-dependent manner upon addition of Cu-acetonitrile (Figure 3.5C). Addition of KCN to remove copper from the complex restored fluorescent emission.

We used FA to assay interaction between the Pic2 and the CuL complex. Pic2, Mrs3, and the related MCF protein Mir1 were expressed in *E. coli*, purified as inclusion bodies, and reconstituted into liposomes by dialysis and sonication. Pic2-containing liposomes were assayed for CuL binding by FA using the 320 nm/400 nm fluorescence characteristics of the CuL complex. Pic2 strongly enhanced anisotropy of the CuL, indicating binding, while Mrs3 and Mir1 had much weaker interactions (Figure 3.5D). Membranes from *E. coli* cells transformed with an empty vector

showed limited interaction with the CuL (not shown). These results suggest that Pic2 has an affinity for the copper ligand that is higher than both Mrs3 and Mir1.

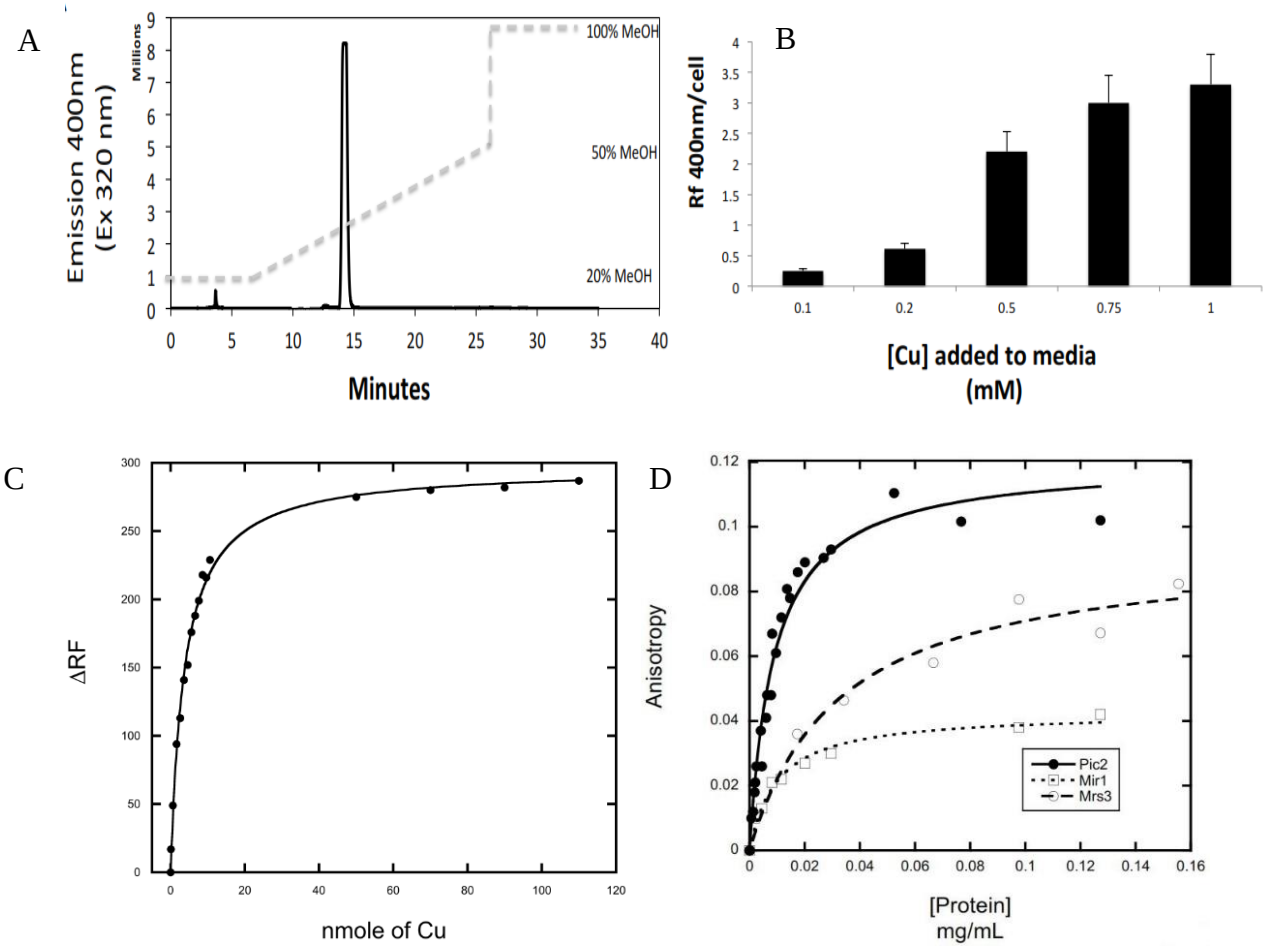

Figure 3.5 CuL uptake assays.

(A) CuL peak under reverse phase chromatography. (B) CuL concentrations with increasing copper addition to the media. (C) Change in relative fluorescence (ΔRF) in CuL fractions titrated with sequential addition of Cu-acetonitrile (D) CuL binding ability of Pic2, Mir1 and Mrs3. Pic2 has the highest binding ability, then Mrs3.

Copper induced heme defect

Mrs3 is required for heme production by providing iron to the mitochondrial matrix. The *mrs3*Δ strain used here has a heme defect as assayed by total heme detected by Soret band (405 nm) after acid-acetone extraction and reverse-phase HPLC when compared to wild-type, *mrs4*Δ

or *pic2*Δ cells (Figure 3.6A) [32]. Due to the connection of *MRS3* and copper related phenotypes we assayed the affects of exogenous copper on heme. Culturing wild-type cells in copper or the heme biosynthesis inhibitor succinyl-acetone resulted in decreased heme synthesis without affecting total cellular iron (Figure 3.6C). The heme levels in wild-type and *mrs3*Δ increased with the addition of exogenous Fe while supplemental copper caused a heme deficit in WT cells similar to levels *mrs3*Δ in non-supplemented media (Figure 3.6B). The copper-induced heme defect was partially resolved upon deletion of *MRS3* (Figure 3.6B). In addition to this biochemical defect we investigated the impact of copper and silver of heme related phenotypes including aerobic growth. Increasing concentrations of copper resulted in toxicity on glucose containing media (Figure 3.6D). However the blockage of heme synthesis reversed this toxicity. This succinyl-acetone (SA) induced rescue of copper toxicity was enhanced in both *pic2*Δ and *mrs3*Δ mutants (Figure 3.6D). In comparison silver toxicity was actually increased by the depletion of heme (Figure 3.6E). Taken together, these results suggest that copper can compete with iron at Mrs3 for the downstream targets of iron homoeostasis.

A

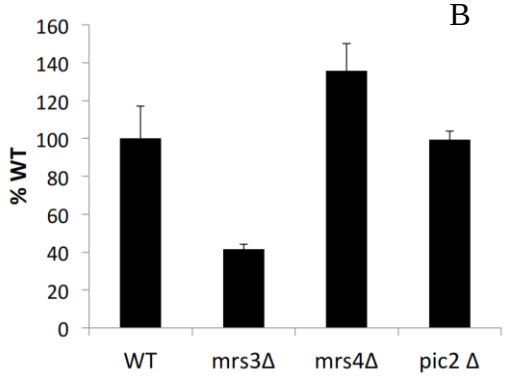
160
140
120
100
80
60
40
20
0
% WT
WT
mrs3Δ
mrs4Δ
pic2 Δ

B

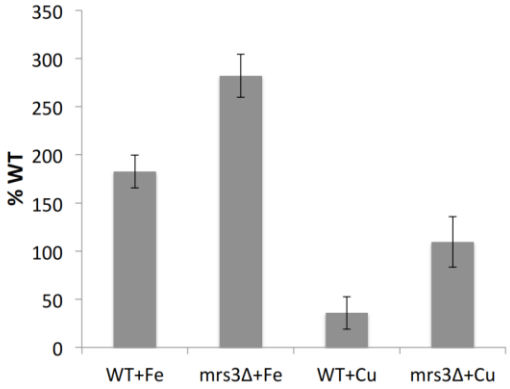
350
300
250
200
150
100
50
0
% WT
WT+Fe
mrs3Δ+Fe
WT+Cu
mrs3Δ+Cu

C

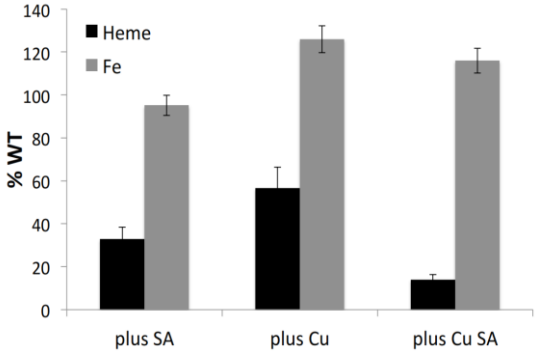
140
120
100
80
60
40
20
0
% WT
Heme
Fe
plus SA
plus Cu
plus Cu SA

D

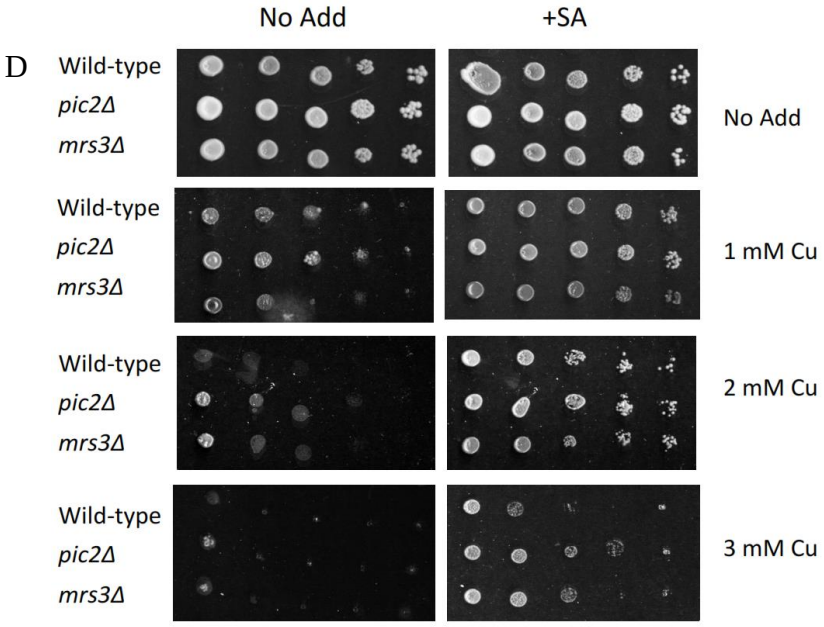
No Add
+SA
Wild-type
pic2Δ
mrs3Δ
No Add
Wild-type
pic2Δ
mrs3Δ
1 mM Cu
Wild-type
pic2Δ
mrs3Δ
2 mM Cu
Wild-type
pic2Δ
mrs3Δ
3 mM Cu

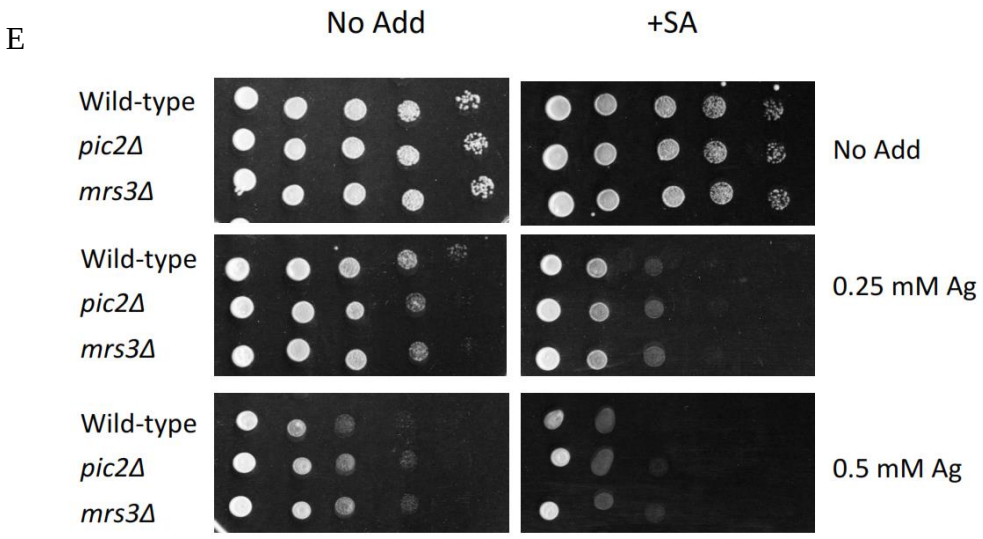

Figure 3.6 Heme and copper related phenotypes in *mrs3*Δ.

(A) Relative heme concentration in *mrs3*Δ, *mrs4*Δ and *pic2*Δ comparing to WT cells. In the mutants, only *mrs3*Δ showed heme defect. (B) Heme level in WT and *mrs3*Δ cells with the addition of iron or copper. By the addition of iron, both WT and *mrs3*Δ cells heme level went higher. When adding copper, WT cells showed defect in heme level but not *mrs3*Δ cells. (C) Relative heme and iron level in WT cells with the addition of SA, copper or both. The iron level did not change when adding them, but heme level showed a decrease when adding copper or SA. When adding both together, it showed a lower heme level in the WT cells. (D) Serial dilution drop test of *pic2*Δ, *mrs3*Δ and WT in different concentration of copper with and without the addition of SA. All the three strains showed copper sensitivity when copper level went high, while WT was more sensitive to *pic2*Δ and *mrs3*Δ. This copper sensitivity could be eliminated by the addition of SA. (E) Serial dilution drop test of *pic2*Δ, *mrs3*Δ and WT in different concentration of silver with and without the addition of SA. The elimination of copper sensitivity could not be repeated with silver when adding SA.

Discussion

MRS3, which encodes a mitochondrial inner-membrane iron transporter, is also involved in mitochondrial copper homeostasis. In vivo phenotypes reported here support Mrs3 having partially overlapping function with the known copper transporter Pic2. Double deletion of *PIC2* and *MRS3* exaggerates multiple copper related phenotypes: 1) defects in expansion of the mitochondrial copper pool 2) a more severe copper dependent respiratory defect 3) failure to activate an IM-tethered hSod1. The exaggerated defects associated with pic2Δmrs3Δ suggest that these two proteins have independent functions in the copper import pathway. However, deletion of *MRS3* does not appear to affect mitochondrial copper uptake in vitro and Mrs3 expressed in *L. lactis* does not mediate copper import or induce silver toxicity. Recombinant Mrs3 shows only a weak interaction with the CuL complex.

One possible explanation for the differences in biochemical versus phenotypic data is that Mrs3 does mediate copper transport in a manner that is undetectable by our measurements. For example, Mrs3 may require specific factors or mitochondrial conditions to function as a copper transporter that are not required by Pic2. These requirements could be related to internal, exchangeable substrates or perhaps concentrations of particular phospholipids that are not present in our in vitro experiments. More likely is that Mrs3 imports copper at low affinity, which is undetectable by our assays. The role for Mrs3 as a low affinity importer is supported by FA data showing weak interaction between Mrs3 and the CuL.

Previous studies suggested that copper and iron uptake did not compete for mitochondrial import based on steady state concentrations [13]. However, it appears that Cu-Fe competition can be observed in WT cells grown in high copper using heme as an assay of available iron. Addition of copper to the medium caused a decrease in heme in WT cells. Meanwhile, copper

supplementation did not dramatically affect the steady state levels of total iron in mitochondria. Extending from the work of Dancis and co-workers which showed requirements for Mrs3/Mrs4 in efficient heme assembly [33], we speculate that the high concentrations of copper may cause competition of copper and iron through Mrs3, which may affect iron delivery to ferrochelatase and decrease the efficiency of heme biosynthesis. Copper could also inhibit ferrochelatase by inappropriate incorporation and this may be induced by the direct transfer through Mrs3. The copper-driven heme defect would be lost with the deletion of *MRS3*. Therefore we suggest that the competition between Fe and Cu arises by Mrs3 acting as a low affinity copper transporter. The in vivo substrate/complex for iron transport in mitochondria is unknown, so we cannot test for competition of CuL (or AgL) and iron using our assays. Ferrous sulfate was used as a substrate for *L. lactis* experiments but we were not able to used $FeSO_4$ for mitochondrial import experiments due to large amounts of non-specific interactions with mitochondrial membranes.

Copper toxicity in prokaryotes is a result of disruption of Fe-S enzymes and has been shown that via this mechanisms can also affect heme and chlorophyll synthesis in *Neisseria gonorrhoeae* and *Rubrivivax gelatinosus*, respectively [34, 35]. The heme synthesis block here in yeast is suggested to via competition between copper and iron for specific transport into the matrix as the yeast coproporphyrinogen III oxidase (Hem13) does not contain iron-sulfur cofactor and deletion of *MRS3* reverses this copper induced affect. This heme depletion induced rescue of copper toxicity suggesting that decreasing copper concentrations in mitochondria can suppress this copper toxicity. It is possible that the competition affects Fe-S formation in the matrix and the decreased in heme synthesis induced by succinyl acetone allows for increased partitioning of iron to Fe-S synthesis. However, we have no supporting evidence at this time. Copper overloading causes severe mitochondrial damage in Wilson patient tissues and models of copper overload disease

including the Long-Evans Cinnamon rat and North Ronaldsay sheep [36-38], but to date no reports exists to suggest this is due to heme or Fe-S defects.

An alternative explanation for the mitochondrial copper defects observed in *mrs3*Δ and *pic2*Δ*mrs3*Δ would be that Mrs3 regulates copper export from the matrix. An increase in copper export in *mrs3*Δ or *pic2*Δ*mrs3*Δ would result in decreased total copper. However, we would not expect this to affect the ability to load the heterologous sensor IM-hSOD1. Also we do not see any enhanced resistance to silver in *L. lactis* assay that might be expected if Mrs3 acted as an exporter. Therefore a role for Mrs3 in regulating copper export from the matrix does not seem likely.

Finally we considered that *MRS3* deletion may cause indirect effects on overall mitochondrial physiology. A previous study found *PIC2* and *MRS3* as high copy suppressors of mitochondrial K^+/H^+ exchanger (KHE) mutants [39]. Under certain experimental conditions, deletion of *MRS3* increased mitochondrial potassium levels three-fold but this was not consistently observe and does not appear to correlate with the level of copper deficiency (not shown). In the KHE study, *PIC2* or *MRS3* overexpression at least partly reversed the mitochondrial morphology defects in the KHE mutants, which had an abnormally high ratio of fragmented to fused mitochondria. Overexpression of *PIC2* mediated only partial return of the tubular network, but overexpression of *MRS3* was able to completely reverse this defect. How mitochondrial morphology affects the matrix copper pool remains unknown, but recent observations show a mitochondrial morphology defect in *coa1*Δ cells, which are also deficient for mitochondrial copper (Zhao and Cobine, unpublished). We also considered that *MRS3* or iron could be important for maintaining bioavailable pools of copper. This would be analogous to the situation for the substrates transported *MTM1* and *GGC1* which are required for maintaining matrix iron homeostasis. However, failure to maintain iron in the bioavailable form in *mtm1*Δ or *ggc1*Δ results

in increased concentration of insoluble iron. We observed decreased total copper levels upon *MRS3* deletion, therefore making this possibility less likely.

In conclusion, we report phenotypic evidence for the involvement of Mrs3 in mitochondrial copper homeostasis, likely by acting as a low affinity copper importer. Our results suggest that a link between copper and iron homoeostasis does exist in mitochondria. The mitochondrial connection of copper and iron through Pic2 and Mrs3 extends the well-established association of these two metals in various aspects of cellular physiology. However, further experiments are required to understand the contributions of multiple factors that give rise to these copper and iron related phenotypes. We are performing synthetic genetic array experiments to understand the complete mitochondrial copper import pathway. Knowledge of the additional components of mitochondrial copper homeostasis, we will be able to refine our transport assays to further understand the connection between copper and iron in mitochondria.

Reference

1. Hassett, R., et al., *The Fe(II) permease Fet4p functions as a low affinity copper transporter and supports normal copper trafficking in Saccharomyces cerevisiae.* Biochem J, 2000. 351 Pt 2: p. 477-84.
2. Dancis, A., et al., *The Saccharomyces cerevisiae copper transport protein (Ctr1p). Biochemical characterization, regulation by copper, and physiologic role in copper uptake.* J Biol Chem, 1994. 269(41): p. 25660-7.
3. Lin, S.J., et al., *A role for the Saccharomyces cerevisiae ATX1 gene in copper trafficking and iron transport.* J Biol Chem, 1997. 272(14): p. 9215-20.
4. Sturtz, L.A., et al., *A fraction of yeast Cu,Zn-superoxide dismutase and its metallochaperone, CCS, localize to the intermembrane space of mitochondria. A physiological role for SOD1 in guarding against mitochondrial oxidative damage.* J Biol Chem, 2001. 276(41): p. 38084-9.
5. Rae, T.D., et al., *Undetectable intracellular free copper: the requirement of a copper chaperone for superoxide dismutase.* Science, 1999. 284(5415): p. 805-8.
6. Leary, S.C., D.R. Winge, and P.A. Cobine, *"Pulling the plug" on cellular copper: the role of mitochondria in copper export.* Biochim Biophys Acta, 2009. 1793(1): p. 146-53.
7. Gennis, R. and S. Ferguson-Miller, *Structure of cytochrome c oxidase, energy generator of aerobic life.* Science, 1995. 269(5227): p. 1063-4.
8. Fontanesi, F., I.C. Soto, and A. Barrientos, *Cytochrome c oxidase biogenesis: new levels of regulation.* IUBMB Life, 2008. 60(9): p. 557-68.
9. Horng, Y.C., et al., *Specific copper transfer from the Cox17 metallochaperone to both Sco1 and Cox11 in the assembly of yeast cytochrome C oxidase.* J Biol Chem, 2004. 279(34): p. 35334-40.
10. Nittis, T., G.N. George, and D.R. Winge, *Yeast Sco1, a protein essential for cytochrome c oxidase function is a Cu(I)-binding protein.* J Biol Chem, 2001. 276(45): p. 42520-6.
11. Tzagoloff, A., et al., *Cytochrome oxidase assembly in yeast requires the product of COX11, a homolog of the P. denitrificans protein encoded by ORF3.* EMBO J, 1990. 9(9): p. 2759-64.
12. Leary, S.C., et al., *The human cytochrome c oxidase assembly factors SCO1 and SCO2 have regulatory roles in the maintenance of cellular copper homeostasis.* Cell Metab, 2007. 5(1): p. 9-20.
13. Cobine, P.A., et al., *Yeast contain a non-proteinaceous pool of copper in the mitochondrial matrix.* J Biol Chem, 2004. 279(14): p. 14447-55.
14. Vest, K.E., et al., *Copper import into the mitochondrial matrix in Saccharomyces cerevisiae is mediated by Pic2, a mitochondrial carrier family protein.* J Biol Chem, 2013. 288(33): p. 23884-92.
15. Cobine, P.A., et al., *Mitochondrial matrix copper complex used in metallation of cytochrome oxidase and superoxide dismutase.* J Biol Chem, 2006. 281(48): p. 36552-9.
16. Palmieri, L., et al., *Yeast mitochondrial carriers: bacterial expression, biochemical identification and metabolic significance.* J Bioenerg Biomembr, 2000. 32(1): p. 67-77.
17. Froschauer, E.M., R.J. Schweyen, and G. Wiesenberger, *The yeast mitochondrial carrier proteins Mrs3p/Mrs4p mediate iron transport across the inner mitochondrial membrane.* Biochim Biophys Acta, 2009. 1788(5): p. 1044-50.

18. Muhlenhoff, U., et al., *A specific role of the yeast mitochondrial carriers MRS3/4p in mitochondrial iron acquisition under iron-limiting conditions.* J Biol Chem, 2003. 278(42): p. 40612-20.
19. Shaw, G.C., et al., *Mitoferrin is essential for erythroid iron assimilation.* Nature, 2006. 440(7080): p. 96-100.
20. Froschauer, E.M., et al., *The mitochondrial carrier Rim2 co-imports pyrimidine nucleotides and iron.* Biochem J, 2013. 455(1): p. 57-65.
21. Luk, E., et al., *Manganese activation of superoxide dismutase 2 in Saccharomyces cerevisiae requires MTM1, a member of the mitochondrial carrier family.* Proc Natl Acad Sci U S A, 2003. 100(18): p. 10353-7.
22. Park, J., et al., *Insights into the iron-ome and manganese-ome of Deltamtm1 Saccharomyces cerevisiae mitochondria.* Metallomics, 2013. 5(6): p. 656-72.
23. Vozza, A., et al., *Identification of the mitochondrial GTP/GDP transporter in Saccharomyces cerevisiae.* J Biol Chem, 2004. 279(20): p. 20850-7.
24. Gordon, D.M., et al., *GTP in the mitochondrial matrix plays a crucial role in organellar iron homoeostasis.* Biochem J, 2006. 400(1): p. 163-8.
25. Todisco, S., et al., *Identification of the mitochondrial NAD+ transporter in Saccharomyces cerevisiae.* J Biol Chem, 2006. 281(3): p. 1524-31.
26. Palmieri, L., et al., *Identification and functions of new transporters in yeast mitochondria.* Biochim Biophys Acta, 2000. 1459(2-3): p. 363-9.
27. Palmieri, L., et al., *Identification in Saccharomyces cerevisiae of two isoforms of a novel mitochondrial transporter for 2-oxoadipate and 2-oxoglutarate.* J Biol Chem, 2001. 276(3): p. 1916-22.
28. Reinders, J., et al., *Profiling phosphoproteins of yeast mitochondria reveals a role of phosphorylation in assembly of the ATP synthase.* Mol Cell Proteomics, 2007. 6(11): p. 1896-906.
29. Gralla, E.B. and D.J. Kosman, *Molecular genetics of superoxide dismutases in yeasts and related fungi.* Adv Genet, 1992. 30: p. 251-319.
30. Jensen, L.T., et al., *Mutations in Saccharomyces cerevisiae iron-sulfur cluster assembly genes and oxidative stress relevant to Cu,Zn superoxide dismutase.* J Biol Chem, 2004. 279(29): p. 29938-43.
31. Kunji, E.R., D.J. Slotboom, and B. Poolman, *Lactococcus lactis as host for overproduction of functional membrane proteins.* Biochim Biophys Acta, 2003. 1610(1): p. 97-108.
32. Barros, M.H., et al., *Involvement of mitochondrial ferredoxin and Cox15p in hydroxylation of heme O.* FEBS Lett, 2001. 492(1-2): p. 133-8.
33. Zhang, Y., et al., *Mrs3p, Mrs4p, and frataxin provide iron for Fe-S cluster synthesis in mitochondria.* J Biol Chem, 2006. 281(32): p. 22493-502.
34. Djoko, K.Y. and A.G. McEwan, *Antimicrobial action of copper is amplified via inhibition of heme biosynthesis.* ACS Chem Biol, 2013. 8(10): p. 2217-23.
35. Liotenberg, S., et al., *Oxygen-dependent copper toxicity: targets in the chlorophyll biosynthesis pathway identified in the copper efflux ATPase CopA deficient mutant.* Environ Microbiol, 2014.
36. Sokol, R.J., et al., *Oxidant injury to hepatic mitochondria in patients with Wilson's disease and Bedlington terriers with copper toxicosis.* Gastroenterology, 1994. 107(6): p. 1788-98.

37. Terada, K. and T. Sugiyama, *The Long-Evans Cinnamon rat: an animal model for Wilson's disease.* Pediatr Int, 1999. 41(4): p. 414-8.
38. Haywood, S. and C. Vaillant, *Overexpression of copper transporter CTR1 in the brain barrier of North Ronaldsay sheep: implications for the study of neurodegenerative disease.* J Comp Pathol, 2014. 150(2-3): p. 216-24.
39. Zotova, L., et al., *Novel components of an active mitochondrial K(+)/H(+) exchange.* J Biol Chem, 2010. 285(19): p. 14399-414.
40. Katherine E. Vest. *Mitochondrial Copper Transport in Saccharomyces cerevisiae.* https://etd.auburn.edu/xmlui/bitstream/handle/10415/3961/KEVestDissertation.pdf?sequence=2&ts=1434682766967

Chapter 4
Characterization of the Role of Fre5 in Mitochondrial Metal Profile in Yeast

Abstract

Iron co-factors, heme and Fe-S clusters are essential to cells. Heme is required for complexes synthesis in electron transport chain, and Fe-S is required for ribosome assembly. Heme and Fe-S clusters are synthesized in mitochondria, so iron trafficking must be tightly regulated. Fre5 is a member of the iron reductase family found in mitochondria. In order to test the function of Fre5 we compared three different strains: wild type BY4741 (WT), *FRE5* knockout mutant (*fre5Δ*) and *fre5Δ* with *FRE5* gene overexpression (FF). We monitored their metal concentrations by inductively-coupled plasma optical emission spectroscopy (ICP-OES) to determine an ionomic profile for each strain. We collected the metal concentration of each strain six times, in these six times we did three times in normal atmospheric oxygen conditions, three times in hypoxia conditions. By comparing six major mitochondrial metal concentrations in these three strains we found in mitochondria *fre5Δ* has lower level of iron and magnesium, higher level of copper and zinc compared to WT. PCA plots showed the patterns for each strain, they can be separated easily in 3D plot. The power test showed the non-parametric transformation is more efficient overall and especially when dealing with iron. Power analysis showed we need about 40 cases to achieve an overall 80% power in this case.

Introduction

Metals such as iron (Fe), copper (Cu), magnesium (Mg), Manganese (Mn), Phosphorus (P) and Zinc (Zn) are essential for physiological and biochemical processes and for normal growth and development of organisms [1]. Understanding the metal ion content of mitochondria and metal ion interactions are vital for insights into both normal respiratory function and the process of protein damage during oxidative stress. For example, copper and iron ions facilitate

the transfer of electrons in the electron transport chain [2], proteins of the tricarboxylic acid cycle utilize metal iron cofactors to catalyze primary metabolic reactions [3]. Manganese and iron are required for antioxidant defense enzymes [4]. Zinc is required for the protein import apparatus in both carrier protein transport to the inner membrane and presequence degradation [5, 6]. Magnesium is essential for many mitochondrial reactions such as DNA, RNA metabolism and ATP synthesis [7]. Mg^{2+} blocks the yeast mitochondrial ATP-induced unspecific channel (YMUC) [8], it also inhibits mitochondrial anion uniport [9]. The regulation of matrix space Mg^{2+} could be important for mitochondrial distribution of many other ions. Under increased ionic strength, Mg^{2+} and Ca^{2+} are released from mitochondria [10]. Manganese is best known as a component of the antioxidant enzyme superoxide dismutase (SOD2), which helps fight free radicals [11]. This trace element is a cofactor for a number of important enzymes, including arginase, cholinesterase, phosphoglucomutase, pyruvate carboxylase, mitochondrial superoxide dismutase and several phosphates, peptidases and glycosyltransferases. In certain instances, Mn^{2+} may be replaced by Co^{2+} or Mg^{2+}. Excessive ingestion of iron, combined with hypochlorhydria, can cause an imbalance in the Mn/Fe ratio [12]. Zinc plays an essential role in numerous biochemical pathways. In its catalytic role, zinc is a critical component of the catalytic site of hundreds of metalloenzymes. In its structural role, zinc coordinates with certain protein domains, facilitating protein folding and producing structures such as ‘zinc fingers’. In its regulatory role, zinc is involved in the regulation of nucleoproteins and the activity of various inflammatory cells [13].

Organisms require Fe for a wide array of metabolic functions, such as cellular respiration, lipid metabolism, gene regulation and DNA replication and repair [14]. When maintained at a balanced level, iron is essential for organism viability. However, excess iron level is toxic and deficient iron level will lead to physiological and developmental disorders. Excessive iron in cells

will generate reactive oxygen species (ROS) by the Fenton reaction. ROS can damage membrane phospholipids, cause vacuolar fragmentation and generate reactive aldehydes that damage proteins, leading to the accumulation of misfolded protein aggregates [15]. While iron deficiency will cause heme defect and Fe-S cluster defect, severe iron deficiency causes cell death.

Iron deficiency is the most common nutritional disorder in the world [16]. Iron deficiency and iron deficiency anemia are especially prevalent among children and women of childbearing age, where they are associated with perinatal mortality. Iron deficiency also impairs neurological development and cognitive function in children, and some of these defects appear to be irreversible [17]. Although the pathogenesis of anemia in iron deficiency is well understood, other manifestations of iron deficiency are not understood at the cellular or metabolic level, and it is unlikely that all of the clinical manifestations of iron deficiency can be attributed to a reduction in the oxygen-carrying capacity of the blood. Iron overload is also a common disorder and is associated with hereditary hemochromatosis, iron loading anemias, and chronic inflammatory diseases of the liver [18, 19]. Iron overload is typically manifest as an accumulation of iron in organs, especially the liver, heart, and pancreas, leading to organ dysfunction and failure. The mechanisms by which excess iron causes organ failure are unknown. In addition to iron, other transition metals, such as copper, manganese and zinc, are critical to cell well-being.

The budding yeast *Saccharomyces cerevisiae* has served as a model eukaryote for the study of basic cellular processes common to all eukaryotic cells, including the uptake and utilization of transition metals, such as iron. Proteins found in higher or multicellular eukaryotes usually are functionally similar to the orthologous proteins in yeast and can frequently be substituted for the yeast protein. This functional similarity coupled with the genetic tractability of yeast have allowed researchers studying human proteins of iron metabolism to quickly focus

their efforts based on the known functions of the yeast ortholog.

Fre5 is a member of the iron reductase family found in yeast mitochondria required for heme synthesis (Chapter 2). We compared four different strains: wild type (WT), *FRE5* null mutant (*fre5Δ*) and *fre5Δ* with *FRE5* gene overexpression (FF). We monitored their metal concentrations by inductively-coupled plasma (ICP) and determined an ionome profile for each strain. We collected the metal concentration of each strain six times. In these six times, we did three times in normal conditions, three times under hypoxia conditions. By comparing six major mitochondrial metal concentrations in these four strains using different statistical methods we could try to understand the relationships of Fre5 and different metals in mitochondria.

Methods

To obtain the data, we first grew the cells in 1L YPD media for 2 days to let them reach the optical density 600nm to 2, then we harvested the cells by centrifugation in 50 ml VWR centrifuge tube at 4000 rpm for 5 min. Then we treated every 1 g cells with 4U lyticase in 15 ml 1.2 M sorbitol at 30 degree Celsius for 2 hours, after that we added 35ml 1.2M sorbitol and centrifuged at 4000 rpm for 10min to wash off lyticase. Then we added small glass beads and 1.2M sorbitol to make it a total volume of 15 ml, and we vortex each one 30 sec for at least 3 times. The 50ml VWR centrifuge tubes were kept on ice when not use. 35 ml 1.2 M sorbitol were added to the tube and centrifuged at 2500 rpm for 10 min, supernatant were transferred to a new 50 ml VWR centrifuge tube. Pellet were repeated the same procedure for another time. Supernatant were centrifuged at 12000 rpm for 20 min, discarded the supernatant, pellets were the crude mitochondria. Crude mitochondria were dissolved in 5 ml 1.2 M sorbitol and 10 ml 22% histidine were added to the bottom of the tube to make it appear two layers. Centrifuged at 12000 rpm for 60 min, the purified

mitochondria were remained in the middle layer. Drew out the middle layer with a 1 ml pippette and used as ICP samples.100 ug purified mitochondria were mixed with 150uL nitric acid, incubated at 90 ℃ for 30 min. Briefly centrifuged, 450 uL milliQ water were added. Run each sample under ICP with at least three duplicates.

Statistical Methodology

ANOVA

The one-way analysis of variance (ANOVA) was used to determine whether there are any significant differences between the means of three or more independent (unrelated) groups [20]. F test was used to compare four strains' mitochondrial metal concentration differences.

$$\mathrm{F} = \frac{\text{Variance between treatments}}{\text{Variance within treatments}} = \frac{\mathrm{SS(Treatments)}/(\mathrm{p}-1)}{\mathrm{SS(Error)}/(\mathrm{n}-\mathrm{p})}$$

In the above equation, p is the number of treatments, n is the number of total cases.

F test is best used when data are derived from a population that follows a normal distribution.

Robust ANOVA

Robust statistics are statistics with good performance for data drawn from a wide range of probability distributions. They are especially useful for the analysis of data from distributions that are not normal. We could use them to produce statistical methods that are not unduly affected by outliers. Estimators that are efficient for clean data from a simple distribution, such as the normal may not be robust to contamination by outliers, and may be inefficient for more complicated distributions. In robust statistics, more importance is placed on robustness and applicability to a wide variety of distributions, rather than efficiency for a single distribution. M-estimators are a general class of solutions motivated by these concerns, yielding both robustness

and high relative efficiency; though possibly lower efficiency than traditional estimators in cases where the underlying data source is normal. So it is important to find the right balance of robustness and efficiency of the estimators. The basic tools used to measure the robustness are breakdown point and influence function. The breakdown point represents the percentage of gross contamination that the estimator can resist while the influence function measures the sensitivity of the estimator to small local changes in the data. For a good robustness, we want a high breakdown point and a bounded influence function [21]. To test the efficiency, we compare estimator variances and in case of tests their test powers.

In order to identify extreme points and determine whether they are outliers we employ M-type robust ANOVA tests. This is important as identification of outliers often depends on model residuals and, if non-robust models are used, residuals will themselves depend on estimates that are possibly swayed by outliers. This can obscure outliers in the residuals. We used the ROBUSTREG procedure of SAS for robust analysis of variance and residual diagnostics based on M estimation.

The M estimator solves

$$\sum_{i=1}^{N} \psi\left(\frac{r_i}{\sigma}\right) x_{ij} = 0,$$

where x_{ij} represents the group indicator functions, $r_i = y_i - \beta_1 x_{i1} - \cdots - \beta_p x_{ip}$ are the model residuals, and σ is a scale parameter. We used Huber's ψ function given by

$$\psi = \begin{cases} -c & x < -c \\ x & |x| < c \\ c & x > c \end{cases}$$

with $c = 1.345$ which corresponds to 95% efficiency at the normal.

Power test

Power analysis is applied in the context of ANOVA in order to assess the probability of successfully rejecting the null hypothesis by assuming a certain ANOVA design, effect size in the population, sample size and significance level. Power analysis can assist in study design by determining what sample size would be required in order to have a reasonable chance of rejecting the null hypothesis when the alternative hypothesis is true [22].

Nonparametric statistics

Nonparametric statistics do not depend on assumptions relating to specific probability distributions. For two-sample problems, an efficient rank-based nonparametric procedure is the Wilcoxon-Mann-Whitney test. Similar to Huber's M estimator, this test has 95.5% efficiency versus the t-test for normal data and it becomes superior to the t-test if the distributions are heavier tailed or the data contain outliers [23]. The extension of the Wilcoxon-Mann-Whitney test to multiple samples is given by the Kruskal-Wallis test. This test has the same efficiency and robustness comparisons against the F-test that the Wilcoxon test has against the t-test. The Kruskal-Wallis test statistic is given by:

$$\mathrm{K} = (\mathrm{N}-1)\frac{\sum_{i=1}^{p} n_i\,(\overline{r_{i\cdot}} - \bar{r})^2}{\sum_{i=1}^{p}\sum_{j=1}^{n_i}(\overline{r_{ij}} - \bar{r})^2},$$

Where n_i is the number of observations in group i; $\overline{r_{ij}}$ is the rank of observation j from group i; N is the total number of observations across all groups; $\overline{r_{i\cdot}} = \frac{\sum_{j=1}^{n_i} n_{ij}}{n_i}$; $\bar{r} = \frac{N+1}{2}$ is the average of all the r_{ij}.

If the data contain no ties then the denomination of K is $\frac{(\mathrm{N}-1)\mathrm{N}(\mathrm{N}+1)}{12}$ and

$$\mathrm{K} = \frac{12}{N(N+1)}\sum_{i=1}^{p} n_i \left(\overline{r_{i.}} - \frac{N+1}{2}\right)^2 = \frac{12}{N(N+1)}\sum_{i=1}^{p} n_i \overline{r_{i.}}^2 - 3\ （N+1)$$

It contains only the squares of the average ranks, the p value is approximated by $\Pr(X^2_{p-1} \geq K)$ [24, 25].

MANOVA

MANOVA is a generalized form of univariate ANOVA, but unlike univariate ANOVA, it uses the variance-covariance between variables in testing the statistical significance of the mean differences. MANOVA is most effective when dependent variables are correlated. It helps to answer whether changes in the independent variables have significant effects on the dependent variables and what are the interactions among the dependent variables and among the independent variables [26].

Principal component analysis

We applied principal component analysis (PCA) as an exploratory data analysis. PCA uses an orthogonal transformation to convert a set of observations of possibly correlated variables into a set of values of linearly uncorrelated variables called principal components. The first principal component has the largest variance possible under the constraint that it is orthogonal to the preceding components [27]. The principal components can be used to find clusters in a set of data. PCA is a variance-focused approach seeking to reproduce the total variable variance, in which components reflect both common and unique variance of the variable. PCA is generally preferred for purposes of data reduction, with more of the total variance concentrated in the first few principal components compared to the same noise variance, the proportionate effect of the noise

is less. PCA thus can have the effect of concentrating much of the signal into the first few principal components, which can usefully be captured by dimensionality reduction; while the later principal components may be dominated by noise, and so disposed of without great loss [28].

Results

First, we used ANOVA to compare iron concentration in different strains using the SAS PROC REG procedure. The results are as below (Figure 4.1). From Figure 4.1A ANOVA table we could see that compared with *fre5Δ*, FF was significantly different. To determine if any outliers interfered the conclusion we applied robust ANOVA test by using PROC ROBUSTREG. From Figure 4.1A Robust ANOVA results we could see that p value in WT changed significantly, it became significant when setting $\alpha=0.05$, meaning there are potential outliers in the data. By comparing them visually in box-plot (Figure 4.1B) we did not visualize any potential outliers. However, we did find three outliers by robust ANOVA analysis (Figure 4.1C). We could see from Figure 4.1B, *fre5Δ* has the lowest iron in the mitochondria, then WT, FF showed highest iron concentration (though in a wide range) and it is significantly different from *fre5Δ*. We then performed non-parametric analysis by using PROC NPAR1WAY to compare the rank among different strains. Figure 4.1D showed the p value was 0.0021, so there are significant difference among strains. Box plot in Figure 4.1E showed FF strain and *fre5Δ* are significantly different in iron levels. Nonparametric analysis result is consistent with the ANOVA test result, meaning the distribution of the data was normal.

A

ANOVA					Robust ANOVA			
Variable	Parameter Estimate	Standard Error	t Value	Pr > |t|	Estimate	Standard Error	Chi-Square	Pr > ChiSq
Intercept	0.03855	0.00397	9.7	<.0001	0.0386	0.0012	1017.54	<.0001
strainff	0.02257	0.00562	4.02	0.0011	0.0375	0.0017	480.43	<.0001
Strainwt	0.00432	0.00562	0.77	0.4543	0.0042	0.0017	6.14	0.0132
Strainfre5	0	.	.	.	0	.	.	.

B

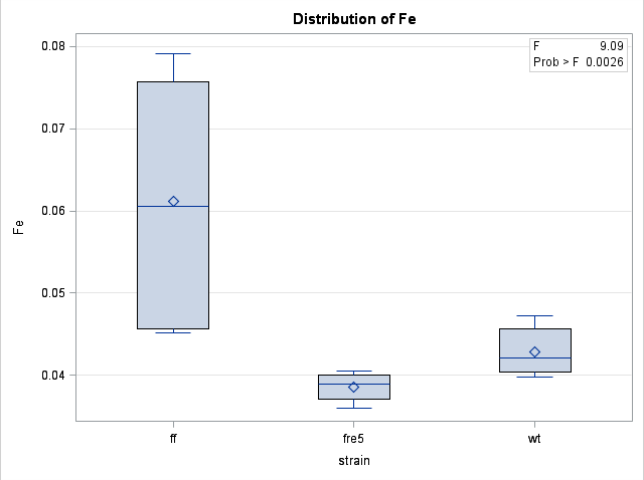

C

Diagnostics		
Obs	Standardized Robust Residual	Outlier
16	-8.1408	*
17	-8.2847	*
18	-7.5564	*

D

Kruskal-Wallis Test	
Chi-Square	12.3626
DF	2
Pr > Chi-Square	0.0021

E

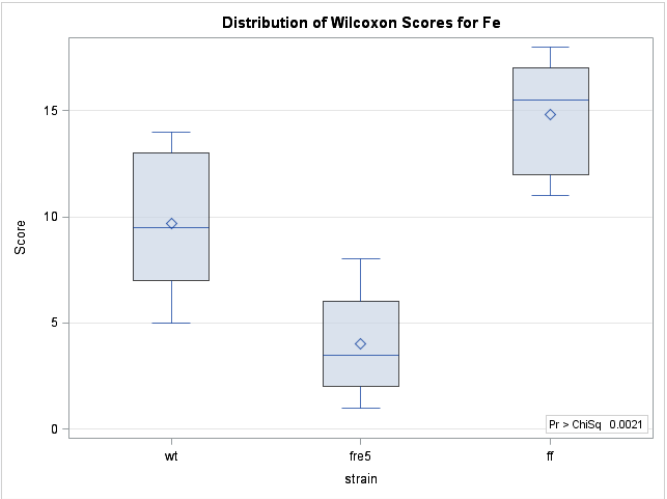

Figure 4.1 Iron ANOVA and nonparametric test results.

A is the ANOVA and Robust ANOVA data table from PROC REG and PROC ROBUSTREG procedure. Three strains' mitochondrial iron level were compared by one way ANOVA, B is the boxplot from the same procedure. C shows the outliers identified by ROBUSTREG procedure. D

is the Kruskal-Wallis test result from PROC NPAR1WAY procedure, E is the boxplot based on Wilcoxon scores.

Then we performed the same analysis with copper. Figure 4.2A ANOVA results showed FF is significantly different compared with *fre5Δ*. And we got the same result from robust ANOVA analysis. By looking at the box-plots, we did not see any potential outliers, and we did not find outlier by robust ANOVA analysis. *fre5Δ* and WT have a wide range in copper concentration in the mitochondria, *fre5Δ* showed higher copper concentration compared with FF. Non-parametric analysis showed the p value was 0.0319 (Figure 4.2C), so there are significant difference among strains. Box plot in Figure 4.2D showed FF strain and *fre5Δ* are significantly different in copper levels. Nonparametric analysis result is consistent with the ANOVA test result.

A

ANOVA					Robust ANOVA			
Variable	Parameter Estimate	Standard Error	t Value	Pr > |t|	Estimate	Standard Error	Chi-Square	Pr > ChiSq
Intercept	0.48741	0.03067	15.89	<.0001	0.4872	0.0326	223.28	<.0001
strainff	-0.1293	0.04338	-2.98	0.0093	-0.1291	0.0461	7.84	0.0051
strainwt	-0.0766	0.04338	-1.77	0.0976	-0.0765	0.0461	2.75	0.0972
Strainfre5	0	.	.	.	0	.	.	.

B

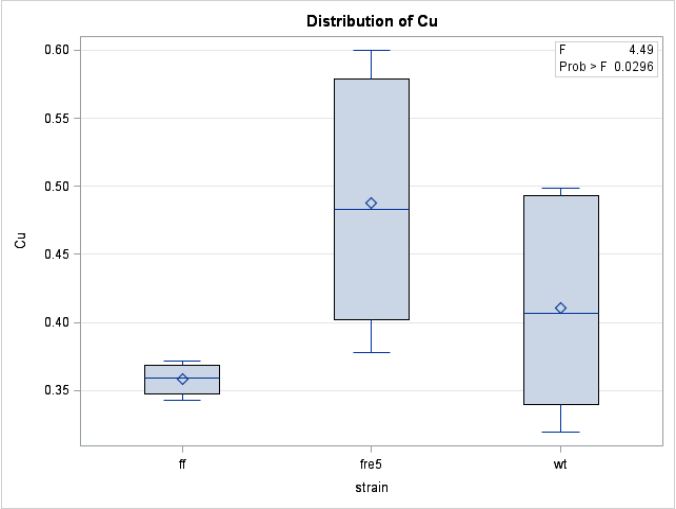

C

Kruskal-Wallis Test	
Chi-Square	6.8889
DF	2
Pr > Chi-Square	0.0319

D

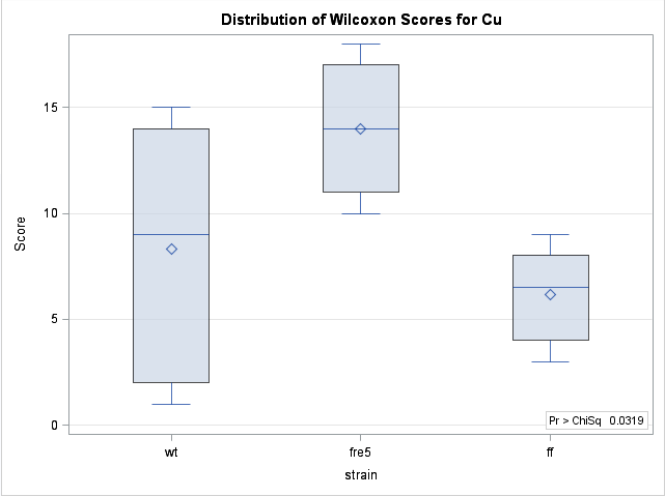

Figure 4.2 Copper ANOVA and nonparametric test results.

A is the ANOVA and Robust ANOVA data table from PROC REG and PROC ROBUSTREG procedure. Three strains' mitochondrial copper level were compared by one way ANOVA, B is the

boxplot from the same procedure. C is the Kruskal-Wallis test result from PROC NPAR1WAY procedure, D is the boxplot based on Wilcoxon scores.

Magnesium is the third metal we tested. Results were shown in Figure 4.3. The p value in ANOVA table showed FF strain is significantly different compared to *fre5Δ*. Robust ANOVA result showed the same result with slightly smaller in p values. By looking at the box-plot of ANOVA we could see that *fre5Δ* and WT showed lower magnesium concentration in mitochondria than FF strain (Figure 4.3B). By robust ANOVA analysis, there is no outlier found. Non-parametric analysis showed the p value was 0.0148 (Figure 4.3C), so there are significant difference among strains. Box plot in Figure 4.3D showed there is one potential outlier, if we ignore that point FF strain and *fre5Δ* are significantly different in magnesium levels. Nonparametric analysis result is consistent with the ANOVA test result.

A

	ANOVA				Robust ANOVA			
Variable	Parameter Estimate	Standard Error	t Value	Pr > |t|	Estimate	Standard Error	Chi-Square	Pr > ChiSq
Intercept	4.30058	0.08178	52.59	<.0001	4.302	0.0889	2339.24	<.0001
strainff	0.36559	0.11565	3.16	0.0065	0.3712	0.1258	8.71	0.0032
strainwt	-0.106	0.11565	-0.92	0.3741	-0.107	0.1258	0.72	0.3949
Strainfre5	0	.	.	.	0	.	.	.

B

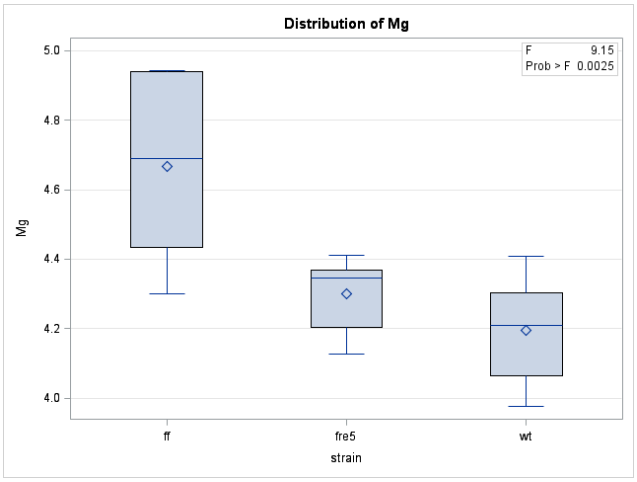

C

Kruskal-Wallis Test	
Chi-Square	8.4327
DF	2
Pr > Chi-Square	0.0148

D

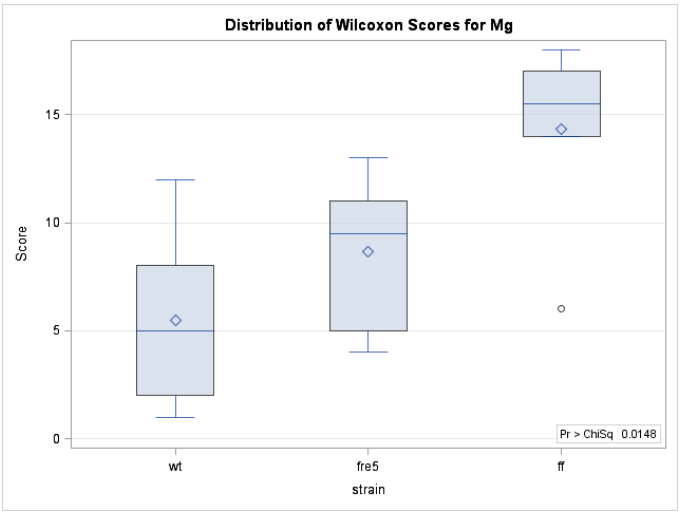

Figure 4.3 Magnesium ANOVA and nonparametric test results.

A is the ANOVA and Robust ANOVA data table from PROC REG and PROC ROBUSTREG procedure. Three strains' mitochondrial magnesium level were compared by one way ANOVA, B

is the boxplot from the same procedure. C is the Kruskal-Wallis test result from PROC NPAR1WAY procedure, D is the boxplot based on Wilcoxon scores.

We then analyzed Manganese with ANOVA approach. The results showed in Figure 4.4. The ANOVA table showed WT is significantly different from *fre5Δ* in manganese level. The box-plot showed that WT had higher level of manganese compared with *fre5Δ* and FF strain. There is one potential outlier in the box plot (Figure 4.4B). However with robust ANOVA analysis, we did not find outlier. Non-parametric analysis showed the p value was 0.0061 (Figure 4.4C), so there are significant difference among strains. Box plot in Figure 4.4D showed FF strain and *fre5Δ* are not significantly different in manganese levels, WT and *fre5Δ* has overlaps as well, we could only see significant difference between WT and FF strain. Based on the box plot of nonparametric analysis, the nonparametric analysis result is not consistent with the ANOVA test result, meaning the manganese data are not normally distributed.

A

ANOVA					Robust ANOVA			
Variable	Parameter Estimate	Standard Error	t Value	Pr > |t|	Estimate	Standard Error	Chi-Square	Pr > ChiSq
Intercept	-0.0187	0.00065	-28.82	<.0001	-0.0187	0.0007	637.62	<.0001
strainff	-0.0004	0.00092	-0.44	0.6655	-0.0004	0.001	0.16	0.6869
strainwt	0.00346	0.00092	3.77	0.0019	0.0034	0.001	10.45	0.0012
Strainfre5	0	.	.	.	0	.	.	.

B

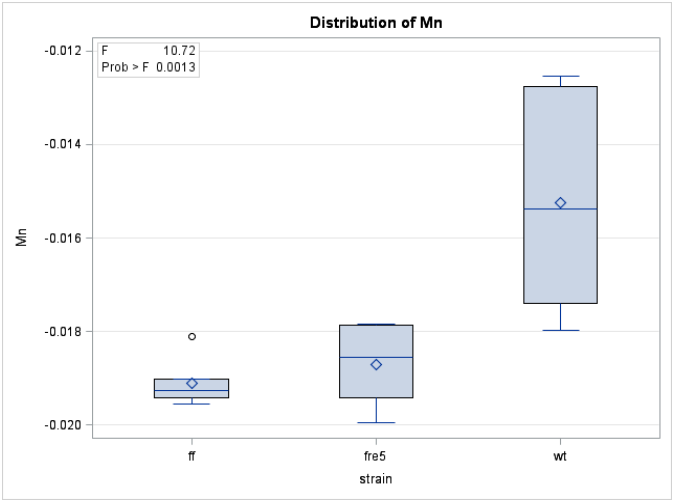

C

Kruskal-Wallis Test	
Chi-Square	10.2105
DF	2
Pr > Chi-Square	0.0061

D

Figure 4.4 Manganese ANOVA and nonparametric test results.

A is the ANOVA and Robust ANOVA data table from PROC REG and PROC ROBUSTREG procedure. Three strains' mitochondrial manganese level were compared by one way ANOVA, B

is the boxplot from the same procedure. C is the Kruskal-Wallis test result from PROC NPAR1WAY procedure, D is the boxplot based on Wilcoxon scores.

Phosphorus is the next metal we analyzed. As shown in Figure 4.5A, the ANOVA table did not show significant difference within strains, the box-plot shows there is no significant difference among strains, and we did not find any outliers by robust ANOVA analysis and by looking at the box plot (Figure 4.5B). Robust ANOVA did not find significant difference either. Non-parametric analysis showed the same result.

A

ANOVA					Robust ANOVA			
Variable	Parameter Estimate	Standard Error	t Value	Pr > |t|	Estimate	Standard Error	Chi-Square	Pr > ChiSq
Intercept	7.4501	0.61613	12.09	<.0001	7.4481	0.6792	120.24	<.0001
strainff	-1.2688	0.87134	-1.46	0.166	-1.2676	0.9606	1.74	0.187
strainwt	-1.0242	0.87134	-1.18	0.2581	-1.023	0.9606	1.13	0.2869
Strainfre5	0	.	.	.	0	.	.	.

B

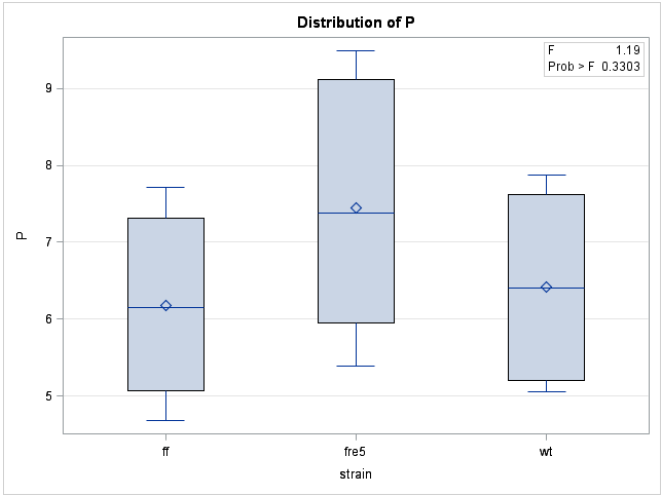

C

Kruskal-Wallis Test	
Chi-Square	3.0292
DF	2
Pr > Chi-Square	0.2199

D

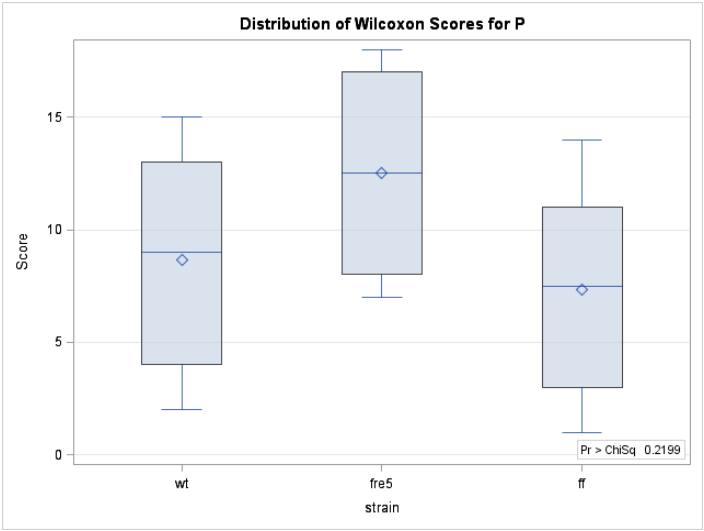

Figure 4.5 Phosphorus ANOVA and nonparametric test results.

A is the ANOVA and Robust ANOVA data table from PROC REG and PROC ROBUSTREG procedure. Three strains' mitochondrial phosphorus level were compared by one way ANOVA, B

is the boxplot from the same procedure. C is the Kruskal-Wallis test result from PROC NPAR1WAY procedure, D is the boxplot based on Wilcoxon scores.

The last metal we analyzed was zinc. ANOVA table showed in Figure 4.6A FF strain and *fre5Δ* are significantly different. Box-plot showed there is no potential outlier. After Robust ANOVA analysis we found the same result, FF strain and *fre5Δ* are significantly different. And there is no outlier based on robust ANOVA analysis. Non-parametric analysis showed the p value was 0.0068 (Figure 4.6C), so there was a significant difference among strains. Box plot in Figure 4.6D showed there is no potential outlier, FF strain and *fre5Δ* are significantly different in zinc levels. Nonparametric analysis result is consistent with the ANOVA test result.

A

ANOVA					Robust ANOVA			
Variable	Parameter Estimate	Standard Error	t Value	Pr > |t|	Estimate	Standard Error	Chi-Square	Pr > ChiSq
Intercept	0.28426	0.01415	20.08	<.0001	0.2841	0.0152	347.54	<.0001
strainff	-0.0657	0.02002	-3.28	0.0051	-0.0655	0.0216	9.24	0.0024
strainwt	-0.0245	0.02002	-1.22	0.2398	-0.0244	0.0216	1.28	0.2575
Strainfre5	0	.	.	.	0	.	.	.

B

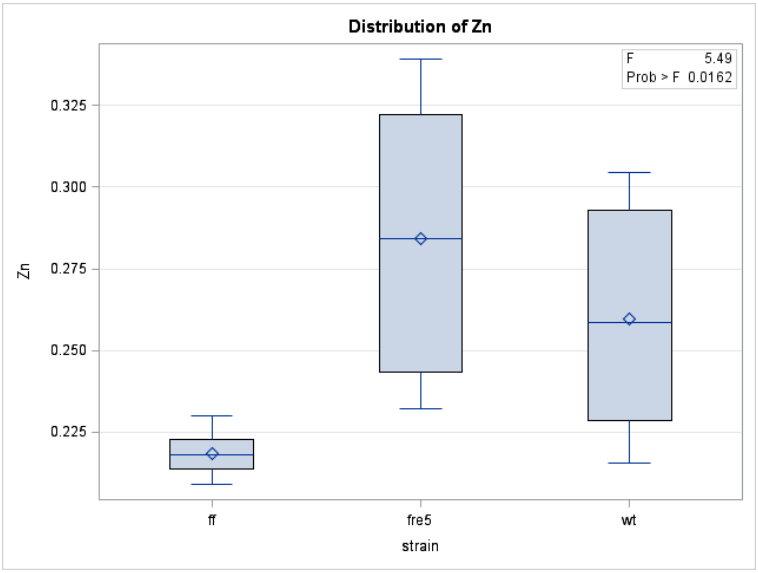

C

Kruskal-Wallis Test	
Chi-Square	9.9766
DF	2
Pr > Chi-Square	0.0068

D

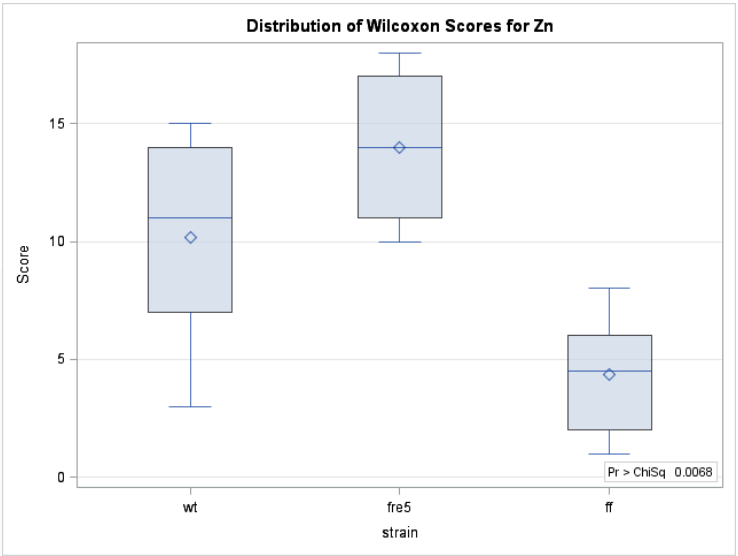

Figure 4.6 Zinc ANOVA and nonparametric test results.

A is the ANOVA and Robust ANOVA data table from PROC REG and PROC ROBUSTREG procedure. Three strains' mitochondrial zinc level were compared by one way ANOVA, B is the

boxplot from the same procedure. C is the Kruskal-Wallis test result from PROC NPAR1WAY procedure, D is the boxplot based on Wilcoxon scores.

To eliminate the colinearity among different metals, we performed MANOVA to test if there is difference among strains as a whole. The result is shown in below. All the tested pointed out that there are significant differences among strains with p value less than 0.0001 (Figure 4.7)

MANOVA Test Criteria and F Approximations for the Hypothesis of No Overall strain Effect
H = Type III SSCP Matrix for strain
E = Error SSCP Matrix

S=2 M=1.5 N=4

Statistic	Value	F Value	Num DF	Den DF	Pr > F
Wilks' Lambda	0.00064310	64.06	12	20	<.0001
Pillai's Trace	1.94294622	62.43	12	22	<.0001
Hotelling-Lawley Trace	86.71664698	68.53	12	12.791	<.0001
Roy's Greatest Root	63.67323462	116.73	6	11	<.0001

NOTE: F Statistic for Roy's Greatest Root is an upper bound.

NOTE: F Statistic for Wilks' Lambda is exact.

Figure 4.7 MANOVA results.

Then we performed PCA to see if we could see a pattern for each strain. We first standardized the data to eliminate scale differences. By the cumulative eigenvalue table and variance explained plot (Figure 4.8A&B) we could see we need to include at least three principal components to explain at least 80% of the data. Figure 4.8C shows the eigenvector values for each principal component.

A

Eigenvalues of the Correlation Matrix				
	Eigenvalue	Difference	Proportion	Cumulative
1	2.49569347	0.81398124	0.4159	0.4159
2	1.68171224	0.68836092	0.2803	0.6962
3	0.99335132	0.45597991	0.1656	0.8618
4	0.53737141	0.25584730	0.0896	0.9514
5	0.28152411	0.27117664	0.0469	0.9983
6	0.01034746		0.0017	1.0000

B

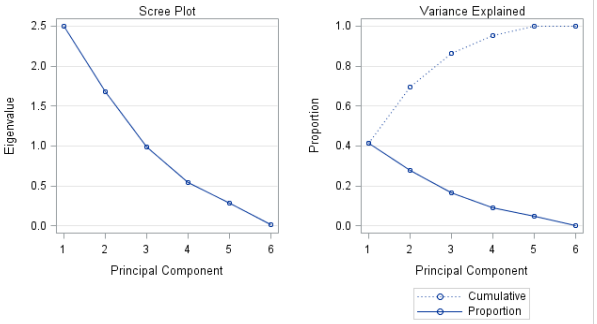

C

Eigenvectors						
	Prin1	Prin2	Prin3	Prin4	Prin5	Prin6
Fe	-.337610	0.108058	0.808823	0.287618	-.025916	0.369801
Cu	0.510417	-.112281	-.060220	0.691431	-.491698	0.058280
Mg	-.330736	0.449149	-.381240	0.595158	0.433945	-.031829
Mn	0.252593	-.624852	0.167005	0.217757	0.681926	-.073654
P	0.405844	0.495997	0.407266	-.027279	0.144667	-.633829
Zn	0.536278	0.370848	-.055487	-.191894	0.288621	0.672067

Figure 4.8 PCA results.

A is the eigenvalues of the correlation matrix and their cumulative percentage, B is the scree plot of the principal components, C is the eigenvectors of each principal component.

To explore the strains' pattern we first scatter plotted two principal components. The plot is shown below (Figure 4.9A). Blue dots are WT strain, red dots are *fre5Δ* and green dots are FF strain. FF strain dots are gathered together, but WT and *fre5Δ* dots have strong overlaps. By just first two principal components we could not separate these three different strains. Then we plotted with three principal components to cover more than 80% data variances by using PROC G3D. With three dimension plot the separation of different strain is more obvious (Figure 4.9B). WT are blue clubs, *fre5Δ* are red diamonds and FF are green spades. We could see six different groups in 3D chart and each group contains three observations. Because we have data from normal condition and hypoxia condition, for each condition we obtained three observations, so we could

conclude that normal condition and hypoxia condition strains have different metal profiles. For *fre5Δ* observations, they mainly shifted on principal component 1 (prin1) axis, WT mainly shifted on principal component 2 (prin2) axis and FF strain mainly shifted on principal component 3 (prin3) axis. By looking at the eigenvectors for each principal component from Figure 4.8C we could see in prin1 copper and zinc have the highest vector coefficient, in prin2 they are manganese and phosphorous and they are iron and copper in prin3. Under normal atmospheric oxygen condition and hypoxia, yeast will undergo different pathways to obtain energy. So in these two different conditions, yeast have different requirements for metal. Iron and copper are two major metals required in electron transport chain, which is the place oxygen has been consumed. Copper is one major vector coefficient for both prin1 and prin3, which is probably the reason why FF strain and *fre5Δ* changed so much under these conditions.

A

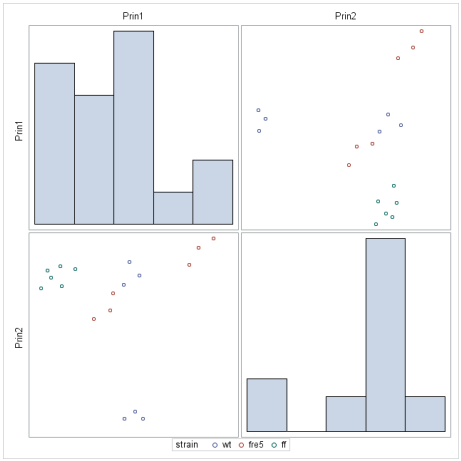

B

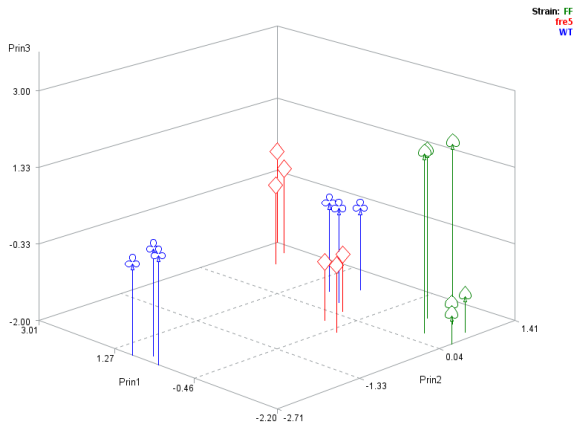

Figure 4.9 Principal Components plots.

A is scatter plot with principal component 1 and 2, B is three dimension plot with principal components 1-3.

At last, we performed power test for the data we collected to test how many data we need to collect to get confident results (to eliminate type II error: accept false null hypothesis). The

results showed that the highest power is associated with manganese with power of 0.726, phosphorous has the lowest power of only 0.217 (Figure 4.10A). To make sure every metal is associated with power higher than 0.8, we need to collect about 100 observations (Fig 4.10B). If we leave out phosphorous and just consider the other five metals, we just need about 40 observations to reach more than 0.8 power, which means we need 13-14 observations for each strain.

A

Computed Power		
Index	Dependent	Power
1	Fe	0.693
2	Cu	0.521
3	Mg	0.695
4	Mn	0.726
5	P	0.217
6	Zn	0.574

B

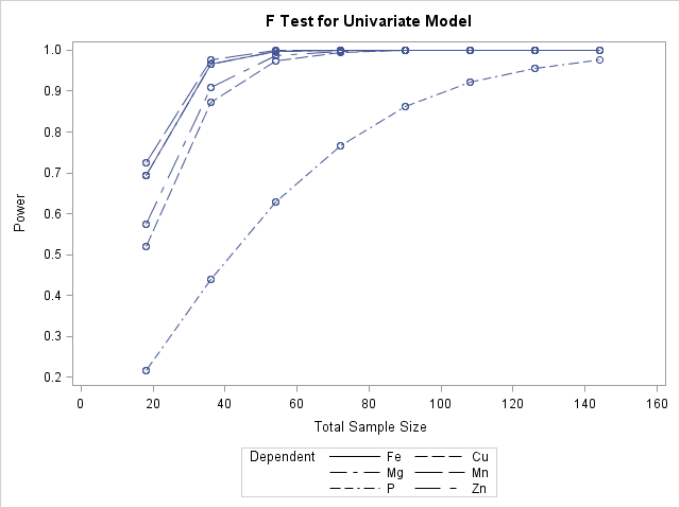

Figure 4.10 Power test result for the six major metals.

A is the power number of each metal, B shows the predict power number when case number in the data grows.

Discussion

We analyzed our data using a general linear model ANOVA, robust ANOVA, non-parametric analysis through rank transformation, MANOVA, principal component analysis and finally a power analysis. The conclusion is that there are significant differences among strains. We achieved this conclusion by eliminating outliers identified by robust ANOVA tests. *fre5Δ* and *fre5Δ* with *FRE5* overexpression strain (FF) are significantly different in iron, copper, magnesium and

zinc. Compared with *fre5Δ*, FF mitochondria have higher levels of iron and magnesium and lower levels of copper and zinc. Although not significantly different, WT showed the same trend of FF strain compared with *fre5Δ* in most cases. The only exception case is magnesium, the reason for that is not clear. As an iron reductase in mitochondria, Fre5 is responsible for the reduction of ferric iron to ferrous iron to make it bioavailable; thus, deletion of *FRE5* could be the cause of insufficient iron acquirement in mitochondria. Overexpressing that will give more reduction power in the mitochondria, so the iron level increased. Iron level is significantly correlated with other metals. Thus, the relationship between iron and copper, magnesium and zinc needs to be tested in other strains to validate this statement. Iron and copper are correlated in other biological pathways. In yeast cells, the multicopper protein Fet3 located in the plasma membrane act as a ferroxidase [29]. There are also other proteins related with both iron and copper, like cytochrome c oxidase in the electron transport chain [30]. The statistical analysis presented here is consistent with the competition observed in Chapter 3 where iron and copper level are oppositely correlated, indicating there is a competition between them. Magnesium and iron levels are correlated in other systems, for example humans that have iron or magnesium deficiency have very similar manifestations. Although manganese and magnesium have similar chemical properties, we did not observe the same pattern in their ion level. And manganese share the same plasma membrane transporter with iron called Smf1 [31], they also share the same vacuole transporter Ccc1 [32], whether they share same mitochondrial membrane transporter is unknown. We did see *fre5Δ* showed a lower of manganese compare to WT, but not FF strain. In the mitochondrial matrix, manganese is the only metal required as a cofactor in SOD2 [33]. With the oxidative stress resistance phenotype, it was possible that *fre5Δ* had higher level of manganese in the mitochondria. However, the results suggest this oxidative stress resistance phenotype is not because of SOD2

activity. Zinc and copper share similarity in that they both have the ability to be the cofactor metal of SOD1, which is the other superoxide dismutase has been found as an abundant cytosolic enzyme [34]. It is also reported that a small percentage of the total SOD1 protein in *Saccharomyces cerevisiae* is located in the intermembrane space (IMS) of mitochondria [35]. SOD1 locating in mitochondria would potentially protect against superoxide radicals released into IMS by the electron transport chain [36]. In the *fre5Δ* mitochondria, copper and zinc levels are higher compared to FF strain, suggesting a potentially higher level of SOD1 in the IMS or cytosol that contributes to this ROS resistance phenotype. It is reported that excess iron in the diet can result in an induced zinc deficiency [37]. This statement suggests there is a negative correlation between iron and zinc. In our study, we also showed a negative correlation between iron and zinc. PCA plots showed the patterns for each strain and that they can be separated easily in 3D plots. Prin3 has copper and iron as its most significant vectors, because we collected data in both normal and hypoxia conditions, their iron and copper level also changed in these two different environments, this might be the reason *fre5Δ* and FF strain shift on prin3 in 3D plot. The reason WT did not shift on prin3 but prin2 was unclear. Prin2 has manganese and phosphorus as its major vectors. The power analysis showed that this study collected insufficient data to draw final conclusion.

The limitation of the study pertains to the data collection. Mitochondria are hard to isolate and the growth condition is not easy to manipulate, especially when attempting to control the levels of metals taken up by each strain. We had only 18 cases overall, maybe the data did not show the actual metal traits for these strains that we need to increase the collection to get more accurate results. Power test showed we need about 40 cases to achieve an overall 80% power if we leave out phosphorus. In the future, if possible, we recommend collecting more cases to minimize the

interference of the outliers and to obtain more accurate results so that we could see the patterns of each strain more clearly.

Reference

1. Rozhdestvenskii, V.I., et al., *[Control of mineral nutrition of higher plants in biological life support systems]*. Kosm Biol Aviakosm Med, 1975. 9(6): p. 30-5.
2. Pascal, N. and R. Douce, *Effect of Iron Deficiency on the Respiration of Sycamore (Acer pseudoplatanus L.) Cells.* Plant Physiol, 1993. 103(4): p. 1329-1338.
3. Jordanov, J., et al., *Structural investigations by extended X-ray absorption fine structure spectroscopy of the iron center of mitochondrial aconitase in higher plant cells.* J Biol Chem, 1992. 267(24): p. 16775-8.
4. Alscher, R.G., N. Erturk, and L.S. Heath, *Role of superoxide dismutases (SODs) in controlling oxidative stress in plants.* J Exp Bot, 2002. 53(372): p. 1331-41.
5. Lister, R., et al., *Zinc-dependent intermembrane space proteins stimulate import of carrier proteins into plant mitochondria.* Plant J, 2002. 30(5): p. 555-66.
6. Moberg, P., et al., *Characterization of a novel zinc metalloprotease involved in degrading targeting peptides in mitochondria and chloroplasts.* Plant J, 2003. 36(5): p. 616-28.
7. Gregan, J., M. Kolisek, and R.J. Schweyen, *Mitochondrial Mg(2+) homeostasis is critical for group II intron splicing in vivo.* Genes Dev, 2001. 15(17): p. 2229-37.
8. Guerin, B., et al., *ATP-induced unspecific channel in yeast mitochondria.* J Biol Chem, 1994. 269(41): p. 25406-10.
9. Manon, S. and M. Guerin, *Evidence for three different electrophoretic pathways in yeast mitochondria: ion specificity and inhibitor sensitivity.* J Bioenerg Biomembr, 1993. 25(6): p. 671-8.
10. Bradshaw, P.C. and D.R. Pfeiffer, *Release of Ca2+ and Mg2+ from yeast mitochondria is stimulated by increased ionic strength.* BMC Biochem, 2006. 7: p. 4.
11. Dendle, P., *Lupines, manganese, and devil-sickness: an Anglo-Saxon medical response to epilepsy.* Bull Hist Med, 2001. 75(1): p. 91-101.
12. Mandal, U., et al., *Management of experimental hypochlorhydria with iron deficiency by the composite extract of Fumaria vaillantii L. and Benincasa hispida T. in rat.* J Nat Sci Biol Med, 2014. 5(2): p. 397-403.
13. Funk, A.E., F.A. Day, and F.O. Brady, *Displacement of zinc and copper from copper-induced metallothionein by cadmium and by mercury: in vivo and ex vivo studies.* Comp Biochem Physiol C, 1987. 86(1): p. 1-6.
14. Lill, R. and U. Muhlenhoff, *Maturation of iron-sulfur proteins in eukaryotes: mechanisms, connected processes, and diseases.* Annu Rev Biochem, 2008. 77: p. 669-700.
15. Corson, L.B., et al., *Oxidative stress and iron are implicated in fragmenting vacuoles of Saccharomyces cerevisiae lacking Cu,Zn-superoxide dismutase.* J Biol Chem, 1999. 274(39): p. 27590-6.
16. Zimmermann, M.B. and R.F. Hurrell, *Nutritional iron deficiency.* Lancet, 2007. 370(9586): p. 511-20.

17. Beard, J.L., *Why iron deficiency is important in infant development.* J Nutr, 2008. 138(12): p. 2534-6.
18. Philippe, M.A., R.G. Ruddell, and G.A. Ramm, *Role of iron in hepatic fibrosis: one piece in the puzzle.* World J Gastroenterol, 2007. 13(35): p. 4746-54.
19. De Domenico, I., D. McVey Ward, and J. Kaplan, *Regulation of iron acquisition and storage: consequences for iron-linked disorders.* Nat Rev Mol Cell Biol, 2008. 9(1): p. 72-81.
20. Van Belle, G., *Statistical rules of thumb*. 2nd ed. Wiley series in probability and statistics. 2008, Hoboken, N.J.: Wiley. xxi, 272 p.
21. Huber, P.J., *Robust statistics*. Wiley series in probability and mathematical statistics. 1981, New York: Wiley. ix, 308 p.
22. Aberson, C.L., *Applied power analysis for the behavioral sciences*. 2010, New York: Routledge.
23. Hettmansperger, T.P. and J.W. McKean, *Robust nonparametric statistical methods*. 2nd ed. Chapman & hall/crc monographs on statistics & applied probability. 2011, Boca Raton, FL: CRC Press. xvii, 535 p.
24. Rasch, D., M.L. Tiku, and Mathematische Gesellschaft der DDR., *Robustness of statistical methods and nonparametric statistics*. Theory and decision library Series B, Mathematical and statistical methods. 1984, Dordrecht BostonHingham, MA, U.S.A.: D. Reidel ; Distributors for the U.S.A. and Canada, Kluwer Academic Publishers. 172 p.
25. Roussas, G.G. and North Atlantic Treaty Organization. Scientific Affairs Division., *Nonparametric functional estimation and related topics*. NATO ASI series Series C, Mathematical and physical sciences. 1991, Dordrecht ; Boston: Kluwer Academic Publishers. xiii, 708 p.
26. Stevens, J., *Applied multivariate statistics for the social sciences*. 4th ed. 2002, Mahwah, N.J.: Lawrence Erlbaum Associates. xiv, 699 p.
27. Jolliffe, I.T., *Principal component analysis*. 2nd ed. Springer series in statistics. 2002, New York: Springer. xxix, 487 p.
28. Jolliffe, I.T., *Principal component analysis*. Springer series in statistics. 1986, New York: Springer-Verlag. xiii, 271 p.
29. Shi, X., et al., *Fre1p Cu2+ reduction and Fet3p Cu1+ oxidation modulate copper toxicity in Saccharomyces cerevisiae.* J Biol Chem, 2003. 278(50): p. 50309-15.
30. Tsukihara, T., et al., *Structures of metal sites of oxidized bovine heart cytochrome c oxidase at 2.8 A.* Science, 1995. 269(5227): p. 1069-74.
31. Culotta, V.C., M. Yang, and M.D. Hall, *Manganese transport and trafficking: lessons learned from Saccharomyces cerevisiae.* Eukaryot Cell, 2005. 4(7): p. 1159-65.
32. Chen, O.S. and J. Kaplan, *CCC1 suppresses mitochondrial damage in the yeast model of Friedreich's ataxia by limiting mitochondrial iron accumulation.* J Biol Chem, 2000. 275(11): p. 7626-32.
33. Weisiger, R.A. and I. Fridovich, *Mitochondrial superoxide simutase. Site of synthesis and intramitochondrial localization.* J Biol Chem, 1973. 248(13): p. 4793-6.
34. Crapo, J.D., et al., *Copper,zinc superoxide dismutase is primarily a cytosolic protein in human cells.* Proc Natl Acad Sci U S A, 1992. 89(21): p. 10405-9.
35. Sturtz, L.A., et al., *A fraction of yeast Cu,Zn-superoxide dismutase and its metallochaperone, CCS, localize to the intermembrane space of mitochondria. A*

physiological role for SOD1 in guarding against mitochondrial oxidative damage. J Biol Chem, 2001. 276(41): p. 38084-9.
36. Zhang, L., L. Yu, and C.A. Yu, *Generation of superoxide anion by succinate-cytochrome c reductase from bovine heart mitochondria.* J Biol Chem, 1998. 273(51): p. 33972-6.
37. Golden, M.H. and B.E. Golden, *Effect of zinc supplementation on the dietary intake, rate of weight gain, and energy cost of tissue deposition in children recovering from severe malnutrition.* Am J Clin Nutr, 1981. 34(5): p. 900-8.

Appendix

SAS codes:

```
data icpf;
input strain $    Ag    Al    B     Ca    Co    Cu    Fe    K     Mg    Mn
      Mo    Na    Ni    P     S     Zn;
datalines;
wt    0.00145594  0.07161692  0.015958872 8.307738569 -0.002014666
      0.348947961 0.041239125 1.538586131 4.301863602 -0.017389677
      0.016781955 0.798474687 0.002201947 7.615968415 6.855715767 0.304323438
wt    0.001324566 0.05705715  0.013699676 8.215102637 -0.000935344
      0.340010261 0.040353089 1.902695657 4.407538439 -0.017982386
      0.008515143 0.96011583  0.001842861 7.870992429 6.667075055 0.292904749
wt    0.000739061 0.064254352 0.013035216 8.355019671 -0.000788421
      0.319418195 0.042920314 1.556946339 4.302589538 -0.017204621
      0.0077441   0.812357862 0.001707526 7.454469804 6.46966954  0.285598688
fre5  0.000671636 0.063049032 0.012639779 8.502207682 -0.00111855 0.550766754
      0.037045622 1.576181989 4.32770963  -0.017867523      0.00545249
      0.799991423 0.001714459 8.576808536 6.977395113 0.311059356
fre5  0.000481837 0.06004008  0.012023232 8.53142803  -0.001239178
      0.578747747 0.039331131 1.613571473 4.410226725 -0.017845374
      0.006876498 0.79094108  0.002746878 9.115645475 7.164258104 0.322316723
fre5  0.000573362 0.058779563 0.011473785 8.34986472  -0.001393034
      0.599550903 0.040521011 1.599666247 4.368913548 -0.017959018
      0.00609526  0.772271224 0.00248221  9.489898949 7.078289833 0.339210479
ff    0.00016908  0.047740278 0.011208315 7.739749025 -0.001439567
      0.34311486  0.075692429 1.499905511 4.30097629  -0.019015528
      0.005503965 0.764809098 0.002247575 7.065952403 6.208737595 0.21391586
ff    0.000166971 0.053421316 0.011243509 8.121501131 -0.00073062 0.351409757
      0.079174999 1.556415572 4.433374985 -0.019301217      0.003424756
      0.809667297 0.002639053 7.317153493 6.446582932 0.222781092
ff    0.000130554 0.051850758 0.010948125 8.034059165 -0.000812514
      0.366834784 0.073320453 1.559842473 4.514885233 -0.018106173
      0.00597408  0.782099441 0.002511566 7.709110049 6.477912288 0.229870067
wt    -0.000424247      0.045943432 0.011210197 8.151038625 -0.000933312
      0.46436345  0.045697991 1.320108516 3.975684617 -0.013565786
      0.007306404 0.78490325  0.00155937  5.052578954 5.737948053 0.21541393
wt    -0.000247608      0.048126378 0.01143348  8.314300509 -0.001827442
      0.498400366 0.047272957 1.42875651  4.114527889 -0.012746295
      0.006180078 0.854702422 0.002227678 5.210241053 6.047718712 0.231773482
wt    0.000132559 0.048050352 0.011270893 8.197801674 -0.000619333
      0.493512025 0.039740933 1.344865436 4.065579399 -0.012544418
      0.006549418 0.805922539 0.001449958 5.351213029 6.046131915 0.228549923
```

```
fre5  -7.94221E-05      0.049940556 0.007579205 8.800746301 -0.000762937
      0.414855964 0.038475947 1.593529616 4.365203484 -0.019166115
      0.007607711 0.997621514 0.002658812 6.176172135 6.235267648 0.257445903
fre5  -3.30819E-05      0.043577377 0.006910835 8.373466114 -0.000478764
      0.378102816 0.039973189 1.339525802 4.127915529 -0.019943189
      0.007390837 0.814315192 0.001764751 5.389139088 5.85440975  0.232010351
fre5  5.62312E-05 0.040111797 0.007000609 8.33239873  -0.000782479
      0.402442129 0.035976005 1.250597508 4.203486922 -0.019413618
      0.00818479  0.794425052 0.001977036 5.952947815 6.097595702 0.243532382
ff    8.66816E-05 0.050444607 0.010461171 10.15430239 -0.00043968 0.371324694
      0.045644901 1.496580939 4.93872015  -0.01921288 0.00352049  1.023485172
      0.002606161 5.070494253 7.203138339 0.218996795
ff    -0.000132195      0.054414657 0.010507716 10.1814082  -0.000791181
      0.347632887 0.045107462 1.543208725 4.864766176 -0.019429488
      0.005340814 1.022858465 0.002557853 4.68248934  7.011677563 0.209001711
ff    4.4347E-05  0.054003156 0.01043495  10.1596764  -0.000615761
      0.368273187 0.047826796 1.516316395 4.944268968 -0.019557676
      0.004310548 1.027871443 0.002565846 5.242644094 7.262628706 0.217108111
;
run;


DATA Metal;
set icpf;
 if strain="wt" then strainwt=1;
 else strainwt=0;
 if strain="fre5" then strainfre5=1;
 else strainfre5=0;
 if strain="ff" then strainff=1;
 else strainff=0;
run;
%macro regfit(metalvar=);

PROC MEANS data=metal clm mean nmiss;
VAR &metalvar;
CLASS strain;
run;
proc reg data=metal;
model &metalvar=strainff strainwt strainfre5;
run;
proc glm data=metal;
CLASS strain;
model &metalvar=strain;
run;

proc robustreg data=metal;
class strain;
model &metalvar=strainff strainwt strainfre5/diagnostics;
run;

proc npar1way data=metal wilcoxon;
class strain;
var &metalvar;
run;
%mend regfit;

%regfit(metalvar=Fe);
```

```
%regfit(metalvar=Cu);
%regfit(metalvar=Mg);
%regfit(metalvar=Mn);
%regfit(metalvar=P);
%regfit(metalvar=Zn);

PROC STANDARD DATA=metal MEAN=0 STD=1 OUT=Zmetal;
  VAR Ag--Zn ;
RUN;

proc glm data=metal;
class strain;
model fe Cu Mg    Mn    P     Zn=strain;
manova h=_all_;
run;

PROC PRINCOMP DATA=Zmetal out=prin;
VAR  Fe     Cu    Mg    Mn    P     Zn ;
RUN;

PROC SGSCATTER DATA=prin;
 MATRIX Prin1 prin2
        / DIAGONAL=(histogram) GROUP=strain;
 PLOT Prin2 * prin1/Group=strain;
RUN;
data princolor;
  set prin;
  length color shape $8.;
  if strain="wt" then do; shape="club"; color="blue"; end;
  if strain="fre5" then do; shape="diamond"; color="red"; end;
  if strain="ff" then do; shape="spade"; color="green"; end;
run;
proc g3d data=princolor;
note j=r f="Albany AMT/bo" "Strain:  " c=green "FF"
         j=r    c=red "fre5"
         j=r    c=blue "WT"
        ;
 scatter prin1*prin2=prin3/
      color=color
      shape=shape
      size=1.5
grid
      rotate=45
      zmax=3
      zmin=-2;
run;
quit;


PROC GLMPOWER DATA=zmetal;
CLASS strain;
MODEL fe cu mg mn p zn =strain;

POWER

STDDEV = 1
ALPHA = 0.05
```

```
NTOTAL = 20
POWER = .;
plot x=n min=20 max=160;
run;
quit;

PROC GLMPOWER DATA=zmetal;
CLASS strain;
MODEL fe cu mg mn zn =strain;

POWER

STDDEV = 1
ALPHA = 0.05
NTOTAL = 20
POWER = .;
plot x=n min=20 max=160;
run;
quit;
```

R codes

```
setwd("c:/data")

metal = read.table(file="metal.txt", header=F)
names(metal) = c("strain","Fe","Cu","Mg","Mn","P","Zn")
metal$strain = as.factor(metal$strain)

## One-way ANOVA
#metal = metal[-18,]
Fe.aov = lm(Fe ~ strain, data=metal)
summary(Fe.aov)
Cu.aov = lm(Cu ~ strain, data=metal)
summary(Cu.aov)
Mg.aov = lm(Mg ~ strain, data=metal)
summary(Mg.aov)
Mn.aov = lm(Mn ~ strain, data=metal)
summary(Mn.aov)
P.aov = lm(P ~ strain, data=metal)
summary(P.aov)
Zn.aov = lm(Zn ~ strain, data=metal)
summary(Zn.aov)

## Rank ANOVA

kruskal.test(metal$Fe,metal$strain)
kruskal.test(metal$Cu,metal$strain)
kruskal.test(metal$Mg,metal$strain)
kruskal.test(metal$Mn,metal$strain)
kruskal.test(metal$P,metal$strain)
kruskal.test(metal$Zn,metal$strain)


## M ANOVA
library(MASS)
Fe.aov = rlm(Fe ~ strain, data=metal)
```

```
summary(Fe.aov)
Cu.aov = rlm(Cu ~ strain, data=metal)
summary(Cu.aov)
Mg.aov = rlm(Mg ~ strain, data=metal)
summary(Mg.aov)
Mn.aov = rlm(Mn ~ strain, data=metal)
summary(Mn.aov)
P.aov = rlm(P ~ strain, data=metal)
summary(P.aov)
Zn.aov = rlm(Zn ~ strain, data=metal)
summary(Zn.aov)


## MANOVA
Y = cbind(metal$Fe,metal$Cu,metal$Mg,metal$Mn,metal$P,metal$Zn)
mfit = manova(Y ~ metal$strain)
summary(mfit, test="Pillai")

Y = scale(Y)
mfit = manova(Y ~ metal$strain)
summary(mfit, test="Pillai")

PY = princomp(Y)
summary(PY)
mfitpc = manova(PY$scores[,1:4] ~ metal$strain)
summary(mfitpc, test="Pillai")

pairs(PY$scores)

library(rrcov)
robpc = PcaHubert(Y)
summary(robpc)
op <- options(contrasts = c("contr.helmert", "contr.poly"))
robmfitpc = manova(getScores(robpc) ~ metal$strain)
summary(robmfitpc, test="Pillai")
plot(robpc)
pairs(getScores(robpc))
getScores(robpc)
```

Conclusion

Iron is an important transition metal involved in many pathways. In this study, I verified Fre5 is a mitochondrial iron reductase by biochemical iron reductase assay, iron related phenotypes and oxidative stress phenotypes. An iron reductase in mitochondria suggests there is intracellular ferric iron that can be reduced to be used for normal physiology. This reduction requirement is not essential for survival as deletion of *FRE5* only caused a heme defect that resulted in mild mitochondrial dysfunction. This study suggests that there is a minimum requirement for heme in the cell, and this minimum requirement is much lower than normal heme concentrations found in yeast cells.

The oxidative stress sensitivity of a *FRE5* overexpression strain is linked with iron concentration in mitochondria and I suggest that the increased iron and increase reductase activity results in damage due to Fenton reactions. An additional source of reactive oxygen species is the electron transport chain particularly Complex III, which produces ROS as a by-product. The decreased heme availability and slight decrease in oxygen consumption in *fre5*Δ strains plus the decrease in reductase activity may contribute to the oxidative stress resistance of this strain.

Iron and copper are correlated in many pathways, this is the first time a mitochondrial transporter (Mrs3) has been found to transport both iron and copper. In the statistical analysis studies, we found negative correlation between iron and copper and high copper causes a heme defect in cell. This defect can be abrogated by the deletion of *MRS3* suggesting that transport by this protein is leading to a biologically relevant competition.

How iron is transferred into mitochondria and the forms that are available in the intermembrane space for transport remains unknown. However, the advances in understanding a

role for the iron reductase Fre5 in mitochondria and the overlap transporter between copper and iron by Mrs3 will be useful in answering these questions in the future.